The Impact of Large-Scale Renewable Energy on Grid Small-Signal and Frequency Stability: Modelling, Analysis, and Control

By

Jae-Woong Shim

A dissertation submitted in fulfilment of

the requirements for the degree of

Doctor of Philosophy

School of Electrical and Information Engineering

The University of Sydney

July 2016

The Impact of Large-Scale Renewable Energy on Grid Small-Signal and Frequency Stability: Modelling, Analysis, and Control

Jae-Woong Shim

A dissertation

Submitted to the School of Electrical and Electronic Engineering,

Graduate School of Yonsei University

in partial fulfilment of

the requirements for the degree of

Doctor of Philosophy

School of Electrical and Electronic Engineering
Graduate School

Yonsei University
Seoul, South Korea

July 2016

The Doctor of Philosophy of Jae-Woong Shim is jointly awarded by

Yonsei University & The University of Sydney.

July 2016

Dedicated to my family

Parents: Jangsoup Shim and Jong Hee Park
Small sister: Ji Youn Shim

Wife: Il-Hoon Kim

Declaration of Originality

I hereby declare that this submission is my own work and contains no material previously published nor written by another person except for specific reference made to the work of others, and this have not been submitted for the award of any other degree or qualification in Yonsei University, the University of Sydney, or any other educational institution.

Any contribution made to the research by others, with whom I have worked at Yonsei University, the University of Sydney, or elsewhere, is explicitly acknowledged in the dissertation.

Author: $Jae\text{-}Woong\ Shim$
Date: July 2016

Acknowledgment

I would like to express my deepest appreciation to my supervisors Prof. Kyeon Hur and Dr. Gregor Verbič. Both professors are respectable, intelligent, and nice. They are the persons whom I want to be a person like. Being their student has been the honourable time to me, and I will be missing the time being at Yonsei University and the University of Sydney.

Prof. Kyeon Hur always tries to understand my situations, listens to my opinions, and strongly supports me. My sight to the world become much wider by kindly allowing me to visit countless places, inspiring me to receive Joint Ph.D, and encouraging me to have interests in the academic society. The topics giving me in many aspects based on his wide background knowledge always cheerfully stimulate my academic curiosity, and make me happy enough to satisfy intellectual appetite. I have no doubt that he is the most influential person in my life except for my family. I would keep his personal and professional advises in my mind with sincere gratitude.

Dr. Gregor Verbič is always with supportive, kind, gentle, and friendly manner. During the research, he always shows me the big vision, clearly explains his professional knowledge, listens attentively to my opinions, and tries to find a way to reach a final goal of our research. I would miss the time having the weakly meetings and visiting several sites together. I am grateful for his friendly advices and kind specialized comments. I may not receive joint Ph.D without his considerate help, as he always actively tried to help me and give advices even after I came back to Korea. I also appreciate warm hospitality from him, his wife Ana, and his fast running sons.

I can say I am a very lucky person to have great scholars as my supervisors. I promise I'll contribute to the world for the future science and technology with knowledge and experience I have acquired during the Ph.D.

I would like to appreciate to dissertation examiners; Prof. Jung-Wook Park, Prof. Yong-June Shin, and Prof. Mithulan Nadarajah. I am grateful to Prof. Jung-Wook Park for providing scientific knowledge through a number of interesting seminars during the Ph.D course, and I also thank to the professional comments during the Ph.D defence process. I appreciate that Prof. Yong-June Shin effectively taught high quality lectures where I learned a lot during my degree, and I am also grateful to his friendly advices. I thank to Prof. Mithulan Nadarajah who gave me kind and valuable comments for the dissertation.

I also highly appreciate to the faculties in the University of Sydney. I have been pleased to conduct my research during my degree with them; Prof. David J. Hill, I'm even still happy that he gave highly professional comments and compliments in regards to the research, and also I learned a lot from his published

papers; Prof. Joe Dong (Zhao-Yong Dong) who is always gentle, kind, and highly professional, and also I learned a lot from his published papers.; Dr. Jin Ma who is gave me the lectures (Power system stability) which was beneficial to me, and I appreciate to him about his professional comments during the research progress.; Prof. Dylan Lu, I won't forget the memories in Seoul with him and I appreciate his hearty friendliness.; Dr. Archie C. Chapman, who is highly professional in his area. I thank to his friendliness.

I would like to express appreciation to the scholars I met during the Ph.D. degree. Prof. Joe Chow in Rensselaer Polytechnic Institute: Beginning of my degree the couple of his seminars in Yonsei University gave me the big impression and a recent meeting in Seoul was highly impressive to me in terms of his academic attitude, interests of our research, and his knowledge. I also learned a lot from his papers and books regarding PMU, PSS, FACTS control, and Generator aggregation. Prof. Kwang Y. Lee at Baylor University: I enjoyed his several seminars in Yonsei University and other places. His research fulfilment has always inspired me. Prof. Vassilios G. Agelidis at the University of New South Wales: His passion toward the research and implementation of installation of renewable and smart devices were highly impressive. Dr. Minsoo Jang at the University of New South Wales: his friendly and kind introduction was grateful. Dr. Prabha Kundur: although I only met him twice in in PES-GM and in his one day seminar at the University of Sydney, his explanation and wide knowledge gave me significant impression, and his book (Power System Stability and Control) provide me the solid knowledge of power system stability.

I would like to say thank you for senior faculties in the Yonsei University; Prof. Tae Kuk Ko, Prof. Young-Hyun Moon, and Prof. Hagbae Kim who gave high quality lectures. Especially, I was glad to collaborate with the lab members of Prof. Tae Kuk Ko.

I'd like to thank to the project ordering organizations. LS Industrial Systems: HVDC/FACTS projects with Dr. Yong-Ho Chung, Dr. Gum-Tae Son, and Dr. Seung-Taek Baek. Korea Electrotechnology Research Institute (KERI) which allows me to start the research of electrical energy storage system; Dr. Seog-Joo Kim, Dr. Sang-Won Min, Dr. Dong Joo Kang, and other members in Smart Power Grid Research Center. OCI company which wanted to develop the algorithm of ESS operation for islanded Microgrid; Alexander Zhou. I learned a lot for the inertia less system operation.

I hope to say thank you to the companies and its employees from which I receive much help: Dr. In Kwon Park in RTDS Technologies Inc., Dharshana Muthumuni and Kimberly Laing in PSCAD, and the staffs in DIgSILENT company allowing me the thesis version of Power Factory.

My gratitude exists in the deep inside of my heart for Dankook University; Profs. Soon-Chan Hong especially who gave me a gentle advice for the anxiety about my future, Kwang-Ho Lee, Kyong Ho Han, Jong-Sun Ko, Seung-Ki Lee, Kee-Sang Lee, Seungrohk Oh, Ki-sik Lee and all other professors.

I highly appreciate to the lab members in Yonsei University; Heejin Kim, he is an intimate mate and I have relied much on him like he does to me; Kyungsung An who is gentle, courteous, and considerate person, I thank him so much in many points; lively and friendly Jaesik Kang; humorous Da Ham Min; cool guy Young Ho Cho; nice guy Jae-Kyeong Kim; rich American and polite guy Sehyun Kim, active and humorous Sang Min Kim, I really thank to him helping me a lot with smiley face; considerate and thoughtful Choong Man Lee, I also thank him so much in many aspects; brilliant Hyun Jae Lee having great appetite; nice guy Kyung Han Jun; sociable Young Joon Lee having relatively good appetite; handsome Jee Hoon Lee; Alcohol Wednesday Woochoul Kim; smiley face Jong Seo Na; funny and sociable Hae Won Seo; polite and friendly Wooyoung Shin; outgoing and humorous Nehal Helaly.

Thank also to past lab members, Jae Yeong Yoo, Tae Sik Nam, Joo Young Moon, Jeong Hyeok Heo, Sukki Jung, Jong Woon Yang who gave me much knowledge of battery characteristics, Won Kyung Kim, Santos Kihwele, Majid Manaf, Hyoung Jin Kim and Mr. Hong. I also thank to a visitor and other lab members; Max Liu, Mehrdad M. Farid, and Jae Young Jang.

All of the lab members in the University of Sydney; Hesamoddin Marzooghi who is kind and helped me a lot to settle down in Australia and gave me technical advices for DIgSILENT/PowerFactory; Mehdi Garmroodi Doiran who help me a lot to learn DPL and DIgSILENT/PowerFactory as well; Zhiheng Zhao, I would not forget the time hanging out with you and play the basketball; Long Liu, it's good memory sharing our concerns of the life and give an advise each other; Chanaka Keerthisinghe friendly and kind guy; Sleiman Mhanna; Mohammad Sadegh Golsorkhi Esfahani; Benjamin Zhang (Wang Zhang); Jaebok Lee who is my friendly lunch mate and an advisor for the life in Australia; Andoni Urtasun; Guo Chen; Liyan Zhang; Md Habibullah; En Kerol; Le An.

My previous house owner and the best friend to me and my wife; TK Kajoranun. My personal life in Australia was always with him and that memory will keep staying in our mind forever.

I thank to my cousins who hung out with me in Yonsei University, Jae-Sung Shim and who thought me how to study effectively when I was young, Prof. Jae Won Shim.

I appreciate to the institutes which provide me financial support; Yonsei University and LS Industrial System and provide me the chances of the study and research; Yonsei University and The University of Sydney, and all the staffs who helped me in these universities.

I would like to express my heartfelt appreciation to my family. My parents, Jangsoup Shim and Jong Hee Park, always have believed me and support me, whenever the situation is difficult or not. Without their sacrifice, dedication, and support, I could not finish my degree. I just can't tell how much all of them mean to me. I love you all so much. I also wish to express my gratitude to 'happy virus' my small sister Ji Youn Shim, who has been always kind and caring. She always understand and entertain me, and she was always there for me, whenever my life gets ascending or descending.

I would like to express my profound appreciation to my wife Il-Hoon Kim. She is always considerate, thoughtful, and supportive. She always believed me without any complaint. I truly appreciate that she has devoted her life to me with the faith, after the marriage. I promise I'll make her happy permanently. I love you so much.

Additionally, I would like to say thank you to all other family members whom I cannot mention in this short acknowledgement.

Lastly, I'd like to say thank you to the Lord, Jesus Christ who is always with me and guides me.
'The Lord is my shepherd, I shall not want. He makes me lie down in green pastures'
Psalms 23:1-2

This certifies that the dissertation
of Jae-Woong Shim is approved.

[redacted]

Dissertation Supervisor: Kyeon Hur

[redacted]

Dissertation Supervisor: Gregor Verbič

[redacted]

Jung-Wook Park

[redacted]

Yong-June Shin

[redacted]

Mithulan Nadarajah

Yonsei University & The University of Sydney

July 2016

Contents

List of Figures

List of Tables

List of Acronyms

AC	Alternative Current
AEMO	Australian Energy Market Operator
AC	Alternative Current
AEMO	Australian Energy Market Operator
AGC	Automatic Generation Control
CPS	Control Performance Standard
CP	Central Point
CSP	Concentrating Solar Thermal Power Plant
DaSOF	Droop control and State-of-Charge Feedback
DC	Direct Current
DG	Distributed Generation
ERCOT	The Electric Reliability Council of Texas
ESS	Energy Storage System
EV	Electric Vehicle
FERC	The Federal Energy Regulatory Commission
FR	Frequency Regulation
HPF	High Pass Filter
HVDC	High Voltage Direct Current transmission system

ISO	Independent System Operator
KDE	Kernel Density Estimation
KEPCO	Korea Electric Power Corporation
LFC	Load-Frequency control
LPF	Low Pass Filter
MIMO	Multiple Input Multiple Output
MISO	Multiple Input Single Output
N4SID	Numerical Algorithms for Subspace State Space System Identification
NEM	Australian National Electricity Market
NERC	North American Electric Reliability Corporation
NYISO	The New York Independent System Operator
PDF	Probability Density Function
PEV	Plug-in Electric Vehicle
PJM	Pennsylvania-New Jersey-Maryland Interconnection
PMU	Phasor Measurement Unit
PRBS	Pseudo Random Binary Signal
PSS	Power System Stabilizer
PV	Photovoltaic
RES	Renewable Energy Sources
SISO	Single Input Single Output
SIMO	Single Input Multiple Output Interconnection
SOC	State-of-Charge
V2G	Vehicle to Grid
VSC	Voltage Sourced Converter

WECC Western Electricity Coordination Council

WPP Wind Power Plant

WTG Wind Turbine Generators

ZCA Zero Carbon Australia Stationary Energy Plan

ABSTRACT

The Impact of Large-Scale Renewable Energy on Grid Small-Signal and Frequency Stability: Modelling, Analysis, and Control

Jae-Woong Shim

Graduate School
School of Electrical and Electronic Engineering
Yonsei University, Seoul, South Korea

School of Electrical and Information Engineering
The University of Sydney, Sydney, NSW, Australia

This dissertation intends to discuss the influence of renewable energy sources (RES) on the stability of power system. Although integration of renewable brings incalculable optimistic aspects, the inherent variability of RES concerning fluctuation of active power may exhibit adverse influence on stability issues regarding small-signal and frequency stability point of views. Thus, this dissertation discusses those two stability perspectives.

From small-signal stability perspectives, the agenda is divided into three parts. First small signal research investigates the influence of time-varying RES on low frequency oscillation, which triggers weak frequency band of vulnerable modes on remote area. Dynamic analysis is carried out to observe the impact of low frequency oscillation and the activation of mode coupling, although most of the research in association with oscillatory stability is conducted on the basis of static analysis. Second study of small signal is to observe the influence of high penetration change on interarea oscillation. Concentrating Solar Thermal Power Plant (CSP) through HVDC provides power on Simplified Australian system, and increases penetration level of specific area. As a consequence, the change of system eigenvalues is explained using a contributive factor, left eigenvector. Third research of small signal is to investigate solar irradiation and wind velocity which inherently embrace stochastic characteristics and affects the generation quantity of photovoltaics (PV) and wind turbine generators (WTG). From this reason, conventional rotating generators may reduce its generation owing to increased quantity of RES. As consequences, power flow from the condition above may lead to stochastic eigenvalue and controllability distribution. Hence, the purpose of this research is to investigate stochastic contribution of Eigen-properties with the change of inertia constant.

From frequency stability perspectives, the future grid might be operated under reduced system inertia and high penetration. The decrease of system inertia constant results in some problems such as deterioration of frequency stability. Against this backdrop, ESS technology emerges as a countermeasure for the implications of large fleet of RES. First chapter of frequency stability aspects introduces ESS methodology which enables ESS to coordinate harmoniously among existing equipment for ancillary service by means of proposed method: droop control and State-of-Charge feedback (DaSOF). The last chapter suggests the method for EV application with DaSOF. This proposed charging method is based on the mix of Smart Charging method and DaSOF method. The efficacy of large group of EV application with this proposed method against variability of RES is investigated and proved on the Jeju island system.

In short, this dissertation explored how much WTG and PV gives rise to influence with regards to a small signal stability aspect. In addition, frequency part provides observations on ESS operation as a countermeasure of RES uncertainty and variability.

Key words : Renewable integration, small-signal stability, frequency stability, system identification, mode coupling, Monte Carlo simulation, stochastic process, Kernel Density Estimation (KDE) methods, Energy Storage System (ESS), frequency regulation, Droop Control, SOC feedback, Load-Frequency Control (LFC), Electric Vehicle (EV), Vehicle to Grid (V2G).

Chapter 1

Introduction

Abstract– **The purpose of this chapter intends to sketch out the background and story-line of the dissertation. This research is based on renewable integration plan in Australia and Korea. Therefore, the circumstances and plans of both countries are introduced in terms of their efforts towards curtailment of carbon dioxide emission. In addition, the objective and outline of this dissertation are addressed in last two sections.**

1.1 Research Background

Harnessing renewable energy sources (RES) is implicated in environmental, socio- economical, technical challenges of the present and future [1]. A rapid rise of global RES share is a current phenomenon towards decarbonization by the support and promotion from governmental action at the international and national level expansion of RES [1].

The research in association with integration of RES has been extensively and vigorously researched in terms of economic benefit; large scale grid integration of renewable energy sources in several countries [2] and policies and economic benefits in Europe [3], [4].

Some of the report in [5] emphasizes the need of interdisciplinary study to embrace diverse area such as the convergence of energy, communications, sensing, and computing technologies to invent economical, reliable, affordable, and environmentally beneficial ways of power network. Likewise, the other research [6] stresses the necessity of inter-

disciplinary research for the integration of high penetrations in aspect of power system planning and risk management, distribution and transmission planning, operations, and interface between the grid and renewables.

Much scholarly and industrial work is increasingly abundant concerning technical issues to embrace the variation of RES into their network. Some of the ISOs and utilities have made the efforts to accommodate the forecasting challenges and short-term performance variability for growing shares of variable renewable generation [7]. The research for geospatial power system model, power system analytics, integrated energy management system and setting-less protection method was conducted [8].

Several research targeting the subject of Western U.S. presents absorbing account of practical RES integration.

The technical analysis found operationally feasible percentage of western interconnection to accommodate solar energy penetration [9], and the operational impacts of very high levels of variable generation penetration rates in the western United States is investigated through the western wind and solar integration study [10]. The ability of ESS was presented to accommodate the large scale integration of RES into the grid and to contribute to the economic dispatch of generation on the WECC system of Arizona, summer peak 2009 [11]. Additionally, pursuing operation strategies and technologies for high penetrations of renewable energy for Oahu Wind Integration Study is verified [12]. The model of utility scale wind and solar PV generation is developed and validated for exact performance in the system [13], and probabilistic method is invented for synthetic forecasts for variety time frame ahead, which is suitable for the use of integration and transmission studies [14]. The inertial and primary frequency response of WTG during the contingency is presented in the research [15]. Flywheels capabilities is investigated on power system to provide higher flexibility with the fast response, when wind penetration level increases [16].

For the mitigation of adverse influence, ESS becomes promising technology and feasible solution. Some of the research team developed a model of optimization for generation and ESS with incorporation of energy regulatory policies, hourly renewable profiles, and optimal operation-based investment [16], and Arizona transmission system in a 2010 summer peak is demonstrated for several topics with regards to bulk energy storage. Regarding the economic dispatch problem, load factor, different levels of ESS, and relaxation of grid circumstances [16]. Increasing system flexibility without infras-

tructure expansion in US ISOs is investigated [17].

A demonstration of the ESS valuation methodology of EPRI and the Energy Storage Valuation Tool for cost-effectiveness of ESS in California is explored [18]. EPRIs ESS Research Program is to obtain better understanding of the costs, value, and benefits of ESS in various applications with huge examples of ESS applications, requirements, and benefits [19]. ESS from commercially available industrial technology can assist wind and solar farms to comply with these grid code requirements for stability and predictability [20]. The different aspects of the V2G services in the use of PHEVs/BEVs based ESS and its impacts of both participations of transportation and power systems in the electricity market with regards to the load demand and ancillary services [21]. An stability assessment methodology by means of Monte Carlo simulation is developed for the quantification of the variable effects on the power system with variable sources into energy storage units, which can evaluate impacts of wind and ESS integration in the point of view of the economic, reliability, and emission effects in a market environment [22].

1.2 The National Challenges

Many of the countries endeavour to harness natural resources for electrical energy to reduce greenhouse gas in accordance with Paris Climate Change Accord in April of 2016. Many of the developed nations have made remarkable efforts to change paradigm of electric power grid and to adopt generation mix. Thus, this section introduces their efforts and long term plans especially in case of two countries; Australia and Korea.

1.2.1 The Challenges of Australian Future Grid

Background and Motivation

The University of Melbourne Energy Research Institute and Australian Energy Market Operator (AEMO) provides a blueprint for Australia to equip with the renewable electricity infrastructure through the reports: Zero Carbon Australia (ZCA) Stationary Energy Plan and 100 Percent Renewables Study Modelling Outcomes Report. They concur in the comprehensive upgrade of Australian power network to envision full utilization of the commercially available technology today: wind power, concentrating solar thermal power plant (CSP) with molten salt storage, PV, etc. ZCA offers a big vision of Australia electric power infrastructure to be a renewable energy powerhouse. According to the report, accumulative emission in Australia produces one of the highest per-capita emissions of carbon dioxide amongst developed countries.

Figure 1.1 indicates the Australian government analysed the carbon dioxide emission from 2005 until 2050 and forecasted the accumulative emission regarding the portion of the source type of greenhouse gas. In Figure 1.1, about two-thirds of total greenhouse gas emissions in Australia are caused by fossil fuel in the stationary energy and transport parts.

Renewable Integration plan

The University of Melbourne Energy Research Institute insists that they suggests a feasible and pragmatic roadmap through ZCA [23] to a new and more sustainable energy system in Australia. The plan proposes 3,500 MW of CSP capacity to be installed in 12 sites in Figure 1.2 and an additional 48,000 MW of wind turbines to supply 40% of electricity demand. Thus, approximately 130 TWh should be generated by wind turbines

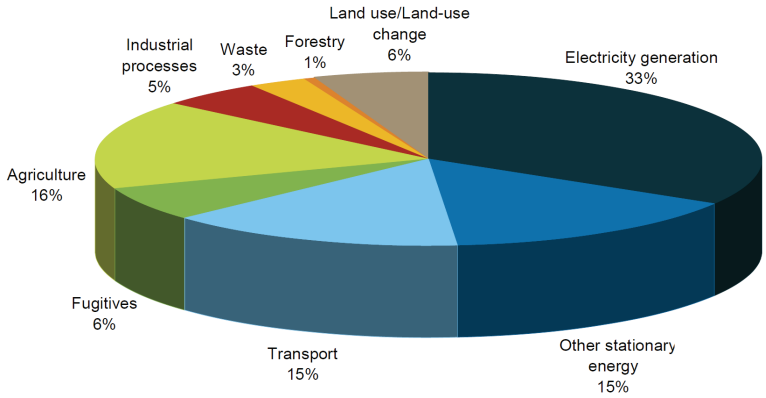

Figure 1.1: Australia projected cumulative emissions 2005 to 2050 [23]

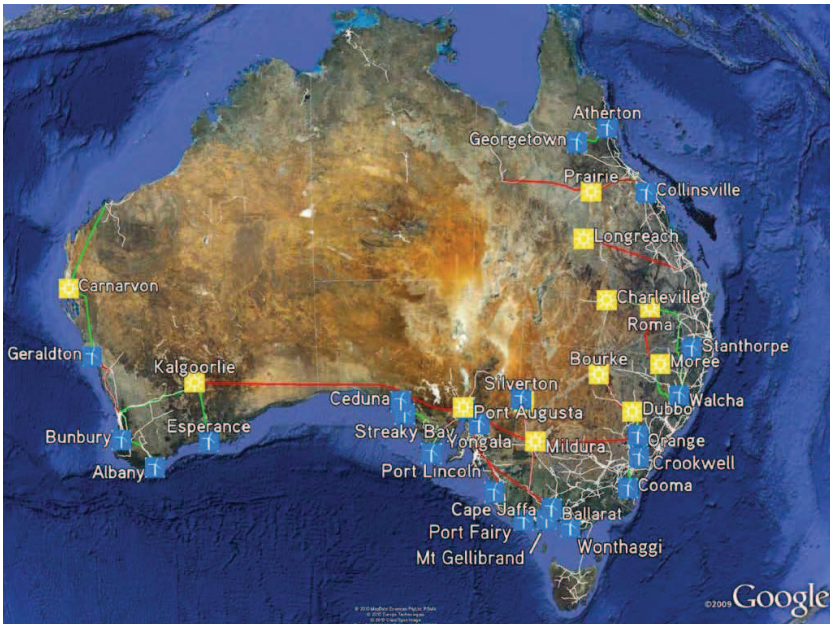

Figure 1.2: WTG and CSP installation sites in the Australian Future Grid Plan [23]

generators (WTG) in each year, and nearly 6,400 wind generators with 7.5MW rating should be installed at 23 distributed sites over Australia.

The Portion of Renewable Capacity

AEMO report in [24] forecast two scenarios according to their assumption; first one is high increase of rooftop PV, and they suggested PV will account for around 50% of generation quantity.

One another scenario forecasted by AEMO assumes wind would be largest capacity (34,500 MW or 35% of total capacity) since wind is likely to be one of the cheapest technology in the future as can be observed in Figure 1.3, 1.4. Both scenarios imply that portion of variable generation is highly increased and the amount of dispatchable generation is significantly decreased.

AEMO report foresees the capacity of RES, especially PV and WTG, will be considerably increased. These non-dispatchable and highly variable generators may give rise to adverse influence on the power system stability. The population of Australia concentrated on the seashore area, and load demand mostly rises in this area; consequently, power network is also narrowly installed near to the seashore. Since the power system flowing corridor is highly narrow and lay on unimaginable long distance, circumstance

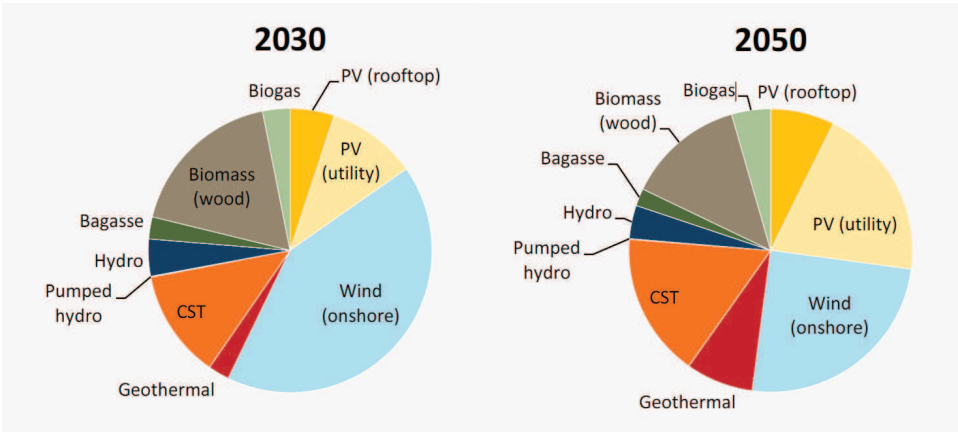

Figure 1.3: Generation capacity of a scenario assumed by AEMO [24]

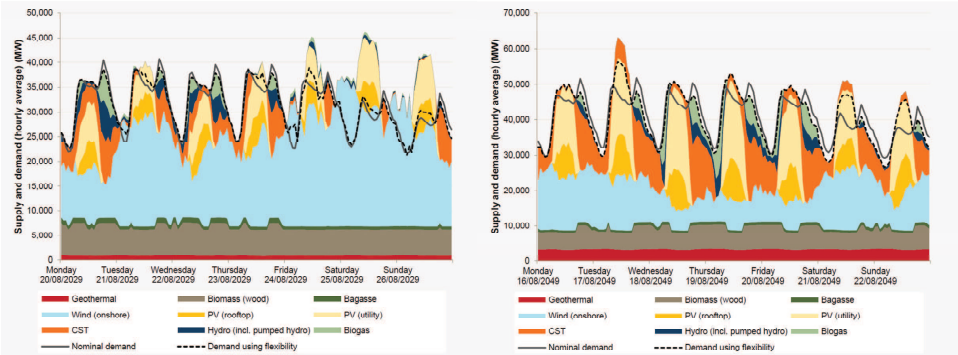

Figure 1.4: Example of one scenario in 2030 and 2050
[24]

in Australia leads to interesting phenomenon such as small interarea oscillation and local oscillation as in [25], which is developed in IEEE working group as an benchmark system targeting the simplified Australian system.

Therefore, this dissertation intends to observe WTG and PV influence on small signal stability and frequency stability as well under the circumstance of highly penetrated network.

Table 1.1: The Portion of Primary Energy by Korean Government – Ministry of Commerce Industry and Energy (Unit:%)

	2012	2014	2025	2035	Annual Growth
Solar Thermal	0.3	0.5	3.7	7.9	21.2
PV	2.7	4.9	12.9	14.1	11.7
Wind Energy	2.2	2.6	15.6	18.2	16.5
Bio Energy	15.2	13.3	19.0	18.0	7.7
Hydraulic	9.3	9.7	4.1	2.9	0.3
Geothermal Thermal	0.7	0.9	4.4	8.5	18.0
Wave Power Station	1.1	1.1	1.6	1.3	6.7
Recycle Energy	68.4	67.0	38.8	29.2	2.0

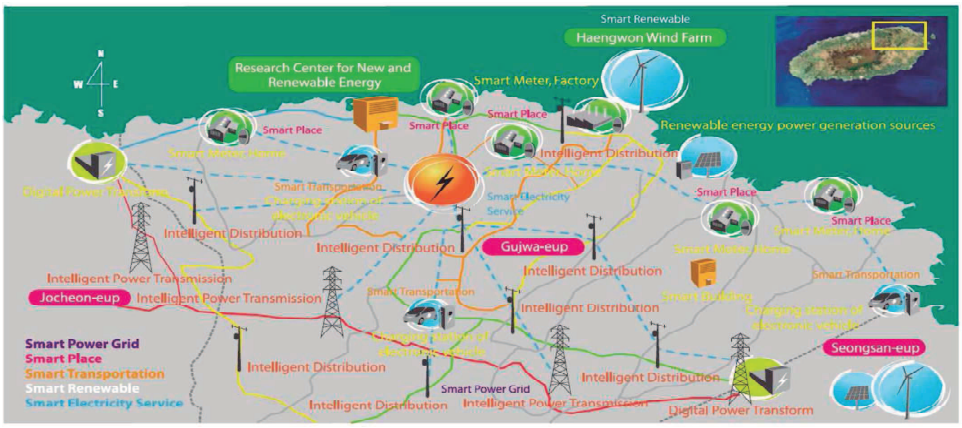

Figure 1.5: Jeju Smart Grid demonstration project
[26]

1.2.2 The Challenges of Korean Network

Korean government recently mapped out the fundamental plan for renewable energy portfolio for mid and long term. The key issues are following: to provide more than 11% of energy until 2050, to foster PV and WTG as core energy source, to establish the road map to reduce generation cost, and to increase the energy annually as in Table 1.1.

The plan report by Korean government mostly focuses on the development of renewable energy and economic benefit of fostering renewable energy, neglecting technical issues. Against this backdrop, the stability issue is one of the important themes to integrate renewable sources; moreover, the plan includes Energy Storage System (ESS) implying frequency and power smoothing issues are placed with underlying consideration.

Recently, Korean government installed the large number of WTGs and PVs on Jeju island and they installed large number of EV charge stations throughout the island as can be seen in Figure 1.5.

Large number of RES in upcoming future would deteriorate power system stability, hence, this dissertation refers to recent studies the utilization of the ESS, and EV [27] and presents implementation of such equipment support to reinforce resiliency in terms of the frequency regulation to stabilize the power system.

1.3 Dissertation Objectives

The intention of the dissertation is to thoroughly evaluate power system stability in terms of low frequency oscillation and frequency variation for the renewable integration. Thus, this research deals with following topics and methods:

- System Identification using Numerical Algorithms for Subspace State Space System Identification (N4SID) to analyse frequency band of wind fluctuation
- Observation of Mode Coupling affected by wind turbine
- Stochastic analysis of WTG and PV generation for eigenvalue, eigenvector, and controllability
- Developing methodology for frequency regulation purposed ESS and its mathematical expressions
- Investigation of implication and harmoniousness of methodology on existing network frequency regulation
- Developing methodology for FR EV for the system adequacy

1.4 Outlines of the Dissertation

The background and the objective of this dissertation are discussed in this section. Each chapter has its own topics regarding stability. Chapters 3 and 4 deliver small-signal stability issues, and Chapters in 5, 6, and 7 provide issues regarding frequency stability. The rest of chapters are organized as follows.

Chapter 2: Theoretical Background of Power System Stability
The definition and classification of power system stability are presented and theoretical stability issues are delivered. Furthermore, conventional frequency control coordination such as primary, secondary, and tertiary controls are explored.

Chapter 3: Impact of RES on Oscillatory Modes - Mode Coupling
This chapter intends to observe a fluctuation impact of RES on the power system. Numerical algorithms for Subspace State Space System Identification N4SID method for System Identification is implemented. Investigation is carried out for Mode coupling, which indicates oscillation of power can trigger other modes in remote area [28].

Chapter 4: The Influence of Penetration Level Change on Eigen-properties

In the small signal stability aspects, high penetrated system may lead to difficulties to foresee system characteristics, as the provided power from renewable generators may change the operating point, and it can be reflected to the eigenvalue change. The eigenvalue normally changes in a continuous way; however, the non-continuous transition of eigenvalues are occasionally observed in here due to the renewable sources. Thus, in this chapter, the change of eigenvalue is investigated in accordance with the increase of penetration level [29].

Chapter 5: Stochastic Eigen-analysis under High Penetration System

In order to analyse eigenvalue for the future, static analysis has weak persuasiveness, for the characteristic of RES exhibits uncertainty and unpredictability. Thus, this chapter introduces the method to stochastically analyse eigenvalues and its contributive factors using Australian system.

Chapter 6: FR ESS Method using Droop Control and SOC Feedback: Methods and Implications.

For the frequency regulation, ESS cannot provide permanently supporting power due to unlimited energy; hence, ESS operation method was proposed considering SOC feedback. FR ESS operation methodology has to be cooperative with existing and conventional frequency regulation practices. Proposed method can harmoniously melt into conventional operation method; thus, this chapter indicates proposed frequency stabilizing methodology through mathematical analysis and its operational functionality in Australian system.

Chapter 7: FR ESS Operation Method using EV

System frequency may fluctuate due to large penetration in the small system, and this frequency fluctuation issues can be alleviated using EV. EV operation method proposed in this chapter, and the contribution of fleet of fast acting equipment is observed for corresponding issues in Jeju Island.

Chapter 8: Conclusion

This chapter concludes the issues discussed above and provides a summary of the each content of the main parts to highlight overall aspect of renewable integration.

Chapter 2

Theoretical backgrounds

2.1 Definition and Classification of Power System Stability

Classification of stability has high importance to build up the alternatives in each case of the stability issues.

Each equipment installed in the power system has its own responsibilities and reinforces the corresponding stability. Categorized stability has different type of cause-and-effect, and if we know cause-and-effect, the solution can be adequately placed for that cause-and-effect.

- $Definition\ of\ Power\ System\ Stability$**:**

  Power system stability is the ability of an electric power system, for a given initial operating condition, to regain a state of operating equilibrium after being subjected to a physical disturbance, with most system variables bounded so that practically the entire system remains intact [30].

The definition of power system stability is defined in [30], and most important one is the ability of power system recovery in several point of views, which can be called resiliency of the power system.

Category of the power system stability is indicated in Fig. 2.1 Rotor angle doesn't have long term, because the stability regarding rotor angle stability can be decided whether power system becomes stable or unstable within short time. Small disturbance angle stability is triggered by small change by generators and loads, and transient stability is triggered by large disturbance by electrical circumstances.

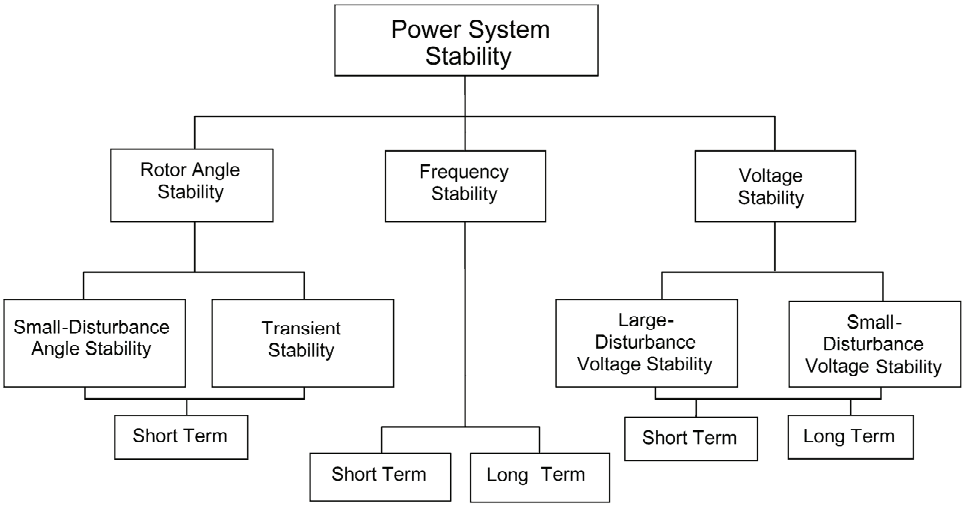

Figure 2.1: Classification of power system stability.
[30]

Frequency stability part can be categorized as one type of the power system stability.

Frequency stability is highly related with the balance issues between generation and consumption by the generation and load. Frequency stability can be analysed in regard with short-term issues, when contingency or the change of the generation or load occur. This stability problem can be resolved by the governor control or automatic generation control (AGC). Additionally, state-of-the-art technology is the ESS for frequency regulation. Frequency stability issues regarding long term can be called adequacy problem, which means power system equipment is installed adequately or not.

Voltage stability topic is also one of the important categorized types of the power system stability. Voltage stability has significant relation with reactive power, although it has relatively low relation with active power. Furthermore, this can be categorized as long-term and short-term.

Through the paper [30], the working group from IEEE/CIGRE defines each stability as follows:

- $Frequency\ Stability$**:**

  Frequency stability refers to the ability of a power system to maintain steady frequency following a severe system upset resulting in a significant imbalance

between generation and load. It depends on the ability to maintain/restore equilibrium between system generation and load, with minimum unintentional loss of load. [30]

- $Rotor\ Angle\ Stability$**:**

  Rotor angle stability refers to the ability of synchronous machines of an interconnected power system to remain in synchronism after being subjected to a disturbance. It depends on the ability to maintain/restore equilibrium between electromagnetic torque and mechanical torque of each synchronous machine in the system [30]

- $Voltage\ Stability$**:**

  Voltage stability refers to the ability of a power system to maintain steady voltages at all buses in the system after being subjected to a disturbance from a given initial operating condition. It depends on the ability to maintain/restore equilibrium between load demand and load supply from the power system [30].

In the dissertation, the most important issue is the uncertainty and variability of the renewable resources and most of the variability issues are related with active power; hence, I would like to discuss the stability of rotor angle and frequency for rest of the dissertation.

2.2 Power System Modelling

The behaviour of a power system can be described by a set of differential and algebraic equations of the form:

$$\dot{\mathbf{x}} = \mathbf{f}_1(\mathbf{x}_1, \mathbf{x}_2, \mathbf{u}) \tag{2.1}$$

$$0 = \mathbf{f}_2(\mathbf{x}_1, \mathbf{x}_2, \mathbf{u}) \tag{2.2}$$

$$\mathbf{y} = \mathbf{g}_0(\mathbf{x}_1, \mathbf{x}_2, \mathbf{u}) \tag{2.3}$$

where $\mathbf{f}_1$, $\mathbf{f}_2$ and $\mathbf{g}_0$ give the vectors of non-linear differential, algebraic and output equations, respectively; and $\mathbf{x}_1 \in \mathbb{R}^n$, $\mathbf{x}_2 \in \mathbb{R}^l$, $\mathbf{u} \in \mathbb{R}^m$ and $\mathbf{y} \in \mathbb{R}^p$ denote the vectors of state variables, algebraic variables, inputs and outputs, respectively. Typically, the system in (2.1) is assumed time-invariant so the time-derivatives of the state variables are not explicit functions of the time. Assuming $\frac{\partial \mathbf{f}_2}{\partial \mathbf{x}_2}$ is nonsingular we can eliminate $\mathbf{x}_2$. Let $\mathbf{x} = \mathbf{x}_1$ and we get

$$\dot{\mathbf{x}} = \mathbf{f}(\mathbf{x}, \mathbf{u}) \tag{2.4}$$

$$\mathbf{y} = \mathbf{g}(\mathbf{x}, \mathbf{u}) \tag{2.5}$$

In small-signal stability analysis, the disturbances are considered small so the system can be linearised around the operating point $(\mathbf{x}_0, \mathbf{u}_0)$ resulting in

$$\Delta\dot{\mathbf{x}} = \left.\frac{\partial \mathbf{f}}{\partial \mathbf{x}}\right|_0 \Delta\mathbf{x} + \left.\frac{\partial \mathbf{f}}{\partial \mathbf{u}}\right|_0 \Delta\mathbf{u} = \mathbf{A}\Delta\mathbf{x} + \mathbf{B}\Delta\mathbf{u} \tag{2.6}$$

$$\Delta\mathbf{y} = \left.\frac{\partial \mathbf{f}}{\partial \mathbf{x}}\right|_0 \Delta\mathbf{x} + \left.\frac{\partial \mathbf{f}}{\partial \mathbf{u}}\right|_0 \Delta\mathbf{u} = \mathbf{C}\Delta\mathbf{x} + \mathbf{D}\Delta\mathbf{u} \tag{2.7}$$

where $\Delta\mathbf{x}$, $\Delta\mathbf{y}$ and $\Delta\mathbf{u}$ represent deviations from operating point values.

2.2.1 Small-signal Stability: Eigen-analysis of Power System

Eigen properties play a significant role in analysing the system response from a small signal stability viewpoint, and this section aims to provide background information.

$$\Lambda = \Psi A \Phi \tag{2.8}$$

$$\Lambda = \begin{bmatrix} \lambda_1 & 0 & \cdots & 0 \\ 0 & \lambda_2 & & 0 \\ \vdots & & \ddots & \vdots \\ 0 & 0 & \cdots & \lambda_n \end{bmatrix} \tag{2.9}$$

$$\Psi = [\psi_1, \psi_2, \cdots \psi_n] \tag{2.10}$$

$$\Phi = [\phi_1, \phi_2, \cdots \phi_n]^T \tag{2.11}$$

where Λ is the diagonal matrix of eigenvalues, λ_n is the nth eigenvalue, Ψ is the left eigenvector matrix, and Φ is the right eigenvector matrix.

The A matrix obtained from (2.6), (2.7) can be transformed to the diagonal matrix eigenvalues Λ in (2.8), (2.9) with the set of left and right eigenvectors, (2.10), (2.11). The A matrix indicates the characteristics of system dynamics, which is reflected from the response of the conventional generators and by a linearised state space matrix from the multi-machine system in [31]. Λ matrix presents the diagonal component of eigenvalues from the A matrix to be readily understandable for the relationship between eigenvalues and inputs/outputs. The differences between those two matrices can be explained as A matrix consists of the generator and system parameters with non-diagonal arrangement, and Λ matrix consists of the eigenvalues of A matrix with diagonal arrangement.

The right eigenvector Φ indicates the activities of the state variables in the modes. The left eigenvector Ψ weighs the contribution to the modes.

$$\Delta x = \Phi z \tag{2.12}$$

$$B' = \Psi B, \qquad C' = C\Psi \tag{2.13}$$

$$\dot{z} = \Lambda z + B' \Delta u \tag{2.14}$$

$$\Delta y = C' z \tag{2.15}$$

$$z_i = \psi_1 \Delta x_1 + \psi_2 \Delta x_2 + \cdots \psi_n \Delta x_n \tag{2.16}$$

where Ψ is the left eigenvector matrix, B' is the controllability matrix, C' is the observability matrix, u is the input matrix, z is the modal variable matrix, x is the state variable matrix, z_i is the ith modal variable, x_i is the ith state variable, and y is the output matrix.

The state space matrix obtained in (2.6), (2.7) can be converted into the transformed state space matrix by derivation from (2.12), (2.13) to (2.14), (2.15); the transformed state space matrix facilitates the investigation of the relationships among input, output, and specific modes. As the transformed state z_i is associated with only the ith mode, the contribution of the activity from states x_i to the ith mode can be explained by left eigenvectors Ψ_i using (2.16).

$$\lambda_i = \sigma_i + j\omega_i \tag{2.17}$$

$$\zeta_i = -\sigma / \sqrt{\sigma_i^2 + \omega_i^2} \tag{2.18}$$

where λ_i, ζ_i, σ_i, and ω_i are the ith eigenvalue, damping ratio, time constant, and angular velocity of the ith mode, respectively.

From (2.17), (2.18), the ith eigenvalue and damping ratio can be analysed on the S-plane consisting of time constant and oscillatory angular speed components. In a large system, local area and interarea modes can be problematic from the small signal stability perspective. Local area oscillation implies that a single generator or generator group has low frequency oscillation with another generator or generator group. Interarea

oscillation is the oscillation between single generators or between groups of generators, as classified in [30]. Interarea oscillation frequency ranges between 0.1 and 1 Hz, while local area oscillation ranges between 1 and 2 Hz based on the definition in [31].

2.3 Frequency Control

2.3.1 Speed Droop Control

When sensors recognize a deviation in generator angular velocity, the governor initiates adjustments of the mechanical input torque to increase or decrease the angular velocity of generator as required. The droop characteristics assigned to governors enable numerous generators to operate in parallel in a power system without competing with one another when unanticipated changes to the system, generation, or load occur. Currently, North American Electric Reliability Corporation (NERC) requires all turbine generators equipped with governors over 75MW should be capable of providing immediate and sustained response to abnormal frequency excursions. Governors should provide less than 5% droop characteristic. [32] In this statement, a 5% droop rate means that the total capability of a generating unit would reacts to a 5% change in the frequency, which implies that larger-rated generators contribute higher power, and smaller generators contribute lower power, as depicted in Fig. 2.2.

A governor with speed-droop operation can be illustrated as Fig. 2.3 and considered as a form of proportional feedback of frequency deviation. When governor gives the signal, the angular velocity of turbine is adjusted and manages the power system frequency.

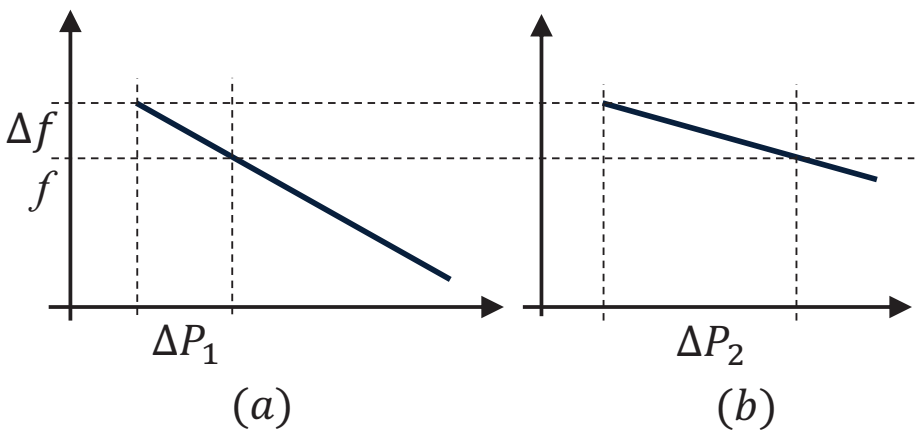

Figure 2.2: Concept of droop control for parallel operation: (a) Gen1: Smaller capacity, (b) Gen2: Larger capacity

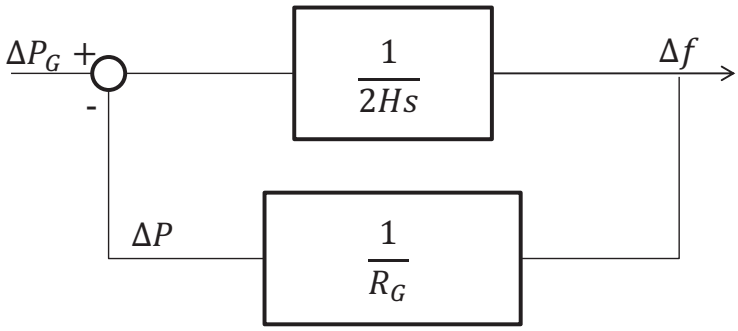

Figure 2.3: Block diagram of a governor speed-droop control

Equation (2.19) indicates the concept of droop control, and aggregated supportive power is described in accordance with (2.20), when frequency deviates. Through (2.21), the individual frequency contribution of a generating unit is (2.22). This calculation can also be applied on the ESS system in this dissertation.

$$R = \frac{\Delta f / f_n}{\Delta P_i / S_n} \tag{2.19}$$

$$\Delta P = \frac{-\Delta f}{f_n}[\frac{S_1}{R_1} + \cdots + \frac{S_k}{R_k}] \tag{2.20}$$

$$\frac{\Delta f}{f_n} = \frac{\Delta P}{[\frac{S_1}{R_1} + \cdots + \frac{S_k}{R_k}]} \tag{2.21}$$

$$\Delta P_i = \frac{S_i}{R_i} \frac{\Delta P}{[\frac{S_1}{R_1} + \cdots + \frac{S_k}{R_k}]} \tag{2.22}$$

where R: droop rate, Δf: frequency deviation, f_n, nominal frequency, ΔP: power deviation, and S_n: power rating

2.3.2 Automatic Generation Control

The primary objectives of AGC are first to eliminate the steady state error and regulates the frequency to the nominal value, and second to carry out previously scheduled interchanging power among interconnected networks [31]. The block diagram of an AGC in Fig. 2.4 depicts prime mover functioning such as a PI controller to equalize system frequency to the nominal value. The key operation of AGC for Independent System Operator (ISO) is to fulfil the pre-determined interchanging power for the day-ahead market to comply with Control Performance Standard (CPS) 1 and 2. Detailed information is in [33–35]

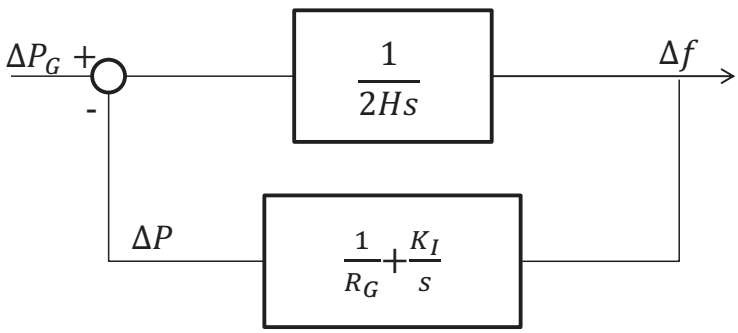

Figure 2.4: Block diagram of Automatic Generation Control

Chapter 3

Impact Analysis of Variable Generation on Small Signal Stability

Abstract–**This chapter aims to analyse the influence of fluctuating renewables on small-signal stability. Most of the research on renewable energy integration assumes that power is provided from a static generation unit and studies how much damping ratio and frequency of fluctuating power changes as a result of changing power and inertia constant. This research is motivated by 'mode coupling' where one oscillatory mode may have an effect on other modes if the mode frequencies are similar. The chapter discusses the impact of fluctuating power sources, Type IV wind turbines in our case, on possible coupling between the fluctuating wind power and the existing modes in the system. Since the fluctuating power may combine a large band of frequency components of fluctuating power, the power system can react to any specific frequency of a variable generator. In this chapter, several influential frequencies were injected through the renewable generator. System identification is used first to obtain the linearised state-space model of the system and the relevant transfer functions, which are then used to identify possible resonant frequencies. DIgSILENT/Power Factory is used next to analyse the system's response to specific frequencies in the time domain.**

3.1 Introduction

Penetration of intermittent renewable energy sources (RES) is steadily increasing following the renewable portfolio targets that have been put in place in many countries around the world to speed up the transition to more RES based power systems. The University of Melbourne Energy Research Institute's study [23] suggests that a 100% renewable scenario can be achieved as early as 2020, although the Australian Energy Market Operator (AEMO) considers the 2030 to 2050 time frame to be more realistic for Australia [24]. To tackle the integration of RES, the analysis of grid characteristics with RES is essential, and used for operation and planning in the long-term future. Without the fundamental work for implications of variable generation, future power system may have difficulty operating stably with high penetration of RES.

Much research effort has been put into studying the impact of RES, mostly solar and wind, on power system stability, focusing predominantly on small-signal [36–40] and transient [40, 41] angle stability. Such initiatives internationally notwithstanding, the influence of RES on power system stability and performance still requires a lot of attention. The common denominator of the existing research is the use of quasi-static analysis, implicitly assuming that variations in the RES' output are slow enough not to impact the system modes. This approach seems to be widely accepted. For example, a comprehensive CIGRE Technical Brochure [42] and a more recent AEMO study [43] don't even mention this assumption. We make an attempt to cover this gap by considering the output of a RES not to be static at the studied operating point but rather consisting of a fixed component and a superimposed fluctuating component of a frequency similar to the existing system's modes.

The problem of mode coupling hasn't attracted much attention in the power engineering community so far. The earliest references date back to 1980s [44]. The phenomenon has been observed in practice, e.g. in the WECC with implications for PSS tuning [45]. To the best of our knowledge, this is the first attempt to study the impact of RES on mode coupling. The goal of this chapter is thus to establish hypotheses about the influence on system stability from variable generators. Unlike the conventional thermal and hydro power plants whose output variation is very slow with no or negligible higher-frequency components, the output of intermittent RES consists of fluctuating components with frequencies that can potentially interact with the existing system

modes. This can change the behaviour of the system or even cause instability in a large scale network. The focal point of our discussion is on the influence of the fluctuating frequency component on the small disturbance stability. Sub-space system identification is first used to obtain a reduced-order linearised model of the system and the relevant transfer functions. Then time-domain simulation is used to analyse the behaviour of the system subject to penetration of fluctuating RES in the selected frequency bands.

The importance of this research can be summarized as following:

- $Influence\ of\ Fluctuating\ RES$: The research indicates which the frequency spectrum of fluctuating RES has an influence on the existing oscillatory modes.
- $Mode\ Coupling\ by\ the\ RES$: Providing simultaneous compensation with conventional generators and other ESSs in network.

The rest of chapter is organized as follows: an introduction discussing the concept of mode coupling and power system oscillations is given in Section 3.2. In Section 3.3, system identification used in the chapter is briefly discussed. In Section 3.4, the results of the case study on test system are given, and Section 3.5 concludes the chapter.

3.2 Background

The main focus of this study is small-signal stability, which is defined as the ability of the power network to keep synchronism under small disturbances, typically changes in either load or generation [30]. The changes are considered to be small enough so the system can be linearised around the operating point. The remainder of this section discusses small-signal stability and mode coupling, which lays the groundwork for the case studies considered later in the chapter.

3.2.1 Small-signal Stability and Mode Coupling

The behaviour of a power system can be described by a set of differential and algebraic equations of the form as (2.1)-(2.7) in chapter 2

The linearised system (2.6), (2.7) can be used to investigate the system's response to small variations in the input or state variables. A possible instability can be due to lack of synchronizing torque, resulting in an increase in rotor angle through a non-oscillatory

or aperiodic mode; or due to lack of sufficient damping torque, resulting in oscillations of increasing amplitude. The oscillations can be either local or global, depending on the machines involved. Global or *inter-area mode oscillations*, involve one group of generators in one part of the system swinging against a group of generators in another part of the system. *Local mode oscillations*, on the other hand, are restricted to a small part of the system and often refer to one generator's motion with respect to the rest of the system.

Mode coupling is a situation where an oscillation mode in one part of the system interacts with a mode of oscillation in a remote part [44]. Mode coupling in Fig. 3.1

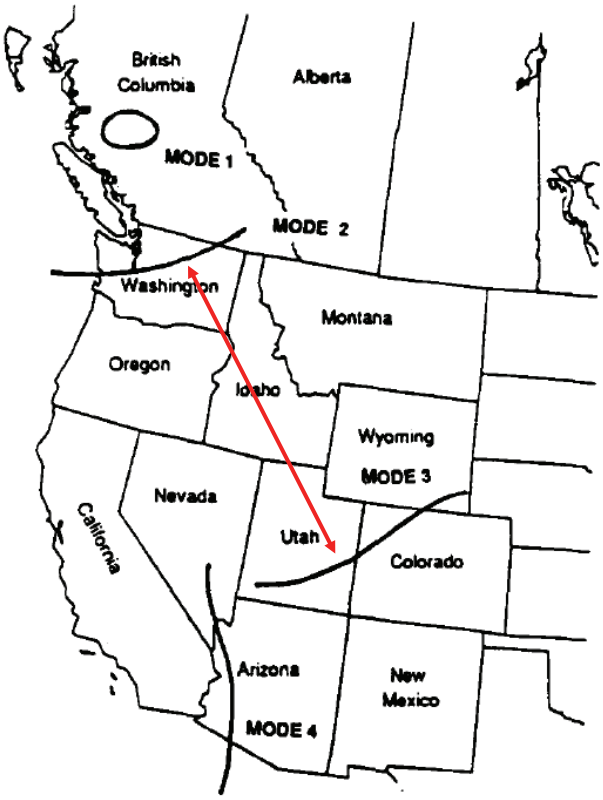

Figure 3.1: The concept of Mode Coupling.
[45]

had been observed in the WECC when studying the placement of PSSs [45]. It was found that a generator in one part of the system had a relatively high participating factor in an oscillatory mode associated with a group of generators located in a remote part of the system. In this particular example, the coupling was triggered due to the mode frequencies being very close. Another possible trigger can be disturbances entering the system at frequencies close to the system modes, i.e. fluctuating RES, which, to the best of authors' knowledge, hasn't been studied yet.

3.2.2 Mode Coupling Triggered by Fluctuating RES

Unlike the conventional energy sources, some RES can exhibit fluctuating behaviour due to the variability of the primary energy source. While geothermal, tidal and solar thermal cannot change the output quickly due to the large inherent inertia, solar PV, wave and wind can. Solar PV doesn't possess any energy buffer so the output can fluctuate due to varying cloud coverage. The resulting fluctuations however will likely be aperiodic. Wave and wind generation, on the other hand, can generate periodic power fluctuations. Unlike wind, wave generation is still in its infancy, so little operational data is available in the literature. In this chapter, therefore wind power is considered as a trigger of possible mode coupling.

The fluctuation in the wind can be thought of as resulting from a composite of sinusoidally varying winds superimposed on the mean steady wind [46]. If the frequency of a sufficient strong wind component matches the frequency of one the system's poorly damped oscillatory modes, the mode gets excited by the fluctuating RES, which results in resonance. This phenomenon is called mode coupling and is not restricted by the electrical distance between the source and the machine participating in the affected mode. In other words, mode coupling can affect both local and inter-area modes.

3.2.3 Wind Power Spectrum

The variability of wind spans multiple time scales. Medium- and long-term fluctuations can be modelled with Van der Hoven's spectral model, while for short-term fluctuations, capturing the turbulent behaviour, either von Karman's or Kaimal spectral models are typically used [47]. Van der Hoven's spectrum is modelled as a stationary random process, whereas the turbulence spectrums, either von Karman's or Kaimal's, are non-

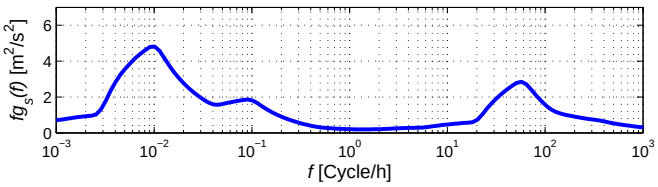

Figure 3.2: Van Der Hoven's wind power spectrum.

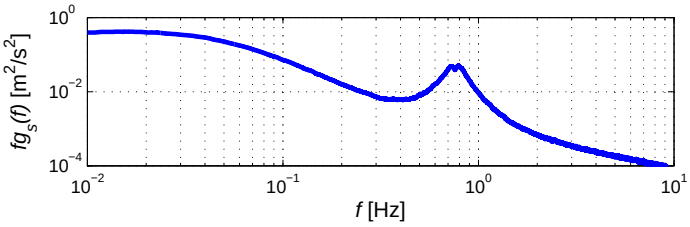

Figure 3.3: Kaimal's wind power spectrum.

stationary. Van der Hoven's spectrum spans the range between 0.001 cycles/h (inter-seasonal variations) and 1000 cycles/h (intra-minute variations). The turbulent short-term power spectrum spans the frequencies between 0.01 and 4 Hz, which covers the typical frequency range of the local and inter-area oscillatory modes (between 0.25 and 2 Hz). The turbulent wind fluctuations should therefore be considered in the analysis of mode coupling due to fluctuation RES. For illustration, a sample Van Der Hoven's and Kaimal wind power spectra are shown in Figs. 3.2 and 3.3, respectively.

Observe in Fig. 3.3 the effect of the rotational sampling of the wind turbine blades caused by the tower shadow. For the most common 3-blade turbine, the sharp spike occurs at the triple of the turbine's rotational speed. The exact frequency thus depends on the rotational speed of the turbine, determined by the design and the control method used. This deserves further attention, as the frequency of the spike could be close to the frequency of an oscillatory mode. This particular issue is however beyond the scope of the chapter.

3.3 Identifying the State Space Model of the System

Power systems are time varying and highly non-linear so it is almost impossible to identify the non-linear models. Instead, linearisation could be used to analyse the impact of a small deviation in system's inputs. DIgSILENT/PowerFactory doesn't allow the user to obtain the linearised state-space model of the system. Instead, the N4SID subspace system identification technique was used which is available in Matlab's System Identification Toolbox [48]. The state-space model has been used to obtain the transfer functions of interest for a particular operating condition, as described later.

One of the most important aspects of system identification is the selection of the probing signal [49]. Firstly, the frequency spectrum needs to cover the frequency band of interest, and, secondly, the amplitude of the signal must be sufficiently high to excite the critical oscillatory modes without pushing the system into a nonlinear zone [50]. The following probing signals are tested: Random Gaussian Signal, Random Binary Signal, Pseudo Random Binary Signal (PRBS), and Sum of Sinusoid Signal. PRBS was chosen due to its superior performance over the widest frequency range.

Intuitively, perturbation of the system with a fluctuating RES is similar to system identification. In response to the perturbation signal with a wide frequency spectrum, most of the frequency band is filtered out except for the oscillatory frequency, where the system resonates with the perturbation signal.

3.3.1 Numerical Subspace State Space System Identification

In our study, system identification was used to identify the transfer functions between the wind turbine, modelled as a controlled current using the in-built converter model, as the input and the angular speeds of the four generators as the outputs to study the resonant behaviour, i.e. the mode coupling between the fluctuating RES and the existing oscillatory modes. The resulting system identification problem is thus Single Input Multiple Output (SIMO). The model with m inputs, p outputs and n states was estimated in discrete domain and the converted into continuous domain resulting in

$$\dot{\mathbf{x}}(t) = \mathbf{A}\mathbf{x}(t) + \mathbf{B}\mathbf{u}(t) + \mathbf{K}\mathbf{e}(t) \tag{3.1}$$

$$\mathbf{y}(t) = \mathbf{C}\mathbf{x}(t) + \mathbf{D}\mathbf{u}(t) + \mathbf{e}(t) \tag{3.2}$$

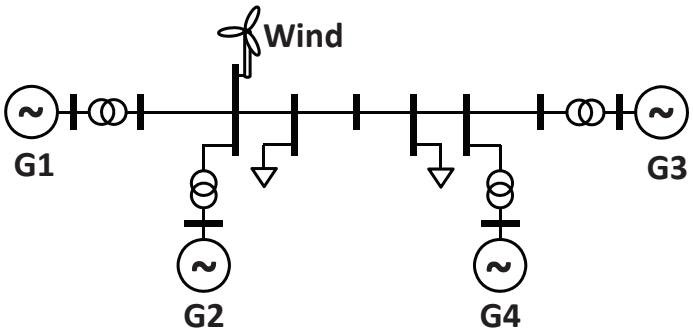

Figure 3.4: Two Area Test System
[31]

where $\mathbf{x} \in \mathbb{R}^n$ is the state vector; $\mathbf{u} \in \mathbb{R}^m$ is the input vector; $\mathbf{y} \in \mathbb{R}^p$ denotes the output vector; and $\mathbf{A} \in \mathbb{R}^{n\times n}$, $\mathbf{B} \in \mathbb{R}^{n\times m}$, $\mathbf{C} \in \mathbb{R}^{p\times n}$ and $\mathbf{D} \in \mathbb{R}^{p\times m}$ are the system matrices. $\mathbf{K}\mathbf{e}(t) \in \mathbb{R}^n$ and $\mathbf{e}(t) \in \mathbb{R}^p$ are, respectively, the disturbances and the noise acting on the system. In our case $m = 1$, $p = 4$ and $n = 13$. The dynamic order of the original system is 49.

3.4 Test System

3.4.1 Test Bed: Two-area System

The four-machine, two-area test system proposed in [31] was used as the test bed. The system consists of four generators located in two areas; G1 and G2 in the east, and G3 and G4 in the west. A wind power plant, modelled as a single 120MW Type IV (synchronous machine with a fully rated converter) wind turbine has been connected to the high voltage bus near G2, and the magnitude of power is assumed as 0.1 pu of the wind turbine. The system is shown in Fig. 3.4. As a result, the power of the slack bus (G1) has been reduced to keep the system in balance.

Three oscillatory modes exist in this system: one interarea mode with the generators in the east oscillating against the generators in the west; and two local modes, one between G1 and G2 and the other between G3 and G4. The case of a thyristor exciter with high transient gain and PSS is considered as can be seen in Fig. 3.5 [31]. To get mode coupling in the system, the renewable generator (sender) needs to have a component

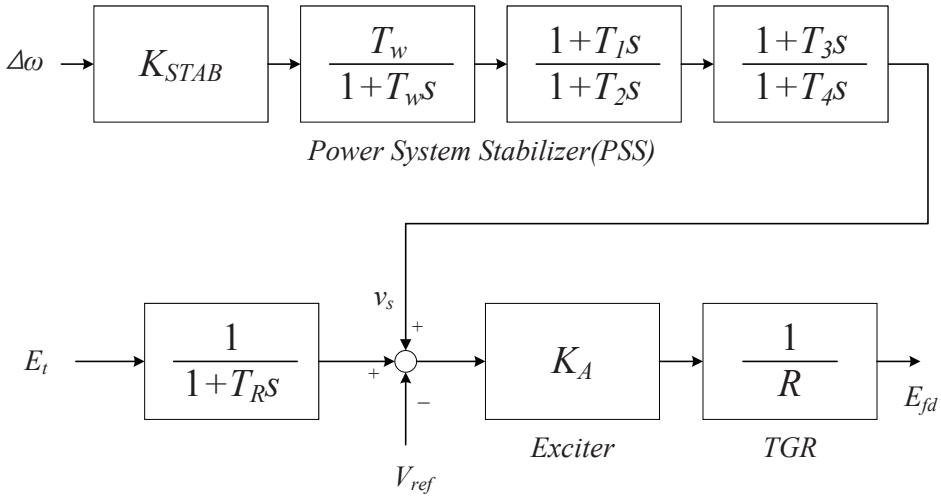

Figure 3.5: High Gain Thyristor Controlled Excitation system with Power System Stabilizer (PSS)

[31]

with a frequency similar to one of the existing oscillatory modes. To this end, some PSS parameters were modified to create two cases with a different oscillatory behaviour—see Table 3.1.

Other parameters were left unchanged, resulting in three study cases: (1) the original case, (2) a case where a local mode (G3, G4) with reduced damping resonates with the wind turbine; and (3) a case with an unstable local mode (G3, G4). In all three cases, the sub-space linearised models of the system were used to obtain the transfer functions between the wind turbine as the input and the angular speeds of all four generators as the outputs. This enabled us to identify possible resonance in the system subject to fluctuations in the wind power. Next, a sinusoidal signal at three different frequencies was injected, representing fluctuating wind power spectral components, and simulated the response of the system in time domain.

3.4.2 Case 1: Standard System

The standard system corresponds to the case with the thyristor exciter with high transient gain and PSS in [31]. Fig. 3.6 shows the oscillatory modes in the complex plane.

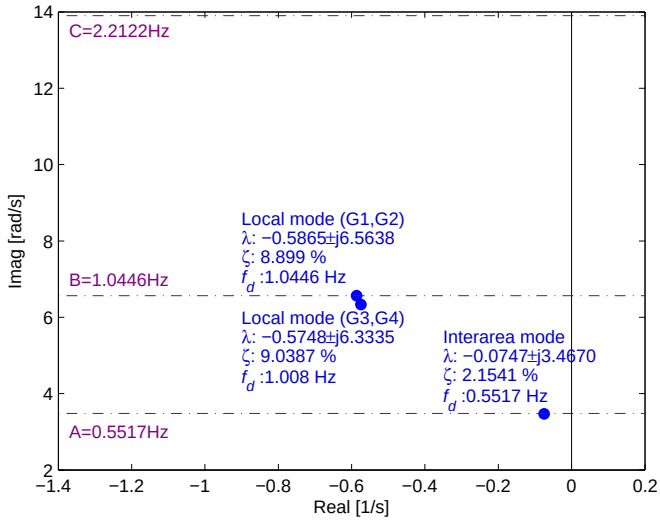

Figure 3.6: Case 1: Oscillatory modes and the frequencies of the injected signals.

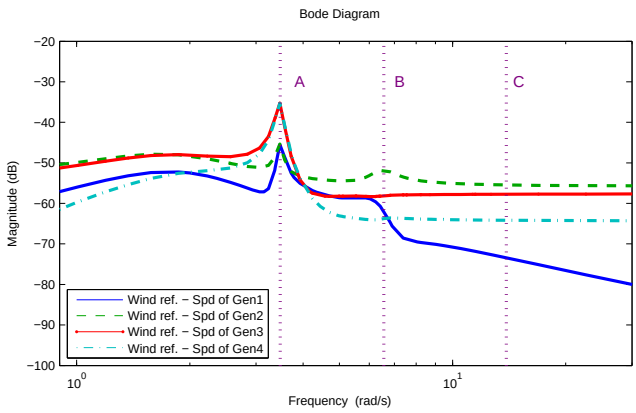

Figure 3.7: Case 1: Oscillatory modes and the frequencies of the injected signals.

Table 3.1: Modified Exciter and PSS Parameters.

	G1			**G1**		
Case	**1**	**2**	**3**	**1**	**2**	**3**
K_{stab}	20	200	200	20	20	20
T_2	0.02	0.02	0.02	0.02	0.02	0.02
T_3	3	30	30	3	30	30
	G3			**G4**		
Case	**1**	**2**	**3**	**1**	**2**	**3**
K_{stab}	20	185	200	20	20	5
T_2	0.02	0.17	0.17	0.02	0.02	0.02
T_3	3	3	3	3	3	5

Observe that the local modes (G1,G2) and (G3,G4) have very similar frequencies.

Fig. 3.7 shows the Bode plots of the transfer functions between the wind power and the machine angular speeds of the four generators.

Three signals with different frequency are injected: (A) interarea mode frequency (0.5517Hz); (B) local mode frequency (1.0446Hz); and (C) a signal with a frequency significantly different from mode frequencies (2.2122Hz). The spike in the bode plot around frequency A indicates that the injected sinusoidal signal might interact with the interarea mode while any interaction for frequencies B and C were not expected. This is confirmed by time-domain simulations, Fig. 3.8. Observe in Fig. 3.8 the amplified response of the four generators subject to a sinusoidal wind power injection with frequency A. As expected, frequencies B and C have negligible impact.

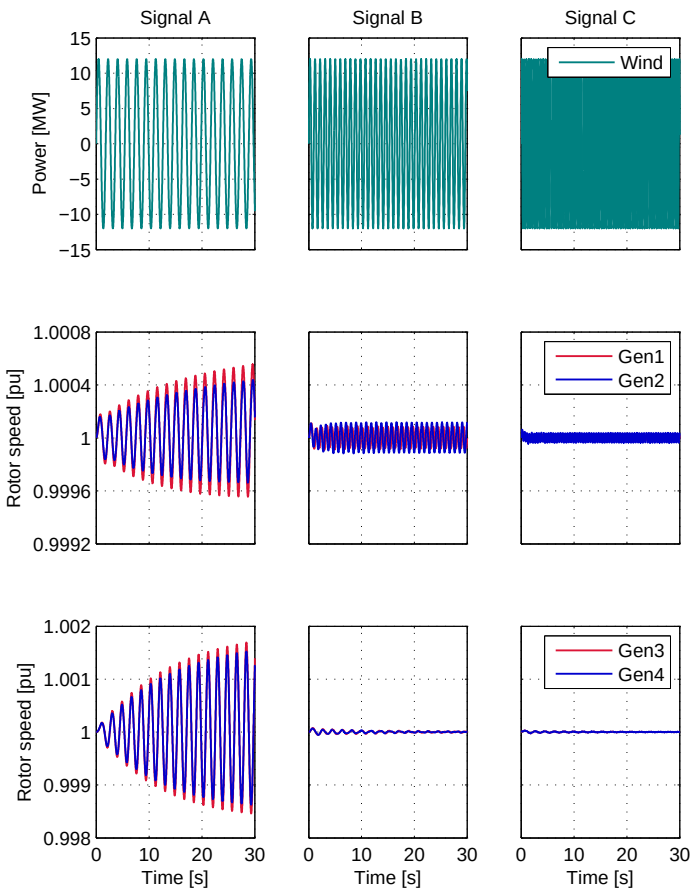

Figure 3.8: Case 1: Time-domain simulation results.

3.4.3 Case 2: Resonant Local Mode

In this case, the parameters of the excitation system were modified to reduce damping of the local mode (G3,G4). Fig. 3.9 and Fig. 3.10 show the oscillatory modes in the complex plane and the Bode plots, respectively.

Unlike in Case 1, the wind turbine input is expected to resonate with the three modes for frequencies A and C. In addition, because the frequencies A and C are similar, frequency B is expected to lie between A and C, to cause resonance. Fig. 3.11 shows the simulation results for the three cases. Three frequencies are injected with the value of (A) 0.6905Hz, (B) 0.8797Hz, and (C) 1.1107Hz, respectively.

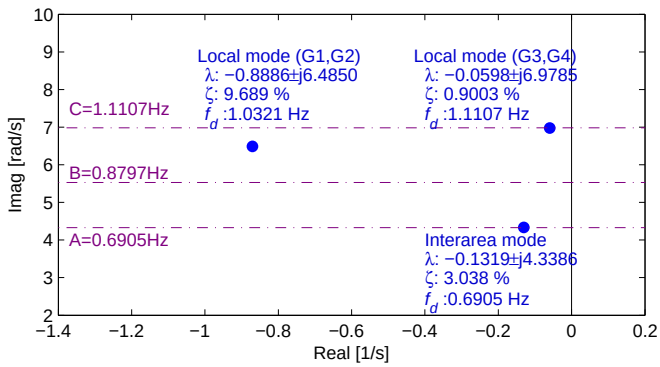

Figure 3.9: Case 2: Oscillatory modes and the frequencies of the injected signals.

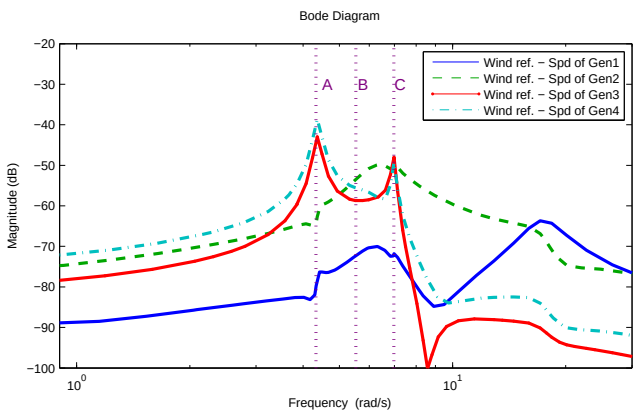

Figure 3.10: Case 2: Bode plots.

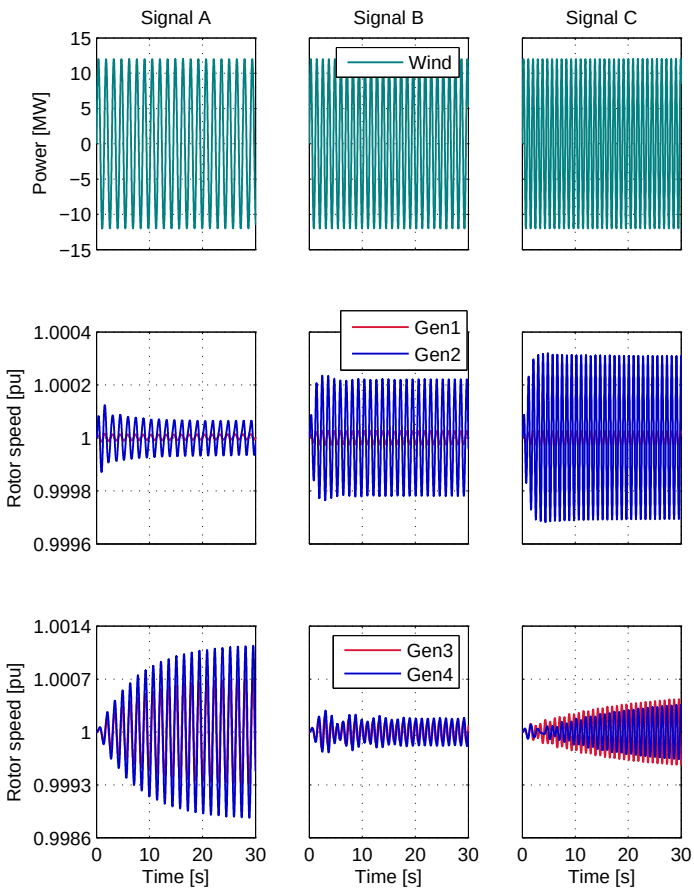

Figure 3.11: Case 2: Time-domain simulation results.

As expected, all three signals cause resonance, with frequency A having the largest impact. As can be seen in Fig. 10 that Signal B, whose frequency lies between the frequencies of the interarea mode and the local mode (G3 and G4), causes slight oscillation of the angular speed of the generators but not significant amplification. The response of G3 and G4 indicates that the injection of a sinusoidal disturbance in one part of the system causes resonance in a distant part of the system, which confirms our assumption and also agrees with what has been observed in the WECC system [45].

3.4.4 Case 3: Unstable Local Mode

In the last case, the local mode (G3,G4) was destabilised to study the impact of fluctuating RES on a poorly damped system. Fig. 3.12 and Fig. 3.13 show the oscillatory modes in the complex plane and the Bode plots, respectively. In this case, only one frequency has been chosen (1.109Hz), matching the frequency of the poorly damped mode (G3,G4).

Figs. 3.14 and 3.15 show the results of time-domain simulation. Observe that, unlike in the previous two cases, the injected signal is now damped. In the first 10 seconds after the disturbance the system seems to have stabilized. However, a longer time-frame of

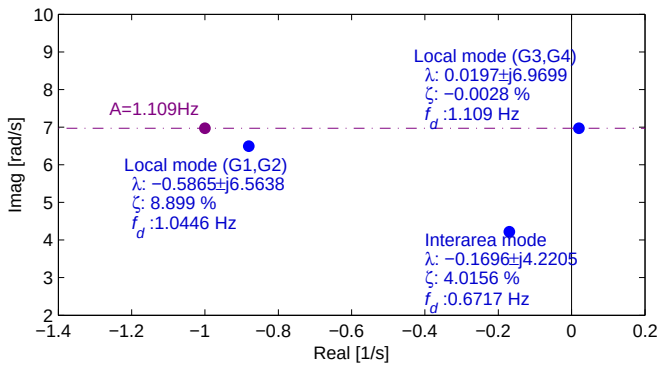

Figure 3.12: Case 3: Oscillatory modes and the frequency of the injected signal.

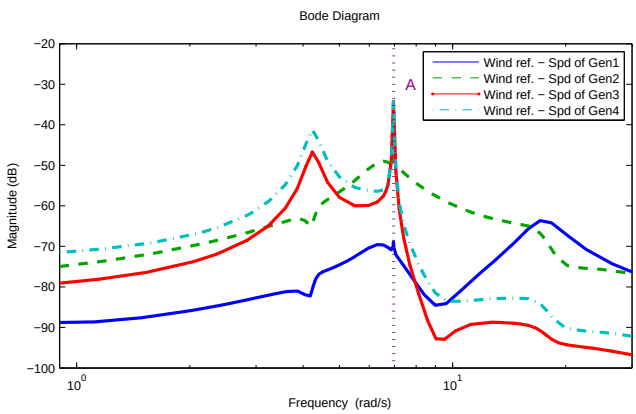

Figure 3.13: Case 3: Bode plots.

200 seconds shows that the oscillations grow in amplitude, which indicates unstable behaviour. This indicates that even a small perturbation at a particular frequency can excite a poorly damped oscillatory mode.

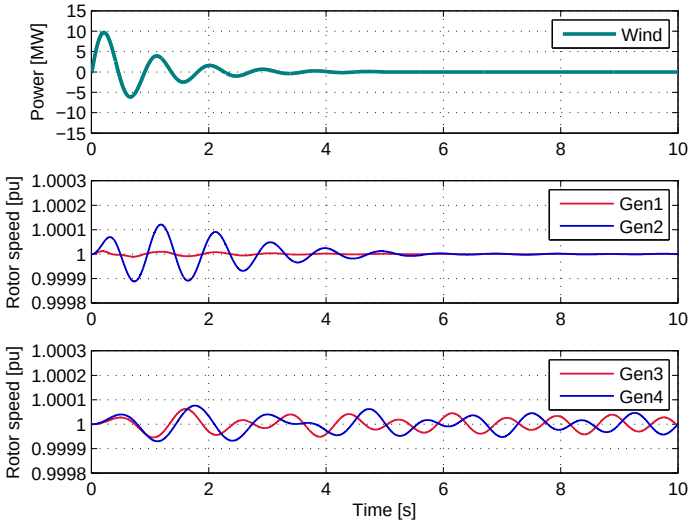

Figure 3.14: Case 3: Time-domain simulation results; short-term evolution.

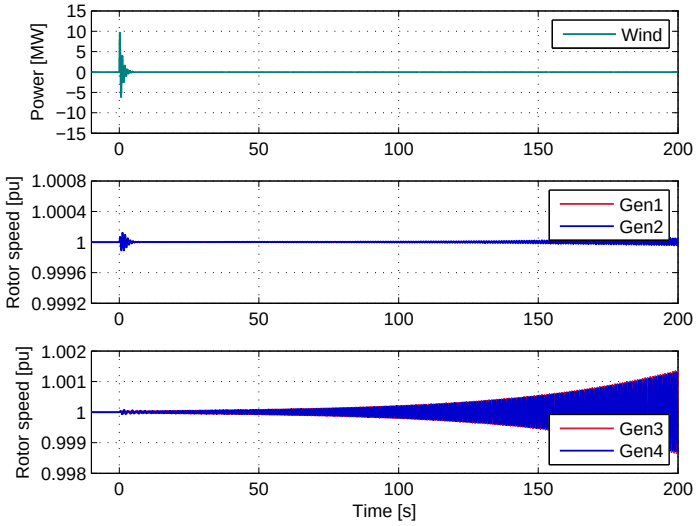

Figure 3.15: Case 3: Time-domain simulation results; long-term evolution.

3.5 Summary

The existing research has so far taken a "quasi-static" approach in stability analysis of future grid scenarios, by assuming that power is provided from static generation units. The focus has thus been limited to how much damping ratio and frequency changes as a result of changing RES penetration. However, it appears that dynamic effects of fast variations in the output of RES should be considered as well.

This chapter has made an attempt to cover this gap by studying the impact of fluctuating wind power on oscillatory stability of a power system. Wind power can have spectral components similar in frequency to oscillatory power system modes. The motivation for the research was thus to analyse possible modal interaction, which can lead to resonance that can negatively affect power system stability. The study cases analysed in the chapter confirmed our expectations. The result was found that fluctuating wind power can indeed amplify power system oscillations, even when the machines participating in the affected modes were located electrically far away from the wind turbine. Due to the increasing penetration of wind power worldwide, the problem of possible modal interaction between RES and the existing power system oscillatory modes certainly deserves

more attention.

Chapter 4

Impact of Large Scale Penetration of Concentrated Solar Thermal Power on Oscillatory Stability of the Australian Future Grid

Abstract–**This chapter analyses the impact of large scale penetration of concentrated solar thermal power (CSP) in the Australian future grid on small signal stability. Our research is motivated by the ten year roadmap for a 100% renewable energy system in Australia proposed by the Melbourne Energy Institute. In this plan, the supply side is dominated by CSP and wind power. Due to the location of the CSP plants, the plan envisages using high-voltage direct current (HVDC) transmission, which will negatively affect the system's inertia. Following the proposed HVDC network augmentation and starting from the current operating state, the penetration of CSP is progressively and deterministically increased in North Queensland. The conventional coal-fired generation is simultaneously reduced to keep the system in balance. The HVDC link effectively decouples the mechanical CSP system from the electrical system, which changes the oscillatory behaviour of the network. The focusing part is specifically on the inter-area oscillatory modes by analysing the root-loci of the corresponding eigenvalues in the complex plane. The analysis using a simple two-area power system shows that the addition of RES**

connected through HVDC links improves damping in the system under typical operating scenarios. A set of more realistic scenarios is then considered by studying a simplified model of the Australian National Electricity Market (NEM). With a larger number of oscillatory modes in the system, the behaviour becomes more complex, which makes general conclusions difficult. The analysis is done in DIgSILENT PowerFactory.

4.1 Introduction

Increasing energy consumption, growing concerns about the negative environmental impacts associated with the use of fossil fuels based energy sources, in particular global warming impacts and dwindling availability, are the main drivers for increasing penetration of renewable energy sources (RES). In many countries around the world, renewable portfolio standards have been put in place to speed up the transition. Although they vary in ambition, they all assume that electric power systems can be based predominantly on RES in the near future. Australia's renewables portfolio target, for example, aims at increasing the penetration of RES to 20% and 50% by 2020 and 2050, respectively [51]. At an international level, proposals like DESERTEC [52] and the Transnational Asian Grid proposal [53] envisage building super grids linking RES and load centres across large distances using high-voltage direct current (HVDC) transmission. Like in the Zero Carbon Australia Stationary Energy Plan [23], concentrated solar thermal power (CSP) plays a major role in both those proposal. Furthermore, many studies [23, 24, 54, 55] suggest that a 100% renewable scenario can be achieved as early as 2020 [5], although 2030 to 2050 time frame is considered more realistic.

The main drawback of those studies is that they only focus on balancing and typically neglect network implications by assuming a copper plate network model. The only exception to this rule is a German study [56] where voltage and frequency stability are also considered. Against this backdrop, our research complements the ten year roadmap for a 100% renewable energy system proposed by the Melbourne Energy Institute [23], shown in Fig. 1.2. The plan envisages an energy system powered by CSP with molten salt storage (supplying 60% of electricity demand) and wind power (40%), with biomass and hydroelectricity as backup options. The plan proposes the use of long-distance HVDC transmission to connect the load centres with the CSP plants lo-

cated in remote desert locations. In this chapter, the stability implications of the HVDC connected RES of the Australian future grid is investigated. The grid of the National Electricity Market (the interconnection spanning the eastern seaboard of Australia) has namely a stringy structure and is thus prone to oscillatory stability. In case of heavy power transfers between Queensland and New South Wales, and Victoria and South Australia, the respective oscillatory stability interconnection limits can drop below the underlying thermal capability of these interconnectors.

The distinctive characteristics of RES (excluding hydro) are raising concerns for reliable and secure operation of power systems with significant RES penetration. Many RES namely use power electronic converters for grid connection, which results in reduced system inertia constant. CSP is an exception to this rule as it uses the conventional steam cycle to convert the thermal energy into electrical, which renders its short-term dynamics very similar to conventional coal-fired power stations. In many cases, though, long-distance HVDC transmission is needed due to the remoteness of CSP plants, which effectively decouples the CSP's mechanical system form the electrical in much the same way as in Type IV wind turbines. Against this backdrop, much research effort has been put into studying the impact of RES, mostly solar and wind, on power system stability, focusing predominantly on small-signal [36–40,57] and transient [40,41] angle stability. Notwithstanding, the influence of RES on power system stability and performance still requires a lot of attention. The goal of this chapter is to develop a model of HVDC connected CSP and analyse its impact on inter-area oscillations of a large-interconnected system.

The rest of chapter is organized as follows: In Section 4.2, the design and control of CSP discussed. In Section 4.3, the results of the case study on test system are given. Section 4.4 concludes the chapter.

4.2 Modelling and Control of HVDC Connected CSP

The interest in CSP has been growing steadily in the recent years, with Spain and the US leading the way [59] in the installed capacity. Unlike solar photovoltaic (PV), CSP converts the energy of sun into thermal energy first and then into electrical energy, using a conventional steam cycle. The main advantage of CSP over PV is the ability of storing thermal energy in molten salt storage tanks with very high efficiency, which significantly

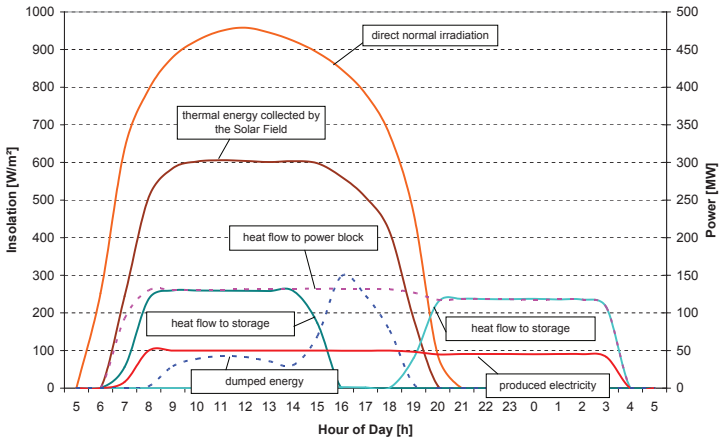

Figure 4.1: Summer energy flows in a CSP plant with thermal storage [58].

increases the capacity factor. With sufficiently enough storage capacity, CSP becomes fully dispatchable, at least for part of the day. Fig. 4.1 shows typical power flows in summer for a CSP plant with thermal storage [60]. Note the constant CSP output from 8am to 3am.

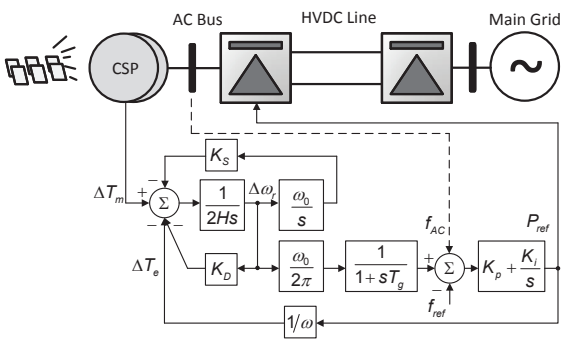

Figure 4.2: Control of a HVDC connected CSP.

4.2.1 HVDC control

In the existing applications, CSP plants are connected directly to AC grids, so the same frequency and voltage control can be used as for the conventional fossil-fuelled power plants. In this chapter, it is assumed that CSP is connected to the main grid through an HVDC link. In principle, two options are possible: (i) current source converter (CSC) HVDC, or (ii) voltage source converter (VSC) HVDC. CSC-HVDC requires a strong AC grid at the connection point, which might not be available for remote CSP applications. It also requires significant reactive-power compensation. Again this backdrop and in line with the Zero Carbon Australia plan [23], VSC-HVDC is selected.

It is assumed that the generator-side converter is controlled to maintain the voltage and the frequency. Controlling the voltage phase angle effectively controls the active power between the CSP plant and the HVDC system. The grid-side converter is controlled to maintain constant DC link voltage, which ensures the transfer of power from the CSP to the grid. Steady-state operation is only considered in our model. In case of a fault, additional control is needed to ensure stable operation. As only electro-mechanical transients were of interest, a fundamental frequency HVDC model is used.

Fig. 4.2 shows the basic HVDC control structure. K_S and K_D are the synchronising and the damping torque coefficients of the synchronous generator, respectively; H is the generator's inertia constant; ω_0 is the nominal frequency; T_g is the generator's time constant (denoting the time delay between the mechanical and the electrical frequencies); and K_p and K_i are the proportional and the integral gains of the PI controller, respectively. The control principle is as follows: the frequency f_{AC} at the AC bus is measured and compared with the reference frequency f_{ref}. [1] When the mechanical torque is change on the turbine, the generator's speed will change accordingly and the frequency deviation added to the $f_{AC} - f_{ref}$. A simple PI controller is then used to generate the power set-point (through AC voltage phase angle) on the generator-side converter to balance the turbine power, which eventually brings the frequency back to its nominal value.

Fig. 4.3 shows time-domain simulation results for a 50% increase in the turbine's output. The response of the generator-side converter is very fast, which results in a negligible frequency deviation.

[1] Note that f_{ref} doesn't need to be the same as the grid frequency but it needs to be controlled tightly because of the steam turbines being prone to vibrations if the frequency deviation exceeds 0.5Hz.

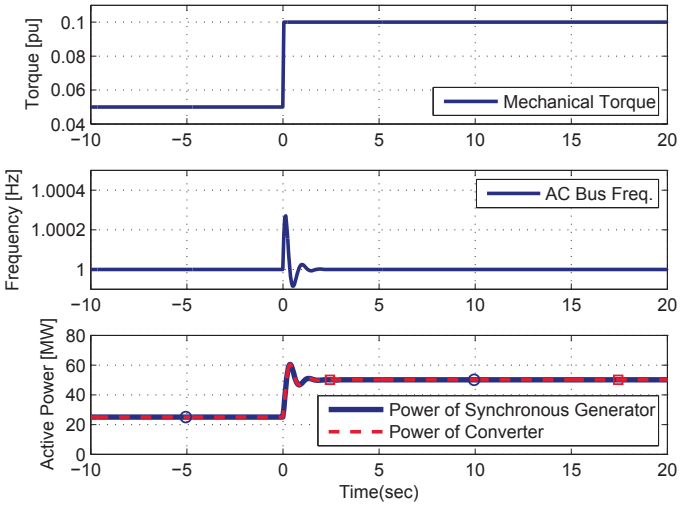

Figure 4.3: HVDC control simulation results.

4.2.2 CSP control

A CSP plant uses a conventional steam-cycle to generate power so in this sense it is very similar to a conventional fossil-fuelled power plant. They differ in the way they generate steam: a conventional fossil-fuelled power plant uses a boiler, while a CSP uses solar collectors. The boiler dynamics is however typically neglected in stability studies, so generic turbine models can be used to model CSP. Implicit in this approach is the assumption of constant steam pressure at the turbine's input (boiler output). For a CSP, this assumption is only valid if thermal storage is available. If this is not the case, the dynamics associated with the steam generation needs to be included as well. In this chapter it is assumed that a CSP plant is with thermal storage so a generic IEEE turbine model is used [31].

Given that the frequency is controlled by the generator-side converter of the HVDC system, no frequency control is in principle needed on the synchronous generator. Using a conventional droop controller does nevertheless seem to be a good idea to cater for emergency situations when the HVDC might not be effective in controlling the frequency. [2] In such situations, a droop controller can help in stabilising the system by

[2] An isochronous frequency governor should not be used because of the HVDC's generator-side con-

adjusting the output of the CSP plant.

4.3 Simulation Results

To study the impact of CSP on small-signal stability, three systems are studied: (i) a single-machine infinite-bus (SMIB) system, (ii) a two-area system, and (iii) a 14-generator model of the Australian National Electricity Market (NEM). In all three cases, the impact of reduced inertia constant on electromechanical modes of oscillations is studied by increasing the penetration of CSP. For each test system several cases are considered depending on the number of operating conventional synchronous generators, which affected the system inertia constant.

4.3.1 Single-machine infinite-bus test system

The first test system is the ubiquitous SMIB test system. The single-line diagram is shown in Fig. 4.4. The conventional generation consists of three machines in parallel. Three cases are studied, depending on the number of machines operating in parallel, Table 4.1. In all three cases, the total generation amounts to 900MW. The system inertia constant varies from 3s in Case 1 to 9s in Case 3. As the CSP is connected through a HVDC link it doesn't contribute to system inertia. Fig. 4.5 shows the penetration of CSP

verter also controlling the frequency.

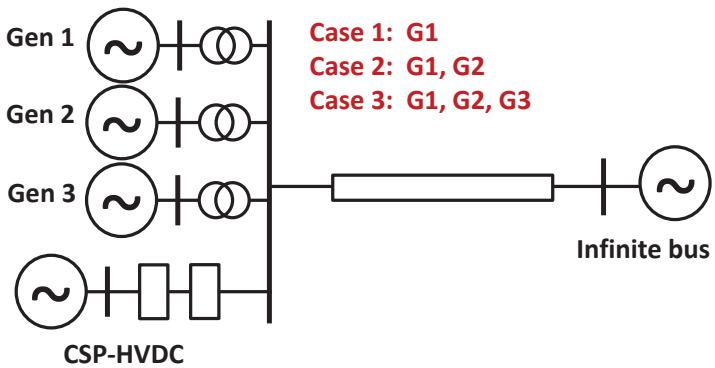

Figure 4.4: SMIB: System configuration.

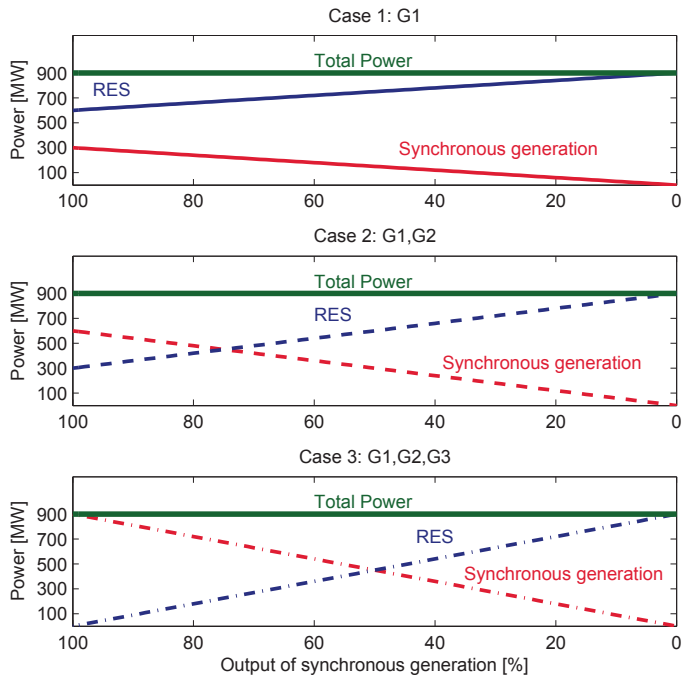

Figure 4.5: SMIB: Power sharing.

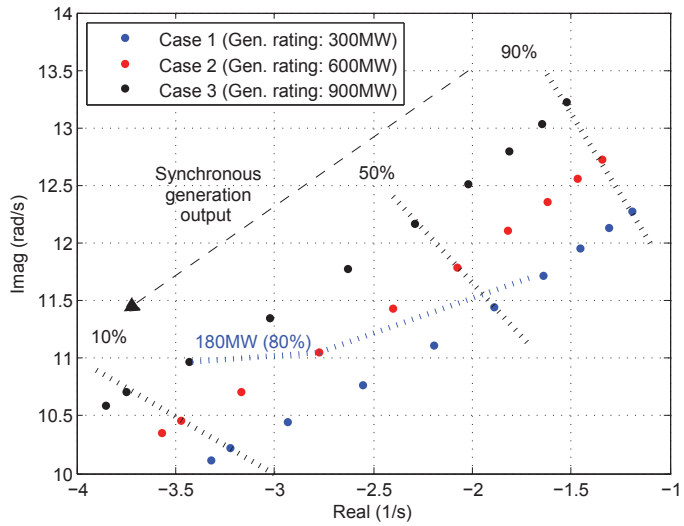

Figure 4.6: SMIB: Movement of the eigenvalues.

Table 4.1: SMIB: Operating conditions.

	Operating generators	**Total generator rating**	**Aggregated inertia const.** H[s]	**Initial power of RES**
Case 1	G1	300 MW	3	600 MW
Case 2	G1,G2	600 MW	6	300 MW
Case 3	G1,G2,G3	900 MW	9	0 MW

Table 4.2: SMIB: Eigenvalues at 80% CSP penetration.

	Eigenvalue	**Oscillation frequency**	**Damping ratio**
Case 1	$-1.6821 \pm j10.9710$	1.7461 Hz	15.16%
Case 2	$-2.7749 \pm j11.0515$	1.7589 Hz	24.35%
Case 3	$-3.4140 \pm j11.7188$	1.8651 Hz	27.97%

with respect to the synchronous generation. The aggregated inertia constant is calculated as follows [61]:

$$H_{total} = \sum_{i=1}^{n_{gen}} H_i n_i \frac{S_i}{S_{base}} \tag{4.1}$$

where n_{gen} is the number of generators; S_i is the rating of ith generator; H_i is the inertia constant of ith generator; and S_{base} is the system's base power.

Fig. 4.6 shows the movement of the eigenvalues for different CSP penetration levels. The system has only one local oscillatory mode. In all three cases, the increase in CSP penetration reduces damping of the electromechanical oscillatory mode. Comparing the three cases with the same absolute CSP penetration of 720MW shows that reducing system inertia constant reduces damping. The damping for the three cases at 80% RES penetration (180MW worth of synchronous generation) are shown in Table 4.2.

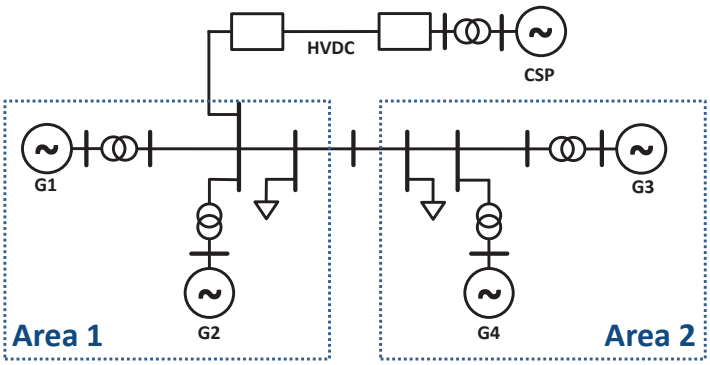

Figure 4.7: Two-area test system.

4.3.2 Two-area test system

The next test system is the four-machine, two-area test system proposed in [31], Fig. 4.7. The system consists of four generators located in two areas; G1 and G2 in the east, and G3 and G4 in the west. A 2GW CSP plant has been connected through a 200km VSC-HVDC link to the high voltage bus near G2. Three oscillatory modes exist in this system: one inter-area mode with the generators in the east oscillating against the generators in the west; and two local modes, one between G1 and G2 and the other between G3 and G4. The case of a thyristor exciter with high transient gain and PSS is considered .

The penetration of CSP is increased from 0MW to 1400MW, which eventually replaced all the synchronous generation in Area 1 with CSP, as shown in Fig. 4.8. Note two distinct cases: in Case 1 only the output of G2 is being reduced while the power of G1 remains constant; in Case 2, the output of G1 is being reduced from 700MW to 0, while G2 has been disconnected from the grid. The operating conditions are summarised in Table 4.3. Note a discrete change in system inertia constant when G2 is disconnected from the grid.

Table 4.4 shows the dominant left eigenvectors associated with the electromechanical oscillatory modes in the base case (no CSP penetration). The participation of the generators can be clearly observed in the inter-area and the local modes, respectively.

Fig. 4.9 shows the movement of the modes as the CSP penetration is increased from 0 to 100% in Area 1. Notice that increasing CSP penetration initially reduces damping of the Area 1 local mode and slightly improves the damping of the inter-area

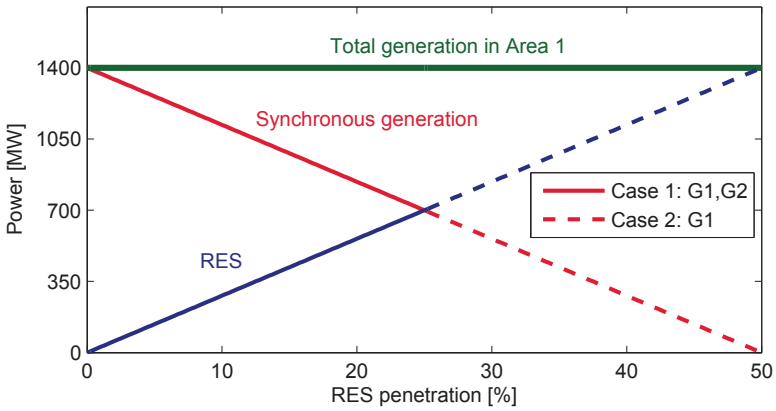

Figure 4.8: Two-area system: Power sharing.

Table 4.3: Two-area system: Operating conditions.

	Operating generators	**Total generator rating**	**Aggregated inertia const.** H[s]	**Initial power of RES**
Case 1	G1,G2	1800 MW	13	0 MW
Case 2	G1	900 MW	6.5	700 MW

Table 4.4: Two-area system: Dominant left eigenvectors.

	Interarea mode	**Area 1 local mode**	**Area 2 local mode**
G1 speed	$0.98\angle 179.4°$	$0.95\angle -179.2°$	non-dominant
G2 speed	$0.72\angle 175.6°$	$1\angle 0°$	non-dominant
G3 speed	$1\angle 0°$	non-dominant	$0.90\angle -179.8°$
G4 speed	$0.73\angle 3.7°$	non-dominant	$1\angle 0°$

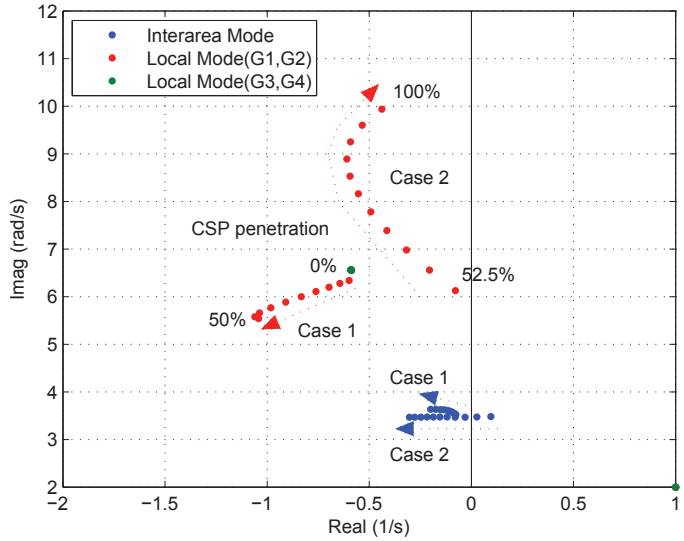

Figure 4.9: Two-area system: Movement of the eigenvalues.

mode. At 50% penetration, G2 gets disconnected from the grid, which moves both the Area 1 local mode and the inter-area mode sharply to the right, with the inter-area mode even becoming unstable. From there on (Case 2), further increase in the CSP penetration initially improves the damping of both modes, however at approximately 70% penetration, the damping of the Area 1 local mode start deteriorating again. The Area 2 local mode remains unaffected.

4.3.3 14-generator model of the NEM

The last test system is a modified 14-generator model of the NEM, which was originally proposed for small-signal stability studies [25]. The schematic diagram of the 14-generator model of the NEM is shown in Fig. 4.10. The system is long and stringy, unlike tightly meshed interconnections found in Europe and the USA. It consists of five states (areas): Snowy Hydro (Area 1), New South Wales (Area 2), Victoria (Area 3), Queensland (Area 4), and South Australia (Area 5). Tasmania is not model explicitly.

The heavy loading scenario (Case 1) from [25] is considered. The total load in the system is 22300MW and the total generation 23030MW. There are high inter-area flows from North to South: Area 4→2: 500MW, Area 2→1: 1134MW, Area 1→3: 1000MW,

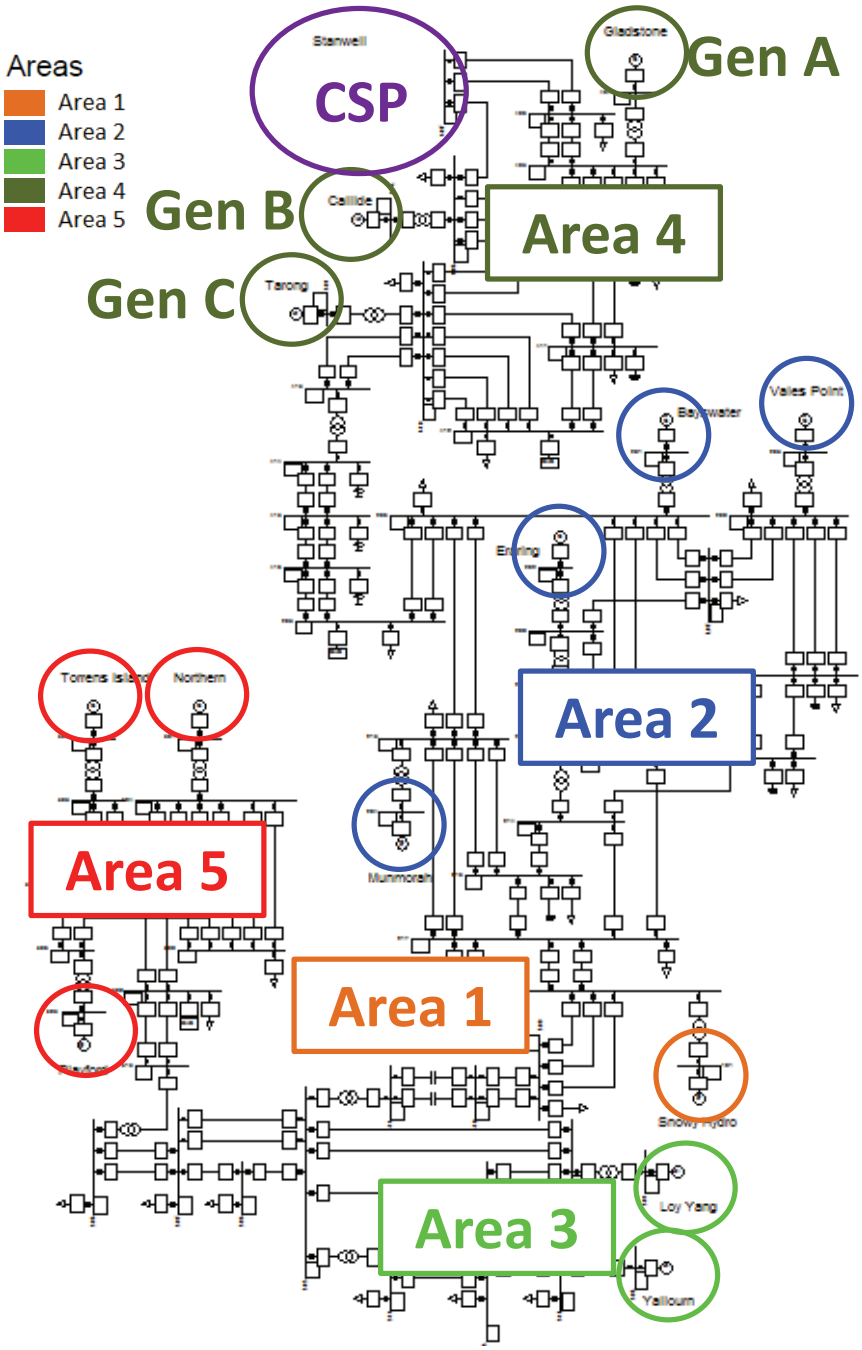

Figure 4.10: 14-generator model of the NEM.

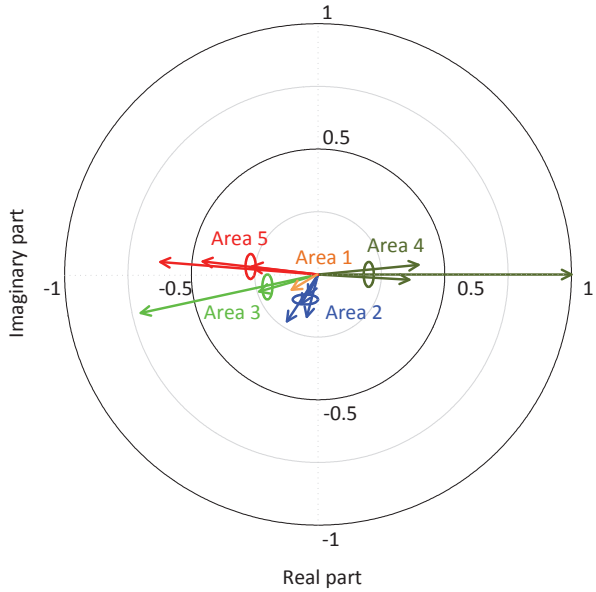

Figure 4.11: NEM: Dominant left eigenvectors and coherent generator groups for the inter-area mode between Area 4 and the rest of the system.

and Area 3→5: 500MW. The generators' excitation systems and power system stabilisers were adopted from [25]. Generic IEEE speed governors were used for conventional fossil-fuel generation.

The system exhibits several modes of oscillation: 3 inter-area modes between 4 main regions and 10 local modes. Without PSSs many of these modes are unstable [25]. Given the penetration of CSP in Area 4, the inter-area mode between Area 4 and the rest of the system is of particular interest. Fig. 4.11 shows the left eigenvectors associated with the generators' speed vectors for that inter-area mode. Five coherent groups of generators (plus Area 1) can be observed, one corresponding to each area. It is obvious from the vector angles that the generators in Areas 1, 2, 3 and 5 swing against the generators in Area 4.

The total generation capacity in Area 4 is 4777.3MW, split into four groups. The conventional generation in the northern part of Area 4 was replaced with CSP. The other three groups were named A, B and C. Like for the SMIB test system, three cases were considered , depending on the number of parallel generators in each group, as shown in

Table 4.5: NEM: Number of parallel generators in Area 4.

	Group A	**Group B**	**Group C**
Case 1	6	3	4
Case 2	5	2	3
Case 3	4	1	2

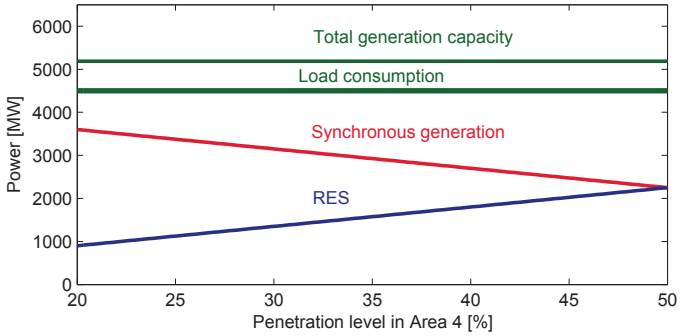

Figure 4.12: NEM: CSP penetration.

Table 4.5.

In all three cases, the total load remains the same. The CSP penetration were increased from 20% to 50%, as illustrated in Fig. 4.12. Depending on the number of generators in the three cases, the system inertia constant varies from 46.86s in Case 1 to 25.13s in Case 3, as shown in Table 4.6. With the increasing CSP penetration, the output of all the generators are reduced proportionally, like in the SMIB test system.

Fig. 4.13 shows the movement of the electromechanical modes' eigenvalues when

Table 4.6: NEM: System Condition in Area 4.

	Total gen. rating	**Aggregate inertia H[s]**
Case 1	4777.3 MW	46.86
Case 2	3666.3 MW	35.2
Case 3	2555.3 MW	25.13

Table 4.7: NEM: Eigenvalues and damping ratios at 40% CSP penetration.

	Eigenvalue	**Damping ratio**
Case 1	$-0.2886 \pm j1.4792$	19.15%
Case 2	$-0.2800 \pm j1.5032$	18.31%
Case 3	$-0.2238 \pm j1.5129$	14.63%

the CSP penetration increases from 20% to 50%. Other eigenvalues don't move significantly so for the sake of clarity they are not shown. Observe how the movement now becomes more unpredictable. Three distinct stages can be observed: Stage A from 20-24% penetration, Stage B from 26-38%, and Stage C between 40-50%. Between the stages, the positions of the eigenvalues experience discrete jumps. To better explain the behaviour of the system, the movement of the dominant left eigenvectors is also plotted, associated with the generators' speed vectors for the inter-area mode of interest. For the sake of clarity, the "weighted average" of the eigenvectors is used in each coherent group calculated as follows:

$$|\psi_{eq}| = \frac{\sum_{i=1}^{m} |\psi_i| n_i H_i S_i}{\sum_{i=1}^{m} H_i n_i S_i} \tag{4.2}$$

$$\theta_{eq} = \frac{\sum_{i=1}^{m} \theta_i n_i H_i S_i}{\sum_{i=1}^{m} H_i n_i S_i} \tag{4.3}$$

where $\psi_i = |\psi_i| e^{j\theta_i}$ denotes the ith eigenvector; m is the number of generator groups; n_i is the number of generators in i^{th}; S_i is the rating of a single generator in i^{th} group; and S_{base} is the system's base power.

Fig. 4.14 shows the movement of the dominant left eigenvectors associated with the inter-area mode for the three cases. Like in Fig. 4.13, the eigenvectors' trajectories are split into three stages, shown with solid lines. Dotted lines show the eigenvectors' discrete jumps. At 20% CSP penetration, Areas 3 and 5 participate the most in the inter-area mode between Area 4 and the rest of the system. As the CSP penetration starts to increase, the generators in Areas 3 and 5 behave in a similar fashion, i.e. the eigenvectors' magnitudes decrease, however they still swing in counter-phase with the

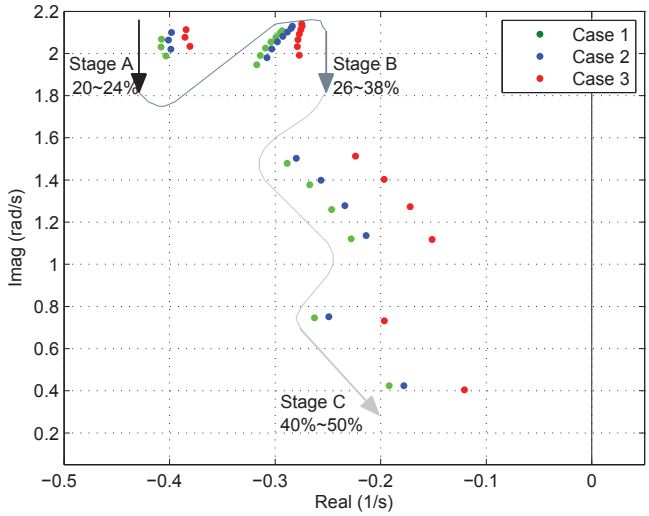

Figure 4.13: NEM: Eigenvalue movement with increasing CSP penetration.

generators in Area 4. The generators in Area 2, on the other hand, swing in counter-phase in Stage 1 (penetration between 20% and 24%), then they suddenly move to the right-hand side of the complex plane (hence Areas 2 and 4 become coherent) in Stage 2 (penetration between 26% and 38%), and finally they jump back to the left-hand side of the complex plane, meaning that they again swing against the generators in Area 4. Also, as the penetration increases from 40% to 50% in Stage 3, the Area 2 eigenvector's magnitude increases, not decreases as it was the case for Areas 3 and 5. Finally at 50% CSP penetration in Area 4, Area 2 participates the most in the inter-area mode between Area 4 and the rest of the system.

Through the CSP penetration, Case 3 exhibits the lowed damping among all three cases due to the lowest inertia constant, as illustrated in Table 4.7, which shows the eigenvalues of the inter-area mode and the damping ratios at 40% CSP penetration for the three cases.

4.4 Summary

Future power systems will rely on large penetration of RES, with CSP considered a very attractive proposition in countries with excellent solar resource, like Australia, The

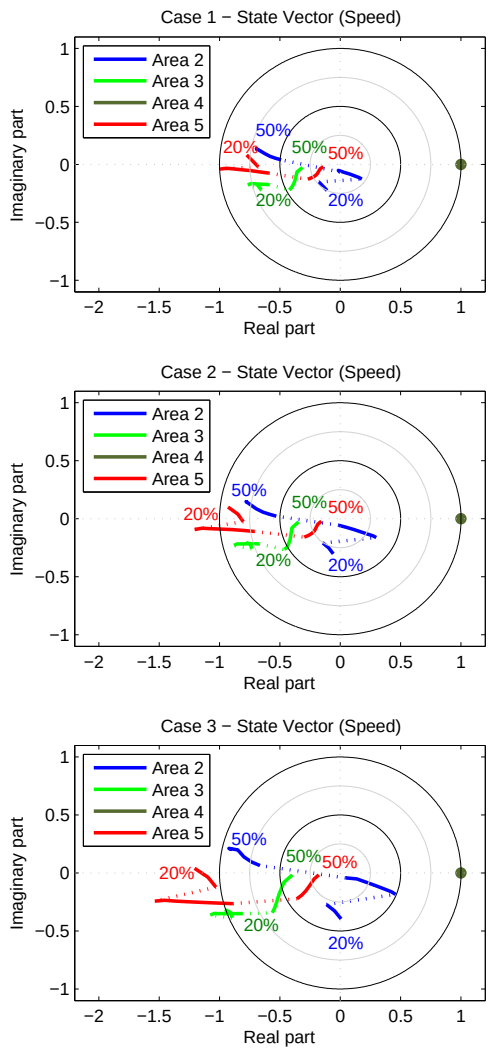

Figure 4.14: NEM: Movement of the dominant left eigenvectors associated with the inter-area mode.

problem with CSP, however, is the large distance between the load centres and suitable locations. Long-distance VSC-HVDC has been proposed as an alternative to conven-

tional AC transmission. This chapter complements the Zero Carbon Australia plan for a 100% renewable power system by analysing small-signal stability with high penetration of VSC-HVDC connected CSP.

First, a model of a CSP plant is proposed, connected to the main AC grid through a VSC-HVDC link. Next, three test systems of different complexities is used to study the movement of the electro-mechanical oscillation modes at different CSP penetration levels. To properly model the displacement of conventional generation, several cases with different number of conventional generators are considered but with the same total capacity, which resulted in different levels of system inertia constant. It is found that less inertia constant always results in lower damping. When it comes to the movement of the eigenvalues associated with the electro-mechanical oscillation modes, general conclusion are not possible. In "topologically simple" systems (SMIB and two-area test system in our case), increasing CSP penetration mostly results in better damping, however it is found for the two-area system that this trend reverses beyond 70% penetration. In the 14-generator test system representing the NEM, the eigenvalue movement becomes even more erratic. With the increasing CSP penetration the damping of the electro-mechanical oscillation modes remains largely unaffected, but the oscillation patterns can change dramatically. In the base case with 20% penetration Areas 3 and 5 had the largest participation in the inter-area mode associated with Area 4 swinging against the rest of the system. With increasing CSP penetration, however, participation of Area 2 becomes more dominant.

Chapter 5

Stochastic Eigenvalue Analysis for Influence of System Inertia Constant Change on Eigen-Properties and Modal Controllability

***Abstract*-The objective of this chapter is to offer a framework of stochastic methodology for stability analysis incorporating uncertainty of renewable sources. This probabilistic method underlies a Monte Carlo approach with random numbers on the basis of Gaussian and Weibull distribution for natural phenomena with conditional probability modelling to reflect photovoltaic and wind converter limits. Through the case studies, the different numbers of operating generators in a specific area are investigated to observe the influence of inertia constant change. The analysis of eigenvalue and controllability is carried out using the kernel density estimation method, and the influence of penetration on the eigenvector is also explored. This analysis method will facilitate the probabilistic stability analysis for the day-ahead or longer term to forecast potential risk. This chapter sheds light mainly on the influence of renewables and reduced inertia constant on the bulk grid from the**

small signal viewpoint, using PowerFactory/DIgSILENT.

5.1 Introduction

Renewable energy source applications exhibiting characteristics such as fast response and no inertia constant are reflected in the paradigm and feature change of the conventional power system [62]. For system planning, renewable resources bring a variety of unexpected factors into play, especially due to the uncertainty from renewables, which may lead to deterioration of power system stability [28]. For a short period of time −on the scale of minutes or hours−prediction and countermeasures for secure operation from the real-time stability assessment enable the network to tolerate harmful contingencies [63]. However, for a longer time period−on the scale of days or months−the requirement of an analysis methodology that incorporates the uncertainty and unpredictability of renewable sources leaves more to be investigated. In this sense, for natural phenomena, a stochastic method from scholarly sources [64] is considered to convincingly and appropriately demonstrate the behaviour pattern of power systems, as opposed to a deterministic method. In this chapter, solar irradiance and wind velocity are formulated using stochastic models−specifically, Gaussian and Weibull based types−and this kind of modelling of natural sources is applied to derive the power generation via photovoltaic (PV) and wind turbine generator (WTG). Then, the implementation of power flow in the Australian national system for the future grid scenarios [23], [24] is carried out to observe stochastic tendencies. Finally, Eigen-analysis of the system is conducted based on the data above. In short, the ultimate purpose of this chapter is to investigate the influence of stochastic natural wind and solar irradiance on eigen-properties of Australian network. The rest of the chapter is organized as follows: Sec. 5.2, future grid scenario of Australia; Sec. 5.3, stochastic modelling of natural sources; Sec. 5.4, modelling of power network; Sec. 5.5, eigenvalue and eigenvector analysis; Sec. 5.6, analysis of case studies for impact of inertia constant; and Sec. 5.7, conclusions.

5.2 Australian Future Grid Scenario

Australian Future Grid mapped out the plan to install WTGs in the southern part of Australia, PVs around Australia, and CSPs in central Australia [23], [24]. In the prac-

tical system, since the generator swing problem is a dominant issue in the Australian power system, to apply renewable sources on the national network the implication of increased penetration level should be taken into deep consideration. Regarding this, a simplified Australian network is developed as the IEEE benchmark system for a small signal stability study [25]. Thus, investigation of corresponding stability issues is tried to be interpreted by Eigen analysis with the stochastic WTG and PV applications based on the Australian future grid plan.

5.3 Probabilistic Modelling of Renewable Generation

The natural characteristics in terms of solar irradiance and wind force may have probabilistically distributed weather conditions at a specific time slot for each day. This phenomenon affects the generation of renewables and the power flow of the large-scale national network, influencing power system stability. This probabilistic study is based on the underlying assumption that solar irradiance and wind velocity are stochastic natural sources.

5.3.1 Solar Irradiance: Gaussian Distribution

For the PV power distribution analysis, solar irradiance is assumed to be a set of random numbers in (5.1) with a type of Gaussian distribution based on practical Australian weather data [65], [66] as Gaussian distribution is used for solar irradiance in previous studies in [67], [68]. The probability density function (PDF) of the Gaussian distribution (5.2) is a fundamental density function and consists of a mean value (5.3) and standard deviation (5.4) explained in [69], [70], which indicates the expectation of a random variable h and the deviation average from the expectation value.

$$h = [h_1, h_2 \cdots h_i \cdots h_n] = \sigma_h Z + \mu_h \tag{5.1}$$

$$f_{gau}(h) = \frac{1}{\sigma_h \sqrt{2\pi}} exp \frac{-(h - \mu_k)^2}{2\sigma_k^2} \tag{5.2}$$

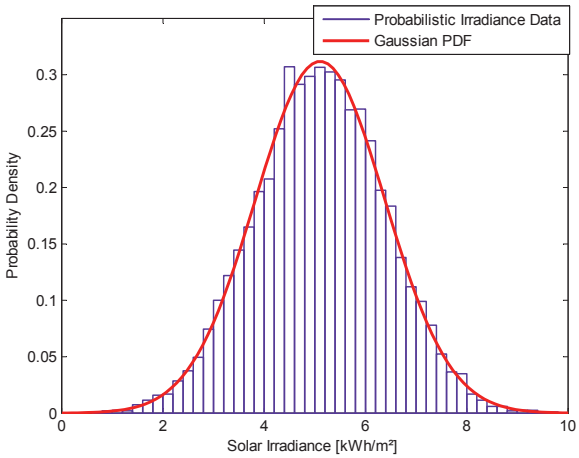

Figure 5.1: Randomly signal based on gaussian distribution for solar irradiance.

$$\mu_k = E[h] = \frac{1}{n}\sum_{i=1}^{n} h_i \tag{5.3}$$

$$\sigma_h = \sqrt{\frac{n\sum h_i^2 - (\sum h_i)^2}{n(n-1)}} \tag{5.4}$$

where h is a set of Gaussian random variable for solar irradiance, h_i is i^{th} sample of a random variable, σ_h is standard deviation of random variable set h, Z is a random variable set of standard normal distribution, μ_h is the mean value of random variable set h, n is the number of samples, and $f_{gau}(h)$ is PDF of solar irradiance.

In the simulation, the random number generator produced around 10,000 samples for the Monte Carlo simulation, as can be seen in the histogram in Fig. 5.1, representing the stochastic solar irradiance, which is used as an input of PV.

5.3.2 Physical Wind Speed: Weibull Distribution

A Weibull distribution function has been widely deployed in wind behaviour analysis [64]. The sample space formulation of probability is generated by the stochastic model

of Weibull distribution in Fig. 5.2.

$$v = [v_1, v_2 \cdots v_i \cdots v_n] = \sigma_v Z + \mu_v \tag{5.5}$$

$$f_{wei}(v) = (\frac{m}{c})(\frac{v}{c})^{m-1} exp[-(\frac{v}{c})^m] \tag{5.6}$$

$$\mu_v = E[v] = c\Gamma(1 + 1/m) \tag{5.7}$$

$$\sigma_v = c[\Gamma(1 + 2/m) - \Gamma(1 + 1/m)] \tag{5.8}$$

$$\Gamma(n) = \int_0^\infty x^{n-1} e^{-x} dx \qquad (n > 0)$$

where v is a set of Weibull random variables for wind velocity, σ_v is standard deviation of random variable v, W is a random variable set of normalized Weibull distribution, μ is the mean value, n is the number of samples, m is the shape parameter, c is characteristic time, and v_i is i^{th} sample of a random variable.

Randomly generated samples for WTG in (5.5) is based on the Weibull PDF in (5.6). This mathematical expression of the Weibull function in (5.6) can be characterized as the mean and standard deviation in (5.7) and (5.8), respectively [69], [70]. The generated random variables are applied to the wind turbine for the calculation of power generation.

5.3.3 Probabilistic Modelling of PV and Wind Generation

Natural characteristics have a high relevance to power generation in the cases of PV and WTG; however, practical generation of PV and WTG has control limits due to converter power rating; thus, it can be probabilistically conducted with converter rating restrictions.

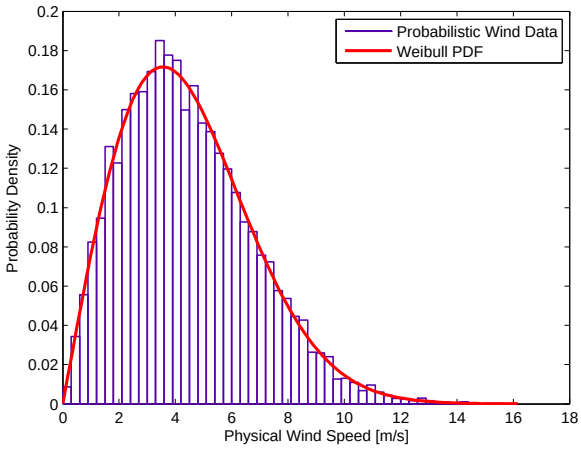

Figure 5.2: Applied random signal based on Weibull distribution for wind application.

Power Calculation for PV and WTG

Based on the stochastic weather and converter conditions, possible outcomes of renewable resource generation can be formulated and itemized for the performance of stochastic experiments as in (5.9), (5.10). PV generation has constraints of power rating as in (5.9), and wind generation is the sum of the three independent random variables and is limited to wind speed of cut-in, cut-out, and rating in (5.10), while concentrating solar thermal power plant (CSP) with HVDC provide constant power in (5.11). These equations provide a mathematical framework for evaluating the outcomes of a probabilistic study.

$$P_{pv}(h) = \begin{cases} 0 & (h_i \leq 0) \\ A_P \cdot r \cdot h_i \cdot PR & (0 \leq h_i \leq H_{rated}) \\ P_{pv,rated} & (H_{rated} \leq h_i) \end{cases} \tag{5.9}$$

$$
\begin{aligned}
P_w(v) &= \sum_{j=1}^{n} P_{w,j}(v) \\
&= \begin{cases} 0 & (v_{j,i} \leq V_{cut\text{-}in}) \\ 0.5 \cdot \rho \cdot A_w \cdot C \cdot \sum_{j=1}^{n} v_{j,i}^3 & (V_{cut\text{-}in} \leq v_{j,i} \leq V_{rated}) \\ P_{w,rated} & (V_{rated} \leq v_{j,i} < V_{cut\text{-}out}) \\ 0 & (V_{cut\text{-}out} < v_{j,i}) \end{cases}
\end{aligned} \tag{5.10}
$$

$$
P_{CSP} = Const(P_{CSP}) \tag{5.11}
$$

where P_{pv} is PV generation, A_p is total solar panel area, r is solar panel yield (%), h_i is i^{th} sample of a solar irradiance random variable set, PR is performance ratio (coefficient for losses), P_{pv},rated is the rated power of PV, H_{rated} is maximum irradiance to generate the rated power of PV, ρ is Air mass density, A_w is turbine sweep area (m^2), C is power efficiency depending on tip speed ratio and pitch angle control, $v_{j,i}$ is i^{th} sample of the wind velocity for j^{th} WTG, $P_{w,j}$ is the jth wind generation, P_w,rated is the rated power of the WTG, $V_{cut\text{-}in}$, $V_{cut\text{-}out}$, and V_{rated} are the cut-in, cut-out, and rated wind velocities, respectively, and P_{CSP} is constant CSP generation.

5.3.4 Bivariate Distribution of Penetration Level and KDE

The produced random numbers are independently distributed on the basis of Gaussian/Weibull distribution. The Kernel Density Estimation (KDE) method [71] enables the penetration levels at Areas 4 and 5 to be visualized as bivariate distribution. Fig. 5.3 indicates the highest and the lowest probability of penetration levels; the red area has the highest probability of penetration level occurrence, and the blue area has the lowest probability of penetration level. The penetration level in (5.12) and (5.13) can be calculated from the output power generated by random variables and can be the function of KDE. This graph in Fig. 5.3 illustrates the estimated joint PDF of KDE based on a combination of the Gaussian and Weibull distributions from conditional outputs, which is the occurrence probability of the penetration level in Areas 4 and 5 mathematically

based on (5.14).

$$K_{a4}(h) = P_{pv}(h)/P_{L4} \tag{5.12}$$

$$K_{a5}(v_i) = P_w(v)/P_{L5} \tag{5.13}$$

$$f(h_i, v_i) = \frac{1}{abl}\sum_{k=1}^{l} K_{a4}(\frac{|h_i - h_k|}{a})K_{a5}(\frac{|v_i - v_k|}{b}) \tag{5.14}$$

where K_{a4} is the function of KDE with penetration level in Area 4, P_{L4} is total load in Area 4, K_{a5} is the function of KDE with penetration level in Area 5, P_{L5} is total load in Area 5, a is the bandwidth of the x-axis, b is the bandwidth of the y-axis, h_i is i^{th} sample of solar irradiance, v_i is i^{th} sample of wind velocity, and l is the number of samples.

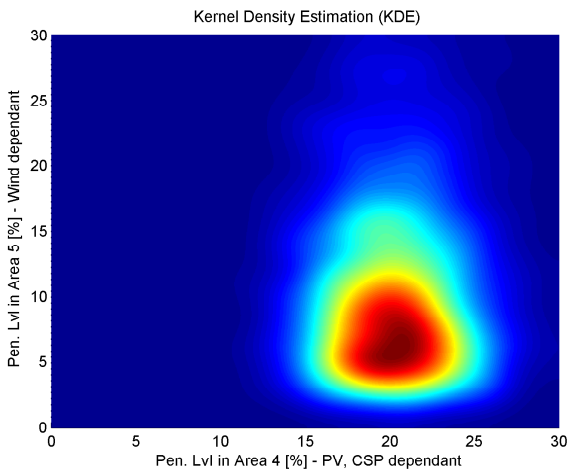

Figure 5.3: Applied penetration levels on the power system with bivariate distribution of KDE.

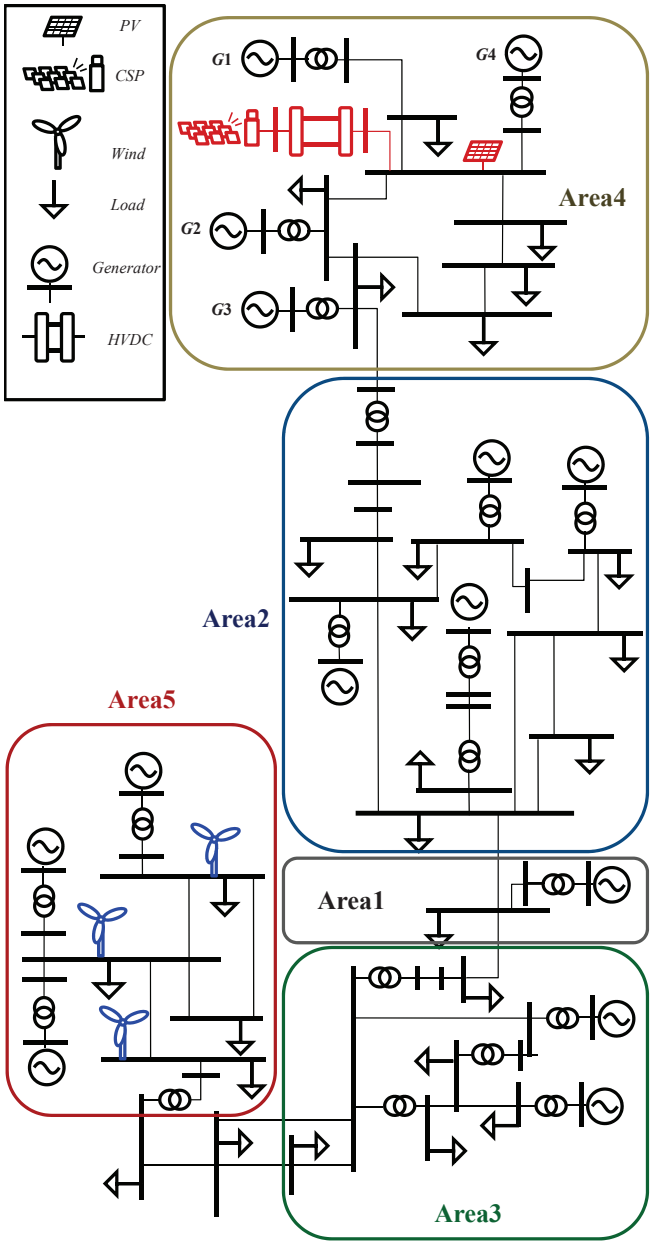

Figure 5.4: IEEE 14-Generator benchmark model; simplified Australian network.

Table 5.1: The Number of Generators and Parameters in a Generator Group in Area 4.

	G1	G2	G3	G4
Case1	4	3	5	6
Case2	3	2	4	5
Case3	3	2	3	4
H (Inertia Constant) [s]	2.6	3.	2.6	4.0
S (Gen. Rating) [MW]	444.4	333.3	444.4	333.3

G1, G2, G3, and G4 from Fig. 5.4 indicate the groups of generators. All of the parameters and values in each generator group are identical.

5.4 Modelling of Power Network

5.4.1 14-Generator Model

A modified 14-generator system [25] is subjected to carry out the simulation of stochastic renewable analysis. This model is an IEEE benchmark system and is designed for small signal stability studies. Observe in Fig. 5.4 a schematic of the Australian National Electricity Market (NEM) model is presented. In [25], the described heavily loaded model including excitation and power system stabilizers (PSS) becomes the objective of our observations.

Under the consideration of renewable sources and load power, the swing equation is transformed into (5.15).

$$\begin{aligned} &\frac{2H_j}{\omega_0}\frac{d\omega}{dt} + D_j\omega_j = \Delta P \\ &= P_{gm,j} - (P_{ge,j} - P_{pv}(h) - P_{w,i}(v) + P_L) \end{aligned} \tag{5.15}$$

where H is inertia constant, ω_0 is nominal angular speed, ω is angular speed, D is damping torque coefficient, P_{gm} is mechanical power of generator, P_{ge} is electrical power of generator, P_{pv} is the generation of PV, $P_{w,i}$ is the generation from i^{th} WTG, P_L is load consumption, and all the letters on subscript position, such as 'j', stands for j^{th} generator.

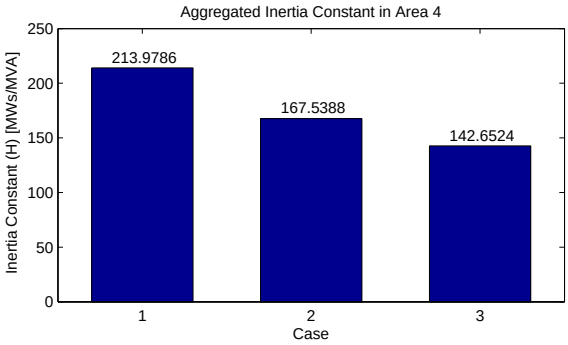

Figure 5.5: Aggregated inertia constant of the coherent Area 4 in each case (Power base: 100 MW)

5.4.2 Case Studies and Aggregation of Inertia Constant

As renewable power generation increases, some of the conventional generators does not have necessity of operation, and this tendency results in a decrease in the inertia constant. Thus, in order to observe the influence of the reduced inertia constant on a specific area of the power system, three case studies are set up in Table 5.1.

Observe in Fig. 5.5 that the decrease of generator numbers in Table 5.1 results in the decrease of inertia constant in specific area according to the calculation by (5.16) explained in [61], [72], and it indicates that the number of operating generator directly related with system inertia constant, i.e. more operating generators: higher inertia constant and less operating generators: lower inertia constant. The aggregated inertia constant in Area 4 can be calculated by (5.16) with the assumption of the generators in each area exhibiting high coherency.

$$H_{Agg,k} = \sum_{j=1}^{m} H_j n_j \frac{S_j}{S_{base}} \tag{5.16}$$

where $H_{Agg,k}$ is the aggregated inertia constant in k^{th} Area, m is the number of generator groups in coherent Area (e.g. Area 4 has four generator groups (G1-G4) in Fig. 5.4), n_j is the number of generators in j^{th} generator group (e.g. G1 in Case 1 has 4 generators), S_i is the rating of jth generator group, H_j is the inertia constant of jth generator group, and S_{base} is system base power.

The assumption is established total generation in Area 4 from conventional and renewable generators is constant in each case. In regards to the scenarios, if the number of generator decreases, each generator should provide a larger quantity of active power for the low level of penetration, because the total power of synchronous generators is pre-determined according to renewable generation. Thus, the power share to a single generator increases, when the number of generators decreases. In other words, when renewable generators provides low amount of power, synchronous generators have to provide higher power and the reduced number of synchronous generators may hit the limitation of the generator.

For this reason, in order to reduce the burden of conventional generators, Area 4 has a minimum penetration level from HVDC transferring CSP power, as indicated in (5.11).

5.5 Eigevalue Analysis

With the aid of recent research [29], the discontinuous change in eigenvalues was explained under the condition of penetration-level change in a specific area. In this chapter, the reciprocal relationship between the penetration levels of two areas is explored. As renewable sources can be characterized as uncertainty and unpredictability, the stochastic approach has the capability to incorporate meteorological possibilities and to foresee a possible range of eigenvalues.

This method increases the predictability of a potential danger due to the renewables from far future network oscillatory stability such as a day-ahead network, operable generator numbers, and the generator retirement planning. Thus, this research will show and verify the influence of the penetration of two areas (Area 4 and 5) through stochastic analysis.

5.5.1 Stochastic Eigenvalue Analysis: Monte Carlo Simulation

Monte Carlo simulation is widely known as a probabilistic analysis method [73] [74] that can be used to evaluate the random behaviour of the renewable model [64] and observe eigenvalue distribution. An advantage of stochastic analysis for the system is to allow predictions related to possible power-system stability situations. In this simulation, in order to balance consumption and supply of power, the reduced power from conventional

generators is determined by (5.17) as much as an increased generation of renewables.

$$P_j = ((S_{k,j} \cdot n_j)/S_{k,tot}) \cdot (P_{k,tot} - P_{k,w}(v) - P_{k,pv}(h)) \tag{5.17}$$

where P_j is power of jth generator group (G_j in Table 5.1), $S_{k,j}$ is rating of jth generator group in Area k, n_j is the number of jth generator group, $S_{k,tot}$ is total rated power in Area k, and P_{pv} and P_w are the generation of PV of WTG in Area k, which are the functions of irradiance (h) and wind velocity (v), respectively.

As a first step of Monte Carlo Simulation in Fig. 5.6, the random numbers are created on the basis of Gaussian and Weibull distributions as in (5.1),(5.5). From these random numbers, renewable generation is calculated as in (5.9),(5.10), and the generation quantity of conventional power plant is decided by (5.17) to keep the uniform generation in the Area; subsequently, the calculated generation is applied on the system in (2.4)−(5.15), and then based on this power flow, modal analysis is conducted in a lin-

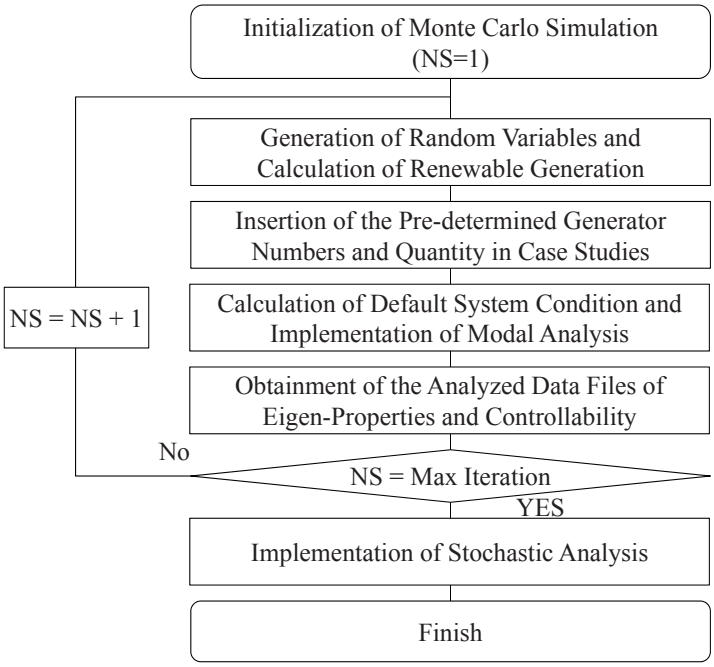

Figure 5.6: Procedure of eigen-analysis based on Monte Carlo simulation.

earised operating point as in (2.6), (2.7), and the result files are saved on the computer. If the number of simulation (NS) does not reach the maximum iterations; 10,000 times as aforementioned, the simulation is conducted from the first step iteratively. This progress is implemented on Digsilent/PowerFactory software using Digsilent Programming Language (DPL).

The analysis of the entire data in each cases to show the stochastic distribution and contour of eigenvalues is carried out on MATLAB software. This procedure is called Monte carlo simulation, and its flow chart is described in Fig. 5.6.

As a result, the graph in Fig. 5.7 shows the eigenvalue distribution on an S-plane the contour of the probabilistic density using the KDE method under the bandwidth conditions of the *x*- and *y*-axis as 9×10^{-3} [1/s] and 28×10^{-3} [rad/s], respectively. In this graph, 'Real (1/*s*)' indicates *x*-axis of S-plane, 'Imag (*rad*/*s*)' stands for *y*-axis of S-plane, and *z*-axis presents the eigenvalue density in the bandwidth conditions.

The selected eigenvalue is one of the least stable eigenvalues and aims to observe the probabilistic distribution influenced by stochastic weather condition together with the changes of distribution in each case, when the inertia constant changes.

The contour of distribution by KDE reflects eigenvalue density; thus, a high contour value presents the highest probability of eigenvalue location, and scattered eigenvalue indicates all of the possible eigenvalue positions. In this simulation, the distribution of eigenvalue moves slightly toward the y-axis, as a result of decreased inertia constant in the cases. Additionally, the eigenvalue distribution is divided into two parts, indicating eigenvalue jumps occurring due to the nonlinearity of the large system.

5.5.2 Analysis of Contributive Factors

Eigenvalues and eigenvectors can be changed non-continuously depending on the penetration level. A previous observation of this phenomenon was first reported in the experiments on PMU measurement [75]. This phenomenon was first observed as a sudden change of phase angle denoting the change of oscillating frequency due to wind power change and fluctuation. In order to obtain insight why this is happening, a study previously attempted to explore this phenomenon [29], and it was found that the influential factor comes from a change in grid penetration level. In this chapter, investigation of the influence of bivariate penetration level in two areas (Area 4 and 5) is conducted to observe which modes are more influenced by generator speed through analysis of con-

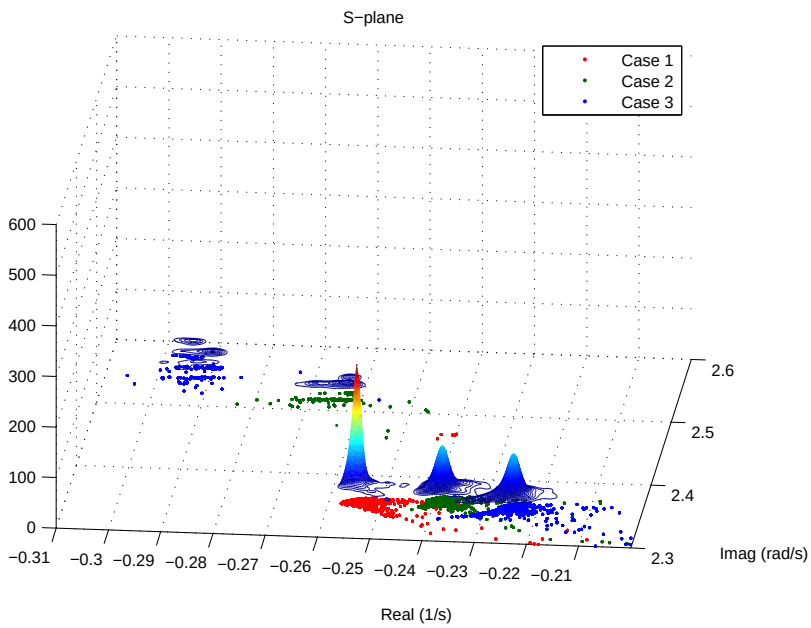

Figure 5.7: Contour of distributed eigenvalues on S-plane.

tributive factors, the left eigenvector.

The graph presented in Fig. 5.8 indicates the magnitude of the aggregated left eigenvector in each area, and explains the non-continuous characteristic of the left eigenvector according to bivariate changes in penetration level.

Along with the linear change of penetration level in two areas, the eigenvector tends to change smoothly around 10% of both Areas; but near by the points from 20% and 10% to 25% and 30% in Area 4 and 5 respectively, contribution of generator speed tends to move non-continuously as in Fig. 5.8.

The graph visually exhibits the tendency of penetration level correlation and implies that the change of penetration level may result in different settling points due to non-linear characteristic of system. This tendency is shown in eigenvector and eigenvalue jumps, although non-linearity cannot shed clear light on the boundary of the transition.

In regard of this, left eigenvectors of the generators only in a coherent area are aggregated, and this calculation of left eigenvector aggregation is denoted in (5.18) and (5.19). In detail, the magnitude and angle of the eigenvector are separately calculated

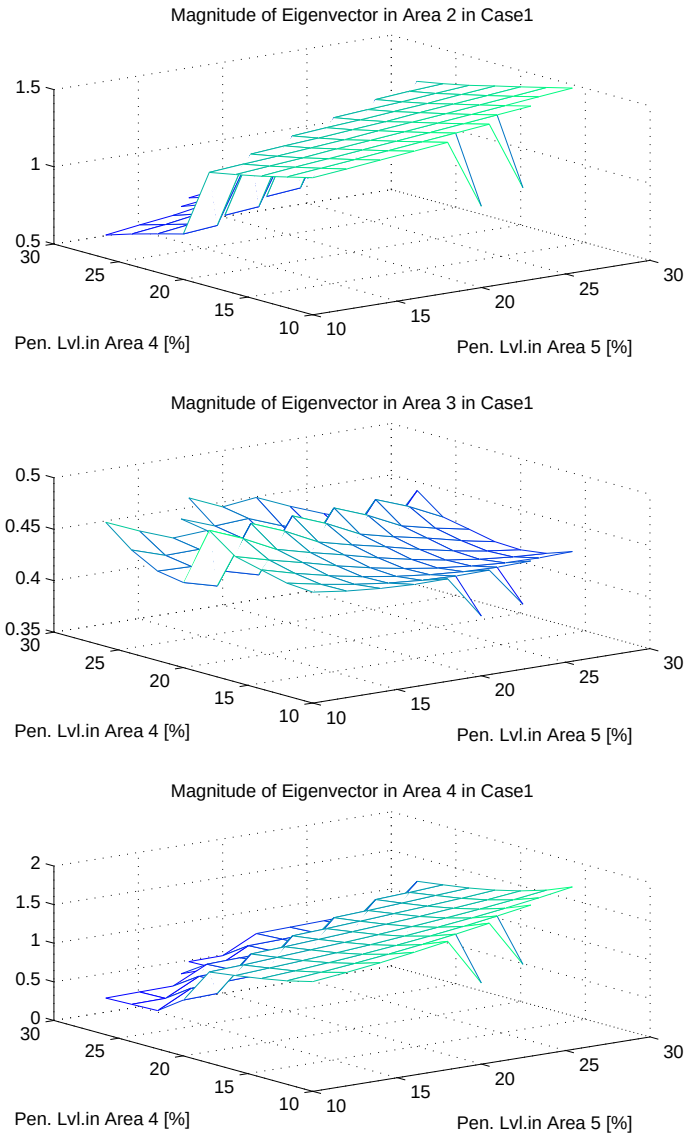

Figure 5.8: The left eigenvector change of Area 4 in Case 1 according to penetration level.

with the coefficients in terms of inertia constant under the assumption of mth electrically coherent area. These numerical expressions in (5.18) and (5.19) indicate that the larger number of operating generators and the larger inertia constant have a higher influence on the left eigenvalue, which is a contributive factor to the modes.

$$\psi_{j,a} = |\psi_{j,a}|\angle\delta_{j,a}, \qquad \psi_{agg,k,a} = |\psi_{agg,k,a}|\angle\delta_{agg,k,a}$$

$$|\psi_{agg,k,a}| = \frac{\sum_{j=1}^{m}|\psi_{j,a}|H_j n_j(S_j/S_{base})}{\sum_{j=1}^{m} H_j n_j(S_j/S_{base})} \tag{5.18}$$

$$|\delta_{agg,k,a}| = \frac{\sum_{j=1}^{m}|\delta_{j,a}|H_j n_j(S_j/S_{base})}{\sum_{j=1}^{m} H_j n_j(S_j/S_{base})} \tag{5.19}$$

where $\psi_{j,a}$ is the element of left eigenvector between for j^{th} generator speed and a^{th} eigenvalue, $|\psi_{j,a}|$ and $\delta_{j,a}$ are the magnitude and angle of $\psi_{j,a}$, $\psi_{agg,k,a}$ is the element of the aggregated left eigenvector in k^{th} Area for a^{th} eigenvalue, $|\psi_{agg,k,a}|$ and $\delta_{agg,k,a}$ are the magnitude and angle of $\psi_{agg,k,a}$, m is the number of generator groups in coherent Area, n is the number of generators in j^{th} generator group, S_j is the rating of the jth generator group, H_j is the inertia constant of the jth generator group, and S_{base} is the system base power.

5.6 Analysis of Inertia Constant Impact

5.6.1 Influence of Generator Torque: Controllability Analysis

Our study in this section is to examine the influence of generator power on the mode, using modal controllability. The left eigenvector observed in the previous section is the influence of generator speed on modal variables. Mode controllability in [31] indicates the influence from generator power to modal variables as in Fig. 5.9 which explains the modal controllability from input (ΔP) to modal variable (z_a) in (5.21); the electrical and mechanical power deviation (ΔP) multiplying B matrix components becomes differential form of rotor angular speed ($\Delta\dot{\omega}$), and multiplying left eigenvector in this result becomes differential form of a modal variable ($\Delta\dot{z}$). The controllability is named

for this relationship between power deviation (ΔP) and modal variable (z_a) and indicates how much power deviation has an influence on the magnitude and angle of modes. The major difference between the left eigenvector and controllability arises from the B matrix. As in (5.20), the B matrix consisting of the inertia constant is multiplied with the left eigenvector for the controllability calculation in (5.21), which implies that the decreased inertia constant leads to the increased impact of a power deviation on a mode, as in (5.20) and (5.21). Accordingly, the aim of our research is to examine and verify the correlation between inertia constant and controllability in regard to the change of inertia constant in each case.

$$B = [b_1, b_2, \cdots b_j]^T = [\frac{\omega_0}{2H_1}, \frac{\omega_0}{2H_2}, \cdots \frac{\omega_0}{2H_j}]^T \tag{5.20}$$

$$\Delta P_j = P_{m,j} - P_{e,j}$$

$$u = [\Delta P_1, \Delta P_2, \cdots \Delta P_j]$$

$$B' = \Psi \cdot B = [\psi_{1a}, \psi_{2a}, \cdots \psi_{ja}] \cdot [b_1, b_2, \cdots b_j]^T \tag{5.21}$$

where B is a matrix from (2.6), b_j is j^{th} element of B matrix for j^{th} generator, ΔP_j is power deviation between mechanical and electrical power in j^{th} generator, $\Delta P_{m,j}$ is the mechanical power of jth generator, $\Delta P_{e,j}$ is the electrical power of jth generator, u is matrix of input from (2.6), B' is transformed matrix from (2.13), (2.14), Ψ is the left

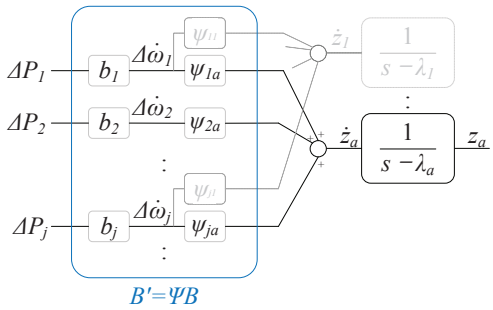

Figure 5.9: Schematic diagram of mode controllability concept (5.21) and (2.14)

eigenvector matrix, $\psi_{j,a}$ is element of left eigenvector between for j^{th} generator speed and a^{th} eigenvalue, λ_a is the ath eigenvalue, z_a is the ath modal variable.

For aggregation of controllability factors among coherent generators in each area, the coefficient is placed, based on inertia constant; consequently, the generator group with higher inertia constant or the larger number of generators has a higher coefficient and obtains a larger share of controllability, as mathematically represented in (5.22).

$$b'_k = \psi_{k,a} \cdot b_k = \frac{\sum_{j=1}^{m} \psi_{j,a} b_j H_j n_j (S_j / S_{base})}{\sum_{j=1}^{m} H_j n_j (S_j / S_{base})} \tag{5.22}$$

$$B'_{Agg} = [b'_1, b'_2, \cdots b'_k]^T$$

$$b_k = \omega_0 / 2H_{Agg,k}$$

where b'_k is modal controllability of kth Area, $\psi_{k,a}$ is the element of the aggregated left eigenvector in k^{th} Area for a^{th} eigenvalue, b_k is B matrix element of kth Area from Aggregated inertia constant in (5.16), and B' is controllability matrix.

5.6.2 Probabilistic Contribution of Generator Input

As a basic premise, only the inertia constant in Area 4 is changing, which intends to observe the implication of inertia constant change of specific area based on Table 5.1 and Fig. 5.5. As can be seen in Fig. 5.10, with regard to a least stable interarea mode, the controllability vectors are stochastically distributed along with the KDE method on the polar coordinates diagram based on the reference at Area 5.

On this polar diagram, the higher magnitude means that the larger impact is delivered on an interarea mode despite the identical power deviation; thus, the decrease of the inertia constant results in increase of generator power influence on a mode associated with the cases. In addition, opposing degrees between Areas can be explained as triggering generators oppositely force to each area.

In physical aspect, if interarea oscillation between conventional generators already exists, occurrence of power deviation from a generator of low inertia constant significantly accelerates or decelerates the rotational velocity. This amplified deviation of

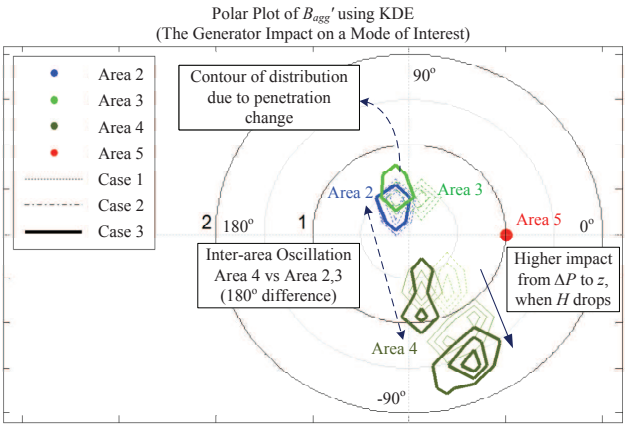

Figure 5.10: Probabilistic influence of input on a mode due to inertia constant change; controllability distribution of each case.

rotational velocity also magnifies the impact on a mode. Furthermore, against the transferred power from the other area, the area with reduced inertia constant will experience larger acceleration or deceleration of rotational velocity.

In Fig. 5.10, Areas 2 & 3 and Area 4 have the inter-area oscillations, since it is located 180 degree against each other. Additionally, Areas 2 and 3, which exhibit no inertia constant change, are not influenced by inertia constant change in Area 4, while the inertia constant change in Area 4 has high influence on controllability of Area 4 itself.

Fig. 5.10 indicates that lower inertia constants lead to higher contributions from the generator input to the modal variable. The case with the highest inertia constant, Case 1, has a smaller contribution of generator change to modal variable, and Case 2, with a medium inertia constant value, results in an increase in the contribution compared to Case 1.

In Case 3, the lowest inertia constant among the three cases contributes more generator change to the mode of interest than other cases. The graph, presenting controllability, shows that the contribution of generator change to the modal variance gradually increases when inertia constant decreases. Fig. 5.10 and (5.22) provide stochastic and theoretical evidence, and considerable insight into the extent to which the change in inertia constant can influence the mode based on generator input.

5.7 Summary

This chapter has attempted to describe a stochastic method based on Monte Carlo simulations to investigate a power system from a small signal perspectives. As a source of natural characteristics, solar irradiance and wind velocity are assumed to be Gaussian and Weibull random variables, and then the generation of WTG and PV is calculated with condition of converter rating restrictions, which may changes the power flow of the system. As an outcome from those values on the network, three main issues have been investigated: probabilistic eigenvalue position, non-continuous characteristics that can be shown at high penetration, and probabilistic contribution of a decrease in inertia constant. Specifically, the eigenvalue distribution shows the probability of placement on the S-plane, and the tendency of non-continuous eigenvector change according to penetration level is observed. Last, the probabilistic contribution of a generator in accordance with inertia constant change in one part of the system is observed through controllability. As may be ascertained from the above outcomes, the results of this study suggest several promising applications for stability analysis embracing stochastic natural phenomena within a power system.

Chapter 6

Harmonious Integration of Faster Acting Energy Storage Systems as Regulation and Reserve Resources into Grid Ancillary Services

Abstract– **The purpose of this chapter is to explain the methodology of handling State-of-Charge (SOC) and regulating frequency by Energy Storage System (ESS) and to explore its mathematical description for observing the effects of compensation ability on power systems. The suggested methodology is formulated on droop control and SOC feedback (DaSOF) by adding the value of frequency offset considering SOC on the frequency deviation, which guarantees resiliency of frequency to be well tuned with existing generators. Throughout this chapter, the mathematical aspects based on the automatic control theory is explored, and analysis of reactions by means of indications such as initial magnitude, cut-off frequency, and settling time is also investigated. The response characteristics regarding the change of parallel installation of ESS and the quantity of energy conservation are examined through the graphical and numerical indications. The DaSOF method also strengthens the security to resist the adverse impact of unanticipated excursions and fluctuations of renewable sources; hence, the effect of DaSOF application on system for certain contingency and renewable integration to theoretical and prac-**

tical bulk system cases will be explored using DIgSILENT/Power Factory.

6.1 Introduction

Recent research from Sandia National Laboratories through a study for DOE Energy Storage System (ESS) program [76] reported the multifaceted benefits associated with the use of electricity ESS for electric-utility-related applications and provided the guide of benefits and market potential assessment, implying ESS would bring significant technical and economic facets in the future. In utility perspectives, the evolution of the network paradigm that is currently underway will result in larger needs of services provided by ESS; besides, the large number of ESS projects have been conducted throughout various utilities such as PJM [77], NYISO [78], ERCOT [79], KEPCO [80], etc. [81–83]; moreover, FERC recognizes the importance of ESS and enacts the law entitled 'Order 755' to encourage ESS installation for the federal utilities [84]. For ESS application on conventional and practical systems, ESS should have co-operative characteristics not only with generators but also with ESS itself. Coordination of frequency regulation by spinning generators is well-constructed in accordance with the order such as inertial response, governor response and Automatic Generation Control (AGC) [35, 85, 86], thus coordination of ESS into frequency regulation practice has significant importance. Moreover, low inertia constant due to renewable resources on the existing or upcoming power system can lead to frequency instability; hence, ESS can be a countermeasure to reinforce the resiliency of the system frequency. In order to resolve these issues, the various methods of ESS application have been extensively studied, and the state-of-the-charge (SOC) feedback attracts scholars' interests. For instance, droop control concept based on releasing or absorbing certain value of power is conceptually introduced [87]. Adjustment of the droop set point to be operated as a Load Frequency Control (LFC) has also been studied [88]. Management of SOC to obtain potential reserve by means of penalty functions are described [89]. Adaptively adjusting droop rate has also been researched for purpose of Vehicle to Grid (V2G) application in consideration of SOC [90, 91]. Micro grid for integrated PV/ESS is explored [92]. DC grid droop control in purpose of matching SOC is expounded in [93, 94], ESS application on Multi-Terminal HVDC is introduced in [95]. SOC control for Hybrid ESS [96], and hierarchical control of SOC in a DC grid are studied [97]. Several studies have attempted

to use droop method with SOC feedback [90, 91, 97–99].

However, research on decentralized control and SOC management for power system coordination of frequency regulation remains in the early stages of development. Thus, this chapter suggests the methodology in autonomous fashion satisfying three issues above (decentralized control, SOC management, and coordinated frequency regulation), and also this chapter offers mathematical expressions and analysis. This chapter is organized as follows: In Section 6.2, modelling of battery and system network is presented, Section 6.3 provides the information of droop control, Section 6.4 describes proposed method, Section 6.5 explains implications and mathematical expressions of proposed method, Section 6.6 presents the frequency stability in case of ESS application with suggested method, and Section 6.7 shows the case of renewables integration.

6.2 Modelling

6.2.1 Battery Modelling

Traditionally, the SOC calculation of Li-ion battery is based on the integration of current [100], [101]. However, the assumption is made as the capacity of ESS can be calculated by energy, the integration of power in (6.1). This calculation can be derived to the transfer function in (6.2) to merge ESS into the network.

$$SOC(t)[\%] = SOC_0 + \frac{1}{E \cdot h} \int_{t_0}^{t} P_{ESS}(t)dt \tag{6.1}$$

$$\Delta SOC_0(s) = \frac{\Delta P_{ESS}(s)}{E \cdot h \cdot s} \tag{6.2}$$

where SOC_0 is initial *SOC(%)*, E: the nominal capacity of battery (MWh), h: weighting factor to change an hour to a second, P_{ESS} is battery power (MW), and $\Delta SOC_0 = SOC - SOC_0$.

6.2.2 System Modelling

The frequency stability is directly related to power balance between mechanical and electrical power in [30, 31]. In this regard, the frequency deviation can be explained as (6.3), caused by the mismatch of power balance consisting of the factor of inertia and damping of the load [31]. In this equation, if rotational velocity (ω) is in pu in this equation, frequency (f) and rotational velocity (ω) are identical.

$$\frac{df}{dt} = \frac{1}{2H}(\Delta P \cdot f_0 + D \cdot \Delta f) \tag{6.3}$$

where H is inertia constant, ΔP is mismatch of power, f_0 is nominal frequency, D is damping component, Δf is deviation of frequency, and all the variables are in pu.

6.3 Droop Control on Generator and ESS

6.3.1 Droop Control on Generator

The purpose of droop control is to share the burden of electrical loads among generators for frequency regulation. The droop rate (R) in (6.4) denotes that when frequency (Δf) deviates, generators offer 100% of rated power. Furthermore, the generators with different droop rate would provide the different degree of the supporting power according to the generator droop rates in (6.4).

$$\Delta f = \Delta P_1 R_1 = \Delta P_2 R_2 \tag{6.4}$$

where Δf is the deviation of frequency, R_1 and R_2 are droop rates of generator 1 and 2 respectively, ΔP_1 and ΔP_2 are the supporting power from generator 1 and 2 due to the frequency deviation.

6.3.2 Droop Control on ESS without SOC Feedback

$$\Delta P_{ESS} = \frac{1}{R} \cdot \Delta f \tag{6.5}$$

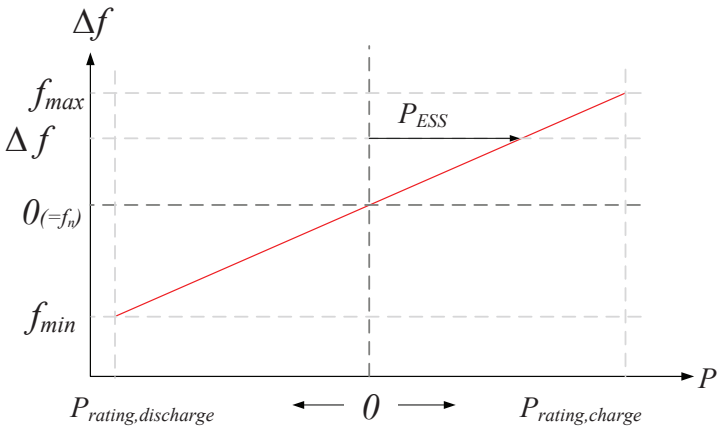

Figure 6.1: Fundamental concept of Droop control in ESS

$$\frac{\Delta SOC(s)}{\Delta f(s)} = \frac{1}{R \cdot E \cdot h \cdot s} \tag{6.6}$$

For the droop control on ESS in Fig. 6.1, inverse droop rate multiplied by frequency deviation in (6.5) would decide the ESS supporting power, and the response of SOC would be transformed to the Laplace form as (6.6). If constant frequency deviation occurs without SOC feedback in (6.6), SOC is gradually increased or decreased in linear fashion due to the step input (Δf).

6.4 Proposed SOC Management with Droop Control

6.4.1 Numerical Expressions for Methodology

In the proposed method, the frequency offset is placed to be subtracted from frequency deviation on droop control as can be seen in (6.7) as an input to calculate the power of ESS. The method with offset is distinguished from normal droop method in Fig. 6.1 and allows ESS to manage its energy.

When it comes to this equation, the calculation of frequency offset is based on SOC by multiplying the factor K_f as calculated in (6.8). The meaning of K_f is the allocation of total operational SOC range (SOC_{tot}) on frequency compensation range from the

maximum compensation frequency ($f_{ofs,max}$) to the minimum compensation frequency ($f_{ofs,min}$) in (6.9). The energy of battery (K_E) can be also defined as (6.10) to calculate SOC from the power as in (6.2). As consequences, the derivation of numerical expressions with regards to droop control and SOC feedback (DaSOF) becomes (6.7) that indicates a key operation.

$$\Delta P_{ESS} = \frac{1}{R}(\Delta f - f_{ofs}) \tag{6.7}$$

$$f_{ofs} = \Delta SOC \cdot K_f \tag{6.8}$$

$$K_f = (f_{ofs,max} - f_{ofs,min})/SOC_{tot} \tag{6.9}$$

$$K_E = E \cdot h \tag{6.10}$$

$$\Delta f = f - f_n$$

$$\Delta SOC = SOC - SOC_{cen}$$

where ΔP_{ESS} is charging power (to ESS), Δf can be both frequency deviation and the reference of frequency offset, f_{ofs} is frequency offset, ΔSOC is SOC deviation from central value, K_f [Hz/%] is the allocation of SOC range to frequency compensation range, $f_{ofs,max}$ is maximum of frequency compensation, $f_{ofs,min}$ is minimum of frequency compensation, SOC_{tot} is SOC control range such as 0 to 100, K_E [MWs] is the total energy of ESS, f_n: nominal frequency, f: system frequency, SOC is measured SOC, and SOC_{cen} is the center of SOC, e.g. 50% when SOC_{tot} is 100%.

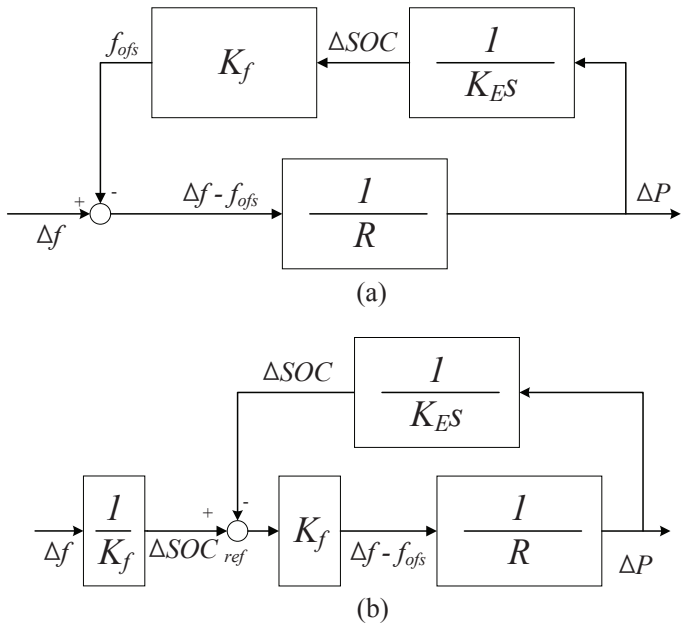

Figure 6.2: Block diagram of proposed DaSOF method in two different perspectives: (a) frequency offset point of view, (b) SOC feedback point of view.

6.4.2 Transfer Functions for the Methodology

Fig. 6.2 derived from (6.2), (6.7)−(6.10) illustrates the suggested methodology in two co-related points of the views; (a) frequency offset feedback and (b) SOC feedback.

For the proposed method, the only added part is K_f for SOC feedback in Fig. 6.2(a), while the $1/R$ part is existing the droop controller in (6.5), and the K_E part is also existing SOC calculation.

For the calculation of SOC deviation in (6.11), the center of SOC is assigned for nominal frequency, which implies that when system frequency reaches nominal frequency f_n (e.g. 60 Hz), SOC reaches the central value (e.g. 50%), which are linked through K_f, as can be explained in (6.11).

$$\Delta f = (SOC_{ref} - SOC_{cen}) \cdot K_f = \Delta SOC_{ref} \cdot K_f \tag{6.11}$$

$$\Delta f - f_{ofs} = \Delta f - \Delta SOC \cdot K_f \tag{6.12}$$

$$\Delta f - f_{ofs} = K_f \cdot (\Delta SOC_{ref} - \Delta SOC) \tag{6.13}$$

where f_n is nominal frequency, SOC_{ref} is SOC reference, and ΔSOC_{ref} is deviation of SOC reference from central SOC.

Fig. 6.2(a) indicates frequency offset (f_{ofs}) determined by SOC deviation plays a feedback role as signal, and frequency deviation (Δf) take a role of the reference.

In this perspective, operation of the controller intends to match frequency offset (f_{ofs}) with frequency deviation (Δf). For instance, if constant frequency deviation occurs, droop input ($\Delta f - f_{ofs}$) tries to be zero by changing frequency offset (f_{ofs}); consequently, the power changes as much as ΔP, and then the release or absorption of power change the SOC (ΔSOC). Subsequently, SOC proportionally follows the frequency deviation as much as K_f according to (6.12).

Fig. 6.2(b) illustrates an block diagram of proposed method in an SOC perspective. In this figure, frequency deviation determines the SOC reference as (6.11), and SOC is subtracted from the SOC reference as in (6.13). By multiplying K_f to this value ($\Delta SOC_{ref} - \Delta SOC$), SOC values are transformed to the difference between frequency deviation and offset ($\Delta f - f_{ofs}$) as in (6.13) for the calculation of the ESS power. Consequently, the SOC traces the SOC reference.

This methodology enables SOC to follow the frequency deviation, which indicates slight frequency deviation results in slight SOC change, and serious frequency deviation lead to significant SOC change. Slight SOC change intends to support small amounts of energy to manage SOC for more serious frequency deviation. Therefore, this behaviour of DaSOF method aims to compromise battery's limited energy on frequency support.

6.4.3 Operation Behaviour from Methodology

In order to investigate the behaviour of proposed method for solid understanding, the basic condition in this section is established as constant frequency deviation in the system input. The characteristics of this method in Fig. 6.3 are briefly explained below.

- All Δf and ΔSOC can be transformed using K_f (Left and right side of y-axis).

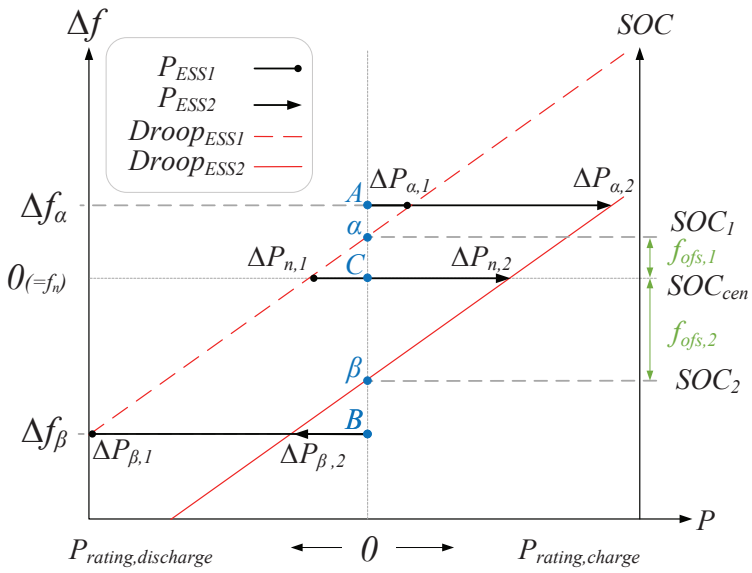

Figure 6.3: Illustration of proposed DaSOF method; subtracting frequency offset from frequency deviation.

- The measured system frequency (Δf) is desired value, and SOC reference (ΔSOC_{ref}) is calculated by (Δf) using K_f in (6.11).
- SOC determines offset of droop rate (f_{ofs}) in (6.8). Thus, f_{ofs} follows Δf, and ΔSOC follows ΔSOC_{ref}.
- ESS power is determined on the horizontal line of Δf.
- ESS power is determined by $\Delta f - \Delta f_{ofs}$ and $1/R$ in (6.7).
- Left y-axis (Measured system freq.) is the reference, right y-axis (SOC) is ESS internal energy, determining feedback signal (f_{ofs}), and ESS power is determined by the gap between both side of y-axis as in (6.7).

In Fig. 6.3, assumption was made as two ESSs exist with different levels of SOCs and two examples of constant frequency deviation. In this point, SOCs of ESSs, SOC_1 and SOC_2, turn into the frequency offsets ($f_{ofs,1}$ and $f_{ofs,2}$) to add it on droop rate. The relationship between two y-axes (SOC and Δf) in Fig. 6.3 are closely connected by K_f,

since those can be transformed by multiplying or dividing K_f as can be ascertained by (6.8), (6.11)-(6.13). The occurrences of frequency deviation Δf_α and Δf_β are linked to point A and B and the point α and β are connected with $f_{ofs,1}$ and $f_{ofs,2}$. Namely, point A, B, and C are dependent on external power system, and the point α and β are dependent on ESS internal system.

For frequency deviation as Δf_α, ESS_1 and ESS_2 absorb the power as $\Delta P_{\alpha,1}$ and $\Delta P_{\alpha,2}$ respectively, which indicates when a grid has excessive power as reflected from increased frequency, ESS_1 with higher level SOC_1 absorbs less power $\Delta P_{\alpha,1}$, and ESS_2 with lower SOC (SOC_2) absorbs higher power $\Delta P_{\alpha,2}$, because ESS_1 has lower chargeable energy capacity than ESS_2.

The power charge/discharge makes SOC move towards to SOC_{ref}; in other words, f_{ofs} (by SOC) moves towards to Δf; as a consequence, point α and β (by $f_{ofs,1}$ and $f_{ofs,2}$) are tracking point A (Δf_α).

For the frequency deviation as Δf_β, if the system requires power support as reflected from decreased frequency, ESS_1 with higher energy discharges higher power $\Delta P_{\beta,1}$, and ESS_2 releases less power $\Delta P_{\beta,2}$, because of lower charged energy in ESS_2 . In this operation, both points α and β are tracking point B.

In this sense, as points α and β are close to the point B, the ESS power decreases, which result in slower movement speed to point B and longer time to reach point B.

Lastly, if the frequency is fluctuating between Δf_α and Δf_β, the ESS power charges/ discharges depending on the frequency to reduce it.

Generally, a power system has a tendency to recover its frequency through the various facilities and interconnected systems such as governor, AGC, and Load Frequency Control (LFC). In this regard, when the power system recovers frequency to the nominal value, both ESSs in Fig. 6.3 try to charge/ discharge the power to manage SOC to central level; for instance, α and β are moving to point C in Fig. 6.3, when power system recovers the frequency to point C.

6.5 Theoretical Implications by DaSOF Method

This section intends to shed a clearer light on tendencies and behaviours of proposed method on power system through the mathematical expressions. To lay the theoretical basis of ESS performance, derived equations and implemented simulations are assumed

without the communication delay, control performance delay, and time constant scattered around the circuit. In case DaSOF ESS is applied on the network, the block diagram of system integrated with ESS can be illustrated as Fig. 6.4 for observation of frequency characteristics neglecting turbine and governor.

6.5.1 The Response of SOC

One of the considerable advantage of the proposed method is to enhance the analysis and evaluation capability by means of automatic control theory for the preparation of the frequency event. In order to efficiently present this method using the transfer function, the derivation can be initiated with an equation in (6.14) from (6.2), (6.7), and (6.8) to reach the formulation as (6.15), which indicates that SOC deviates such as first order filter by input of frequency deviation with DaSOF method. Equation (6.15) is readily understandable transfer function to take a look at the relation between ΔSOC and Δf with block diagram in Fig. 6.2(a).

$$\Delta SOC(s) = \frac{1}{K_E \cdot s}(\frac{1}{R}\Delta f(s) - \Delta SOC(s) \cdot K_f) \tag{6.14}$$

$$\frac{\Delta SOC(s)}{\Delta f(s)} = \frac{1}{K_f + RK_E s} \tag{6.15}$$

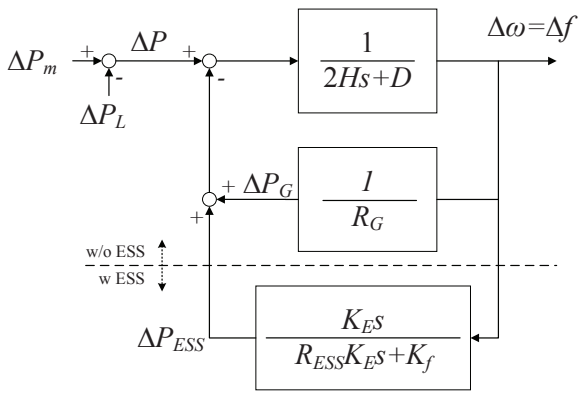

Figure 6.4: The block diagram of DaSOF ESS application on the system.

6.5.2 The Response of Power

From the excursion in consequence of a system condition change, e.g. demand or supply change, the frequency deviation can be supported by ESS power as much as droop characteristic at the initial point, and gradually reduces supporting power. For the DaSOF method, the equation of power response can be derived from (6.2), (6.7), and (6.8) to (6.16), and can be formulated to ESS transfer function as in (6.17), which becomes the type of high pass filter (HPF), especially the washout filter form with the gain $1/R$ and the time constant RK_E/K_f.

$$\Delta P_{ESS}(s) = \frac{1}{R}(\Delta f(s) - \frac{\Delta P_{ESS}}{K_E s} \cdot K_f) \tag{6.16}$$

$$\frac{\Delta P_{ESS}(s)}{\Delta f(s)} = \frac{K_E s}{R_{ESS} K_E s + K_f} \tag{6.17}$$

This relation between input and output would allow improving predictability and analysability to investigate ESS reaction in terms of power response in (6.17).

Initial Value of Frequency with DaSOF ESS

The characteristic of composite regulation in terms of aggregated droop control is introduced in Kundur's book [31], which can be extended to explain DaSOF ESS applied system in this section. The initial and final points are intimately linked with composite droop rate (R_{eq}). Right after contingency, initial status of ESS can approximately assume the Laplace operator goes to infinite; subsequently, transfer function results in inverse droop rate of ESS, as can be seen in (6.18).

In case distributed DaSOF ESSs can support the frequency of system, initial support starts with equivalent droop rate of parallel ESSs and generators in combined fashion as in (6.19). In this sense, equivalent droop rate of ESSs can be calculated by (6.20) such as parallel impedance calculation, which implies that if the same values of droop rate on two ESSs are applied in parallel, droop rate becomes half and allows to provide doubled power from certain frequency deviation.

The implication of frequency deviation supported by both ESSs and generators can

be described as in (6.21) with expression of equivalent droop control [31].

$$\frac{\Delta P(s)}{\Delta f(s)} = \lim_{s\to\infty} \frac{K_E s}{R_{ESS} K_E s + K_f} \cdot s \cdot \frac{1}{s} \simeq \frac{1}{R_{ESS}} \tag{6.18}$$

$$R_{eq} = \frac{1}{(\frac{1}{R_{ESS,1}} + \cdots \frac{1}{R_{ESS,n}}) + (\frac{1}{R_{G,1}} + \cdots \frac{1}{R_{G,n}})} \tag{6.19}$$

$$R_{ESS,eq} = \frac{1}{(\frac{1}{R_{ESS,1}} + \frac{1}{R_{ESS,2}} + \cdots \frac{1}{R_{ESS,n}})} \tag{6.20}$$

$$\Delta f(s) = \frac{1}{D + 1/R_{eq}} \cdot \Delta P(s) \tag{6.21}$$

where R_{eq} is equivalent droop rate of ESSs and generators, $R_{ESS,eq}$ is equivalent droop rate of ESSs, $R_{ESS,n}$ and $R_{G,n}$ are droop rate of nth ESSs and generators in pu respectively, and D is load damping component.

Final Value Theorem for Frequency with/without DaSOF ESS

Final value theorem allows for the examination of the final value of the time function by analysing its Laplace form at s=0 indicated in (6.22), [102].

$$\lim_{t\to\infty} g(t) = \lim_{s\to 0} sG(s) \tag{6.22}$$

where $\mathcal{L}[g(t)]$=$G(s)$, $g(t)$ is a function of time, and $G(s)$ is a function of Laplace formation.

Total transfer functions of excluding and including ESS in Fig. 6.4 are formulated into (6.23) and (6.24) respectively.

The power deviation of load is assumed as step function ($\Delta P_L(s)/s$) as an input event. As a result, both (6.23) and (6.24) are converged into the same result in (6.25), when s becomes zero. This result in (6.25) implies that the power support of ESS di-

minishes in the long term, and only the support of generators remains. Thus, the factor of ESS does not remain in (6.25), and the characteristics of generators and loads only remain in (6.25), indicating that deviation of power is highly dependent on generator droop rate and load damping.

$$\Delta f_{ss} = \lim_{s \to 0} \frac{s \cdot \Delta P(s)/s}{2Hs + D + 1/R_G} \tag{6.23}$$

$$\Delta f_{ss} = \lim_{s \to 0} \frac{s \cdot \Delta P(s)/s}{(2Hs + D + 1/R_G) + (K_E s/(R_{ESS} K_E s + K_f))} \tag{6.24}$$

$$\Delta f(s) = \frac{1}{D + 1/R_G} \cdot \Delta P(s) \tag{6.25}$$

where Δf_{ss} is steady state of frequency deviation, R_G is droop rate of generator, H is inertia constant, D is load damping component, ΔP is deviation of power in pu, R_{ESS} is droop rate of all ESSs, K_E [MWs] is the energy of ESS, and K_f [Hz/%] is the coefficient

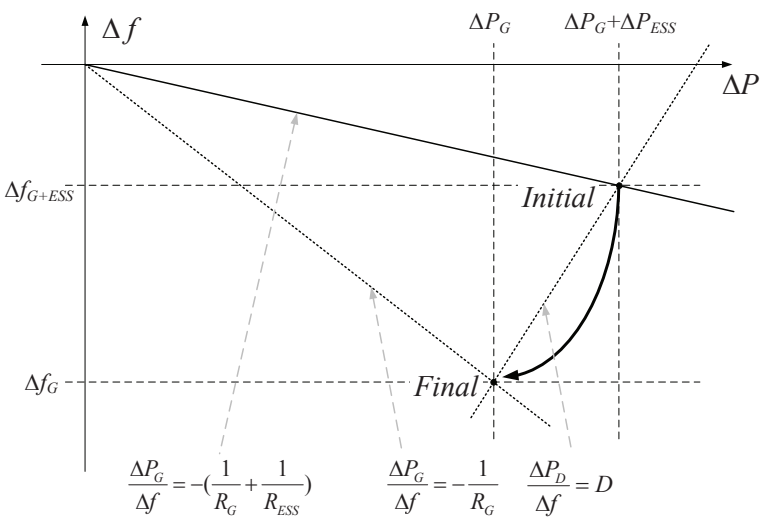

Figure 6.5: Net frequency sensitivity for initial and final values of frequency with DaSOF ESS, composite governor and load characteristics.

for allocation between SOC and frequency compensation range.

Graphical Description of Initial and Final Point

As indicated in previous two sections, initial and final points of frequency compensated by DaSOF ESS can be calculated by (6.21) and (6.25), and those equations can be illustrated as Fig. 6.5 based on the analysis method of the net frequency sensitivity in Kundur's book [31].

Fig. 6.5 shows the initial compensation is provided by ESS and the generator power ($\Delta P_G + \Delta P_{ESS}$); consequently, the frequency deviates slightly to Δf_{G+ESS}. On the other hand, long-term power compensation of ESS is not sufficient due to SOC management, and only generators provide the power (ΔP_G) without ESS support. Subsequently, frequency deviation moves to final point in Fig. 6.5. The trajectory from the initial to final points moves as first order function.

Verification of Initial and Final Point

In this section, the investigation is carried out for three subjects; Case-a: generators only with governor control that is applied to the other cases as well, Case-b: ESS with droop only (w/o DaSOF), and Case-c: ESS with DaSOF method under the condition with step load change at 50 [s].

Under the assumption of the constant load change leading to frequency deviation (Δf) in Fig. 6.6, ΔSOC_{ref} would experience the variation according to frequency deviation (Δf) change. Subsequently, ΔSOC changes as the form of first order low pass filter (LPF) in (6.15), which exhibits the response with the time constant as RK_E/K_f and the gain as $1/K_f$, when the time goes to infinite as can be observed in Fig. 6.6(b) Case-c. This phenomenon in Fig. 6.6 can be explained as this method considers the limited energy of ESS, which intends to maintain SOC for slight frequency deviation (Δf) in preparation of much severer frequency drop.

In Fig. 6.6, after the load change at 50 [s], the frequency drops in short time and remains constantly in Fig. 6.6(a) Case-a by the influence of the droop control by generator governor.

Case-b illustrates ESS droop control without SOC management and ESS offers con-

stant power, which leads highly reduced deviation of frequency in Fig. 6.6(a) and constant battery power in Fig. 6.6(c) and linear decrease of SOC in Fig. 6.6(b). However, ESS with the limited energy exhibits the limited performance duration to support the power. For instance, when ESS power in Fig. 6.6(c) provides constant power in response to frequency deviation, the supporting power make all reserve and SOC run out as shown in Fig. 6.6(b) Case-b, which indicates ESS cannot achieve sustainable frequency regulation due to the failure of SOC management.

Case-c in Fig. 6.6(c) illustrates the response of the DaSOF ESS power in (6.17) indicating that the power acts like HPF.

The proposed method in Case-c allows for compromising between frequency deviation and stored energy to pursue both supporting frequency and preserving the potential supportable energy in ESS for further deviation. After the demand change, the initial supporting power of the battery equals to the power in Case-b; however, the quantity of

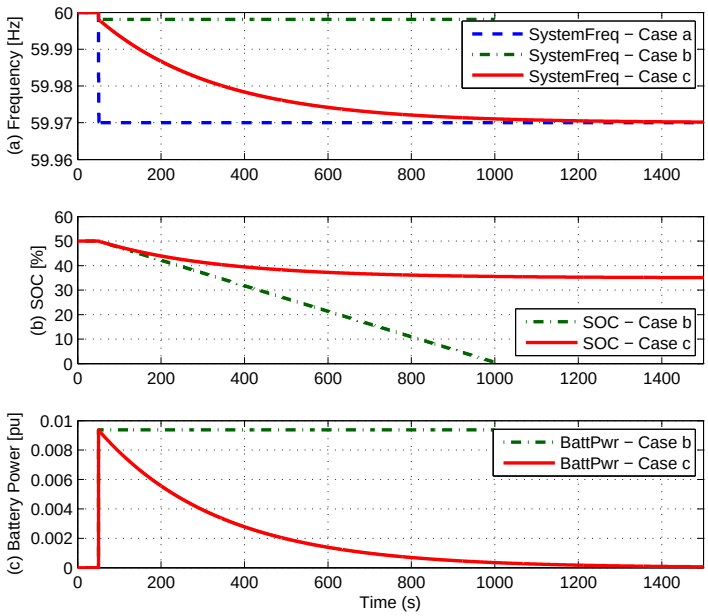

Figure 6.6: Outline of frequency deviation: Case-a: Without ESS, Case-b: with droop control, and Case-c: with DaSOF method.

power gradually becomes zero such as high pass filtered value in Fig. 6.6(c), and the deviation of SOC also remains constant such as low pass filtered value due to (6.15).

Consequently, the deviation of frequency starts with the full support of the ESS as Case-b, but finishes without support of the ESS such as Case-a. This operation can be explained as ESS is managing SOC for the long term.

Such considerations are of particular importance to understand the behaviour of proposed method to compromisingly seek the support of frequency and the conservation of energy.

6.5.3 The Influence of ESS Size and Droop Rate

In order to investigate ESS performance from given transfer functions at (6.17), the selectable parameters are R_{ESS}, K_E, and K_f, denoting droop rate, ESS energy, and frequency compensation range, respectively. Regarding this, the indications of responses in terms of ESS power, such as cut-off frequency and settling time, are directly associated with the characteristics of both network frequency and ESS energy management, thus the cut-off frequency and settling time of the ESS power on the basis of (6.17) are worthwhile to be explored.

Response Characteristics of DaSOF Condition Change

In this section, the influences of the ESS size change and the droop rate change on both cut-off frequency and settling time are investigated though three cases by comparing different ESS sizes (X) and the number of parallel converters (Y). In regard to this, (6.26) indicates cut-off frequency of ESS transfer function at (6.17), composed of the factors (R_{ESS}, K_E, and K_f) with Y and X. The equation (6.27) stands for settling time (5%) from a calculation method in (6.28) [102], when damping ratio is over 0.69. Table 6.1 presents gain from (6.5), cut-off frequency from (6.26), and settling time from (6.27) in each case for different X and Y situations.

$$f_a = \frac{1}{2\pi}\left|\frac{K_f}{(R_{ESS}/Y)(K_E \cdot X)}\right| \tag{6.26}$$

$$t_{s,ESS} = \frac{4.5(R_{ESS}/Y)(K_E \cdot X)}{K_f} \tag{6.27}$$

Table 6.1: Response Characterisics of ESS

	The Cases	X	Y	Gain (db)	Cut-off Freq.	Settling Time
Case1	Single ESS	1	1	5 (13.98)	7.3683 e-04	972
Case2	Two ESS in parallel	2	2	10 (20)	7.3683 e-04	972
Case3	Two Times Larger ESS	2	1	5 (13.98)	3.6841 e-04	1944

$$t_s = \frac{4.5\zeta}{\omega_n} \qquad (\zeta > 0.69) \tag{6.28}$$

where f_a is cut-off frequency of ESS, Y is the parallel number of ESS, X is total ESS size compared to single ESS size, $t_{s,ESS}$ is settling time of ESS, t_s is settling time to arrive at settling point within 5%, ζ is damping ratio, and ω_n is natural undamped frequency.

Firstly, 'Single ESS' in Case 1 stands for indication of comparison consisting of one ESS and one converter, which gain, cut-off frequency, and settling time are listed in Table 6.1.

Secondly, in Case 2 for 'Two ESSs in parallel', droop rate (R) becomes half of the original value and gain becomes double according to (6.20). In regards to the usable size of ESS (K_E), it becomes twice of single ESS. As consequences, the cut-off frequency and settling time are constant, because X/Y is one in (6.26) and (6.27); however, gain (Y/R) is increased as twice of Case 1 in Table 6.1 owing to the decrease of droop rate in half by (6.20). In this sense, distributed ESS can independently regulate frequency all together in decentralized manner for the certain frequency deviation in power system.

Thirdly, 'Two times larger ESS', Case 3, indicates the case with double-sized ESS without the change of droop rate. As a result, the coverage of this case can be extended to much lower frequency band, because settling time increases as in Table 6.1 and the ESS, embracing higher energy, can support the power for longer time, although initial value linked with gain is identical to the Single ESS case.

Analysis of DaSOF ESS on Bode Plot and Time Domain

Fig. 6.7 and 6.8 compare the three case studies in Table 6.1 using bode plot in Fig. 6.7 and its time response in Fig. 6.8 concerning DaSOF transfer function in (6.17). The graphs in Fig. 6.7 and 6.8 imply DaSOF method enables ESS to serve as high pass filter, and the number and size of connection can differ the characteristics of DaSOF ESS.

Compared to Case 1, Case 2 is also undoubtedly bound up with the increase of gain; therefore, the magnitude of Case 2 increases on the bode plot in Fig. 6.7, and the initial value is magnified twice of Case 1 on time frame in Fig. 6.8; however, the compensation frequency range and settling time between Case 1 and 2 can be identical as analysed in Table 6.1.

The frequency coverage of Case 3 is extended to lower frequency band without the change of gain in Fig. 6.7. In this regard, on the time domain, the value of Case 3 initializes as that of Case 1 but provides durable support for the longer time and lower frequency band.

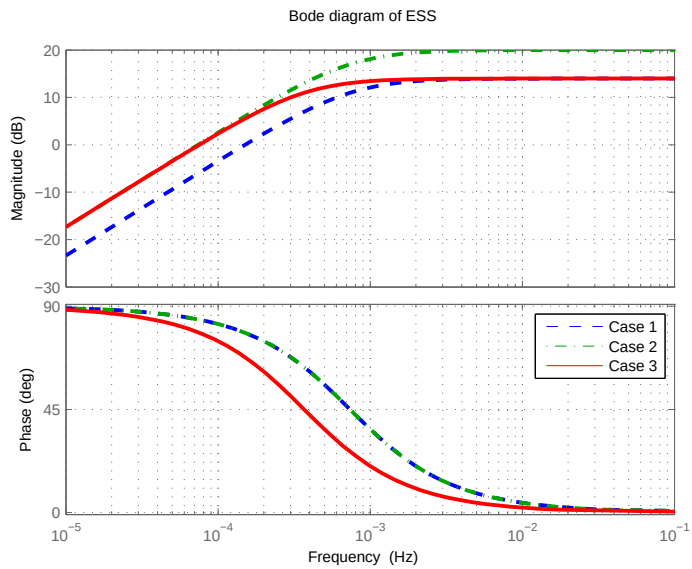

Figure 6.7: Bode plot of DaSOF transfer function: Case 1: Single ESS, Case 2: Two ESSs, Case 3: Two times larger ESS.

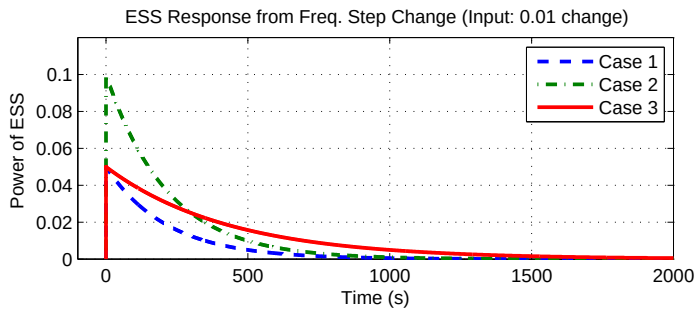

Figure 6.8: Response of DaSOF method: Case 1: Single ESS, Case 2: Two ESSs, Case 3: Two times larger ESS.

Fig. 6.9 displays the interrelationship between K_E and R with X and Y to observe cut-off frequency change in regard to the case studies. Fig. 6.9 attempts to address that when parallel ESS number (Y) increases (droop rate (R/Y) decreases), cut-off frequency rises; however, when operational energy of ESS ($K_E \cdot X$) increases, cut-off frequency

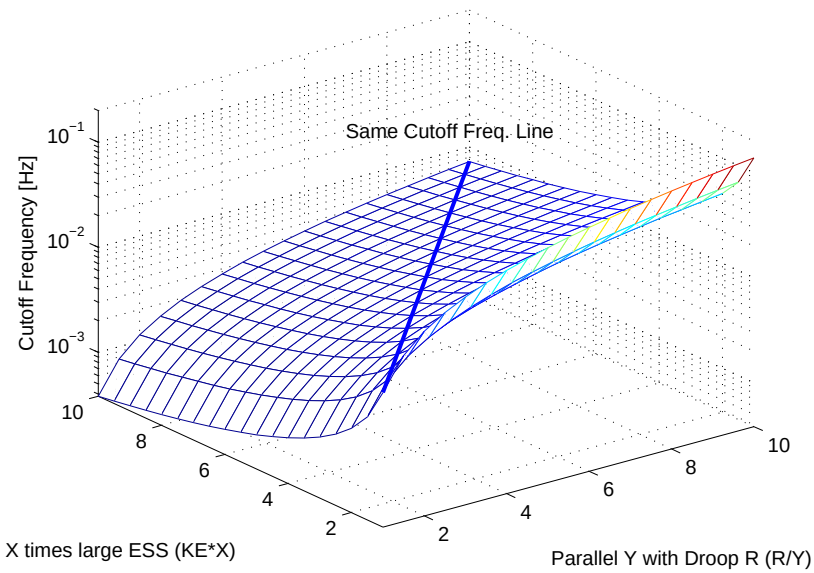

Figure 6.9: Cut-off Frequency in terms of total ESS size (X) and droop rate change (Y)

decreases according to (6.26). Furthermore, it can be noticed that cut-off frequency constantly remains where X and Y match.

On the other hand, the tendency of settling time exhibits inversely proportional to cut-off frequency, thus the higher value of cut-off frequency in Fig. 6.9 converts into lower value, and the lower value converts into higher value as can be shown in (6.27).

For the parameter selection, It can be considered as K_f can be determined for how much frequency range ESS covers in (6.9), then initial value of ESS power can be determined with droop rate as in (6.5), and the size of ESS (K_E) can be determined for the duration of energy supply or the coverage of frequency using settling time or cut-off frequency in (6.27), (6.28), respectively.

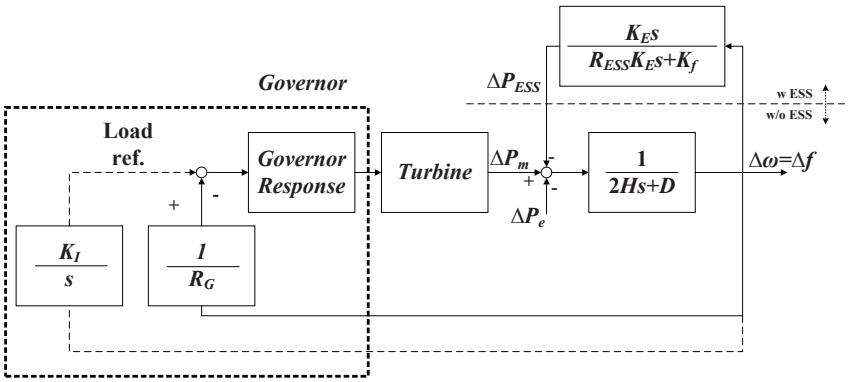

Figure 6.10: Block diagram of system for frequency stability study.

Table 6.2: Parameters for Frequency Stability

Variable	H	K_E	R_G	D	K_f	K_I	R_{ESS}
Value	5	1.8	0.05	0.01	0.1 /60	20	0.2

Droop rate of ESS is considered with system rating, and frequency and SOC are pu. (60Hz and 100% respectively)
System base and rating is 1 GW. Single ESS size is 500kWh.

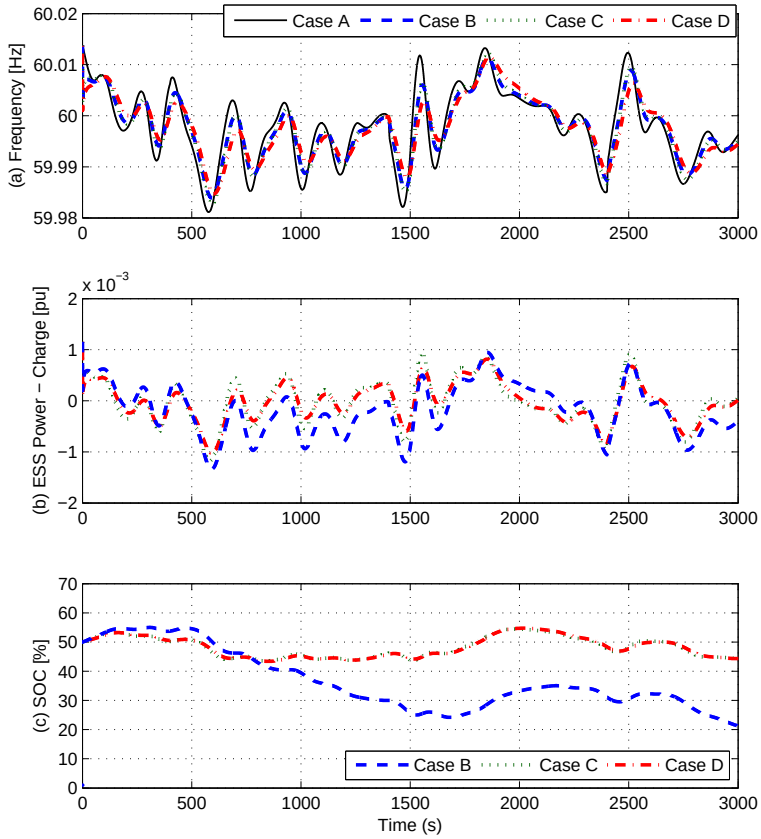

Figure 6.11: The DaSOF ESS effects on renewable Integration case: Case A: w/o ESS, Case B: with droop control only, Case C: five DaSOF ESSs, Case D: ten DaSOF ESSs.

Table 6.3: The Cases for System in Fig. 6.10

The Cases	Control Method	The Number of ESS	Single ESS Size	System Inertia Constant(H)
Case A	-	0	-	5
Case B	Droop only	5	500kWh	5
Case C	DaSOF	5	500kWh	5
Case D	DaSOF	10	500kWh	5

Wind Rating: 200MW with variable Load.
All the parameters are the same as Table 6.2.

6.6 Frequency Stability in Case of DaSOF ESS

For the verification of DaSOF ESS on the power system, the system configuration is formulated by including Turbine and Governor responses based on the reheat steam turbine generator model [31] as depicted in Fig. 6.10.

The transfer functions in terms of Governor and Turbine responses are assumed as (6.29) and (6.30) respectively, which indicates the time delay of valve adjustment in (6.29) and simplified transfer function for the disturbed values of the turbine power and control valve position in (6.30).

DaSOF ESS in Fig. 6.10 aims to provide the power (ΔP_{ESS}) from external power event in electrical power ΔP_e, which includes fluctuations of renewable generation and contingencies from load, line, etc.

$$G_{Gov}(s) = \frac{1}{1 + sT_G} \tag{6.29}$$

$$G_{Tur}(s) = \frac{1 + sF_{HP}T_{RH}}{(1 + sT_{CH})(1 + sT_{RH})} \tag{6.30}$$

Output power and the droop rate of ESS are calculated with the system base as in Table 6.2, and DaSOF ESSs are installed on the system as can be illustrated in Fig. 6.10. The load event with 0.01 [pu] occurs at 100 [s].

Advantage of DaSOF method for the system

The efficient and harmonious operation of ESSs for a system should be investigated; accordingly, the aim of this chapter is to exploit droop control and SOC feedback for complementary operation with the conventional electric power system.

The benefits of this droop control method are:

- $Harmonious\ operation$: Enabling ESS to naturally operate and coordinate with the existing frequency regulation for reciprocal compensation between generators and ESSs
- $Parallel\ operation$: Providing simultaneous compensation with conventional generators and other ESSs in network.
- $Decentralized\ control$: Controlling ESS for frequency regulation and SOC management in a decentralized fashion.
- $SOC\ consideration$: Determining the quantity of supportable power in consideration of battery SOC.
- $LPF\ of\ frequency$: Smoothing sudden changes of frequency, and increasing the analysability of the compensable frequency band.

In Fig. 6.12, supporting power from ESS is provided to power system as in left side of Fig. 6.12, and it supports the frequency regulation with conventional frequency control devices against the disturbances (RES and Load). This power balance problem among Load, RES, conventional generation, and ESS is reflected in frequency deviation (Δf), which works as ESS reference input. For the ESS internal procedure in right side of Fig. 6.12, supporting power change the SOC and f_{ofs}, which follows Δf.

The role of ESS is to assist FR in considering the condition of system and device against perturbation from the generation, RES, and load as in Fig. 6.12, which make generator and ESS operates complementarily and harmoniously.

In this regard, the small size ESS compared to the system does not have a huge influence on the system side, and SOC would experience the significant change due to the compensation of frequency conducted almost only by generators. However, if the huge number of ESS installed in parallel, and if total ESS reserve is large capacity, the compensation of total ESS would have a significant influence on the system frequency,

and deviation of frequency Δf would be decreased. As a result, since the change of $f_{ofs,ref}$ (Δf) would not be significant, the change of SOC and f_{ofs} would be decreased as well.

6.6.1 Frequency Coordination with Conventional System

A reduced number of conventional generators would be the root of two problems in terms of frequency regulation: reducing the inertial energy and lowering the aggregated droop slope of the system. Both problems are located in the primary response, the fastest time domain in the frequency control sequence in Fig. 6.13. The role of each ESS within the existing frequency compensation procedure should be clearly defined for well-balanced ancillary service provision under high penetration.

The following role of ESS was suggested for existing FR.

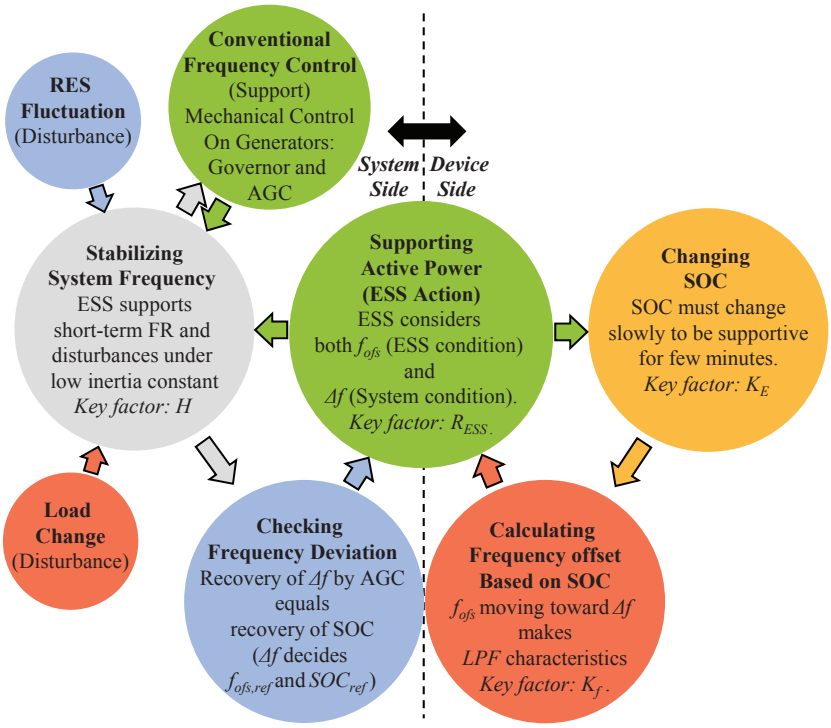

Figure 6.12: An overall picture of the proposed approach description.

- Primary control: The static reserve (ESS) supports inertial energy and governor control.
- Secondary control: Generators take charge of frequency recovery; subsequently, the ESS recovers SOC.

Mutual compensation between conventional generators and ESS can be enabled with this method. Its characteristics as a high pass filter allow ESS to be placed in primary reserve, and the re-dispatch and AGC action of generators are responsible for eliminating a steady state error of frequency; meanwhile, frequency recovery leads to the SOC recovery of the ESS.

Therefore, the ESS operation melts into the frequency regulation of the conventional system, enabling complementary operation.

6.6.2 Frequency Control with Governor System

The study outcome to be presented in this section has assumed that conventional generation units regulate the frequency with governor.

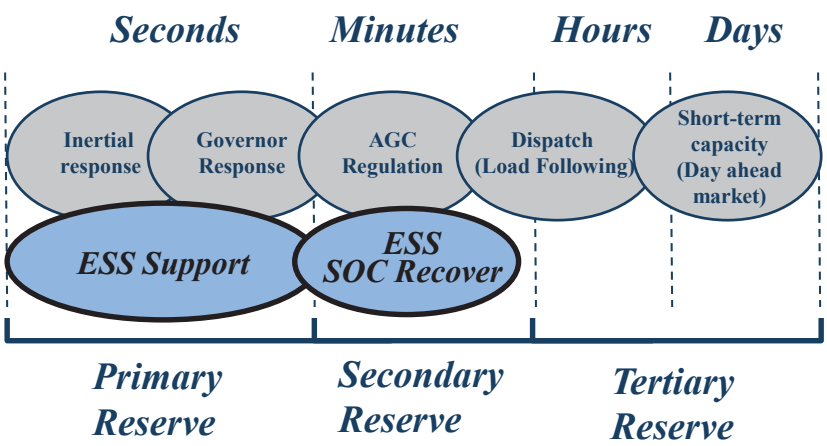

Figure 6.13: Coordinated operation of the energy sources: Multiple values from the ESS along a time line.

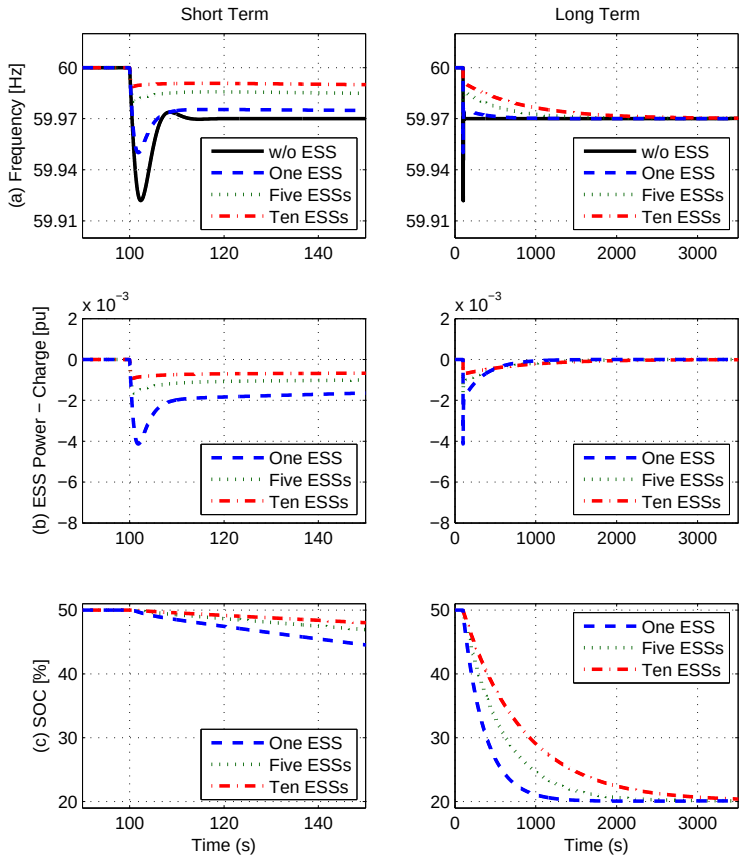

Figure 6.14: The influence of increased number of ESS for Long Term and Short Term: w/o ESS, Single ESS, Five ESSs, and Ten ESSs.

The Influence of ESS Numbers

In order to figure out the differences among ESS installation numbers, It is intended to increase the number of ESS, resulting in the increase of both X and Y on (6.26) and (6.27).

Apart from previous cases in Fig. 6.3 where assumption is made as frequency deviation is constant value, practically system frequency would not experience constant frequency deviation due to the influence of ESS compensation. Moreover, the increase of ESS numbers leads to increased initial power support by ESS, and the system would receive the increased power support at the beginning. Thus, the increased number of ESS tends to reduce the grid frequency deviation right after contingency.

In ESS point of view, the initial power and supporting duration due to the input of ESS which is system frequency compensated by ESS itself in Fig. 6.14(a) have the differences among the cases of ESS number change. Basically, the cut-off frequency and time constant of ESS do not experience the change, since the multiplication between the total energy of ESS (K_E) and droop rate (R) in (6.26) and (6.27) remains constant. However, the differences between the cases are coming from different level of ESS input frequency deviation, and it leads the change of ESS power and SOC. In short, when the contingency happens, the higher number of ESSs supports higher power for the system, and for this reason, the frequency deviation decreases. Therefore, due to the decreased frequency deviation meaning decreased ESS input value, the SOC and power from the larger number of ESSs changes less then that of the lower number of ESSs.

Fig. 6.14 for the comparison of one, five, and ten ESSs in parallel illuminates the fact that the supporting power from the plural ESSs reduces frequency deviation in short term and changes settling time in long term as the number of ESS increases in Fig. 6.14(a) as aforementioned. The initial power from each ESS in short term of Fig. 6.14(b) is reduced as ESS number increases and its responses have differences in long term. Because of these different power responses, the trajectories of SOC have also differences in responses, and the steady state values of SOC are based on (6.25) in long term of Fig. 6.14(c). The result in this section indicates the larger number of ESS connected in parallel manner can be effective for the short term frequency stability, as the fleet of ESS all together provides high power.

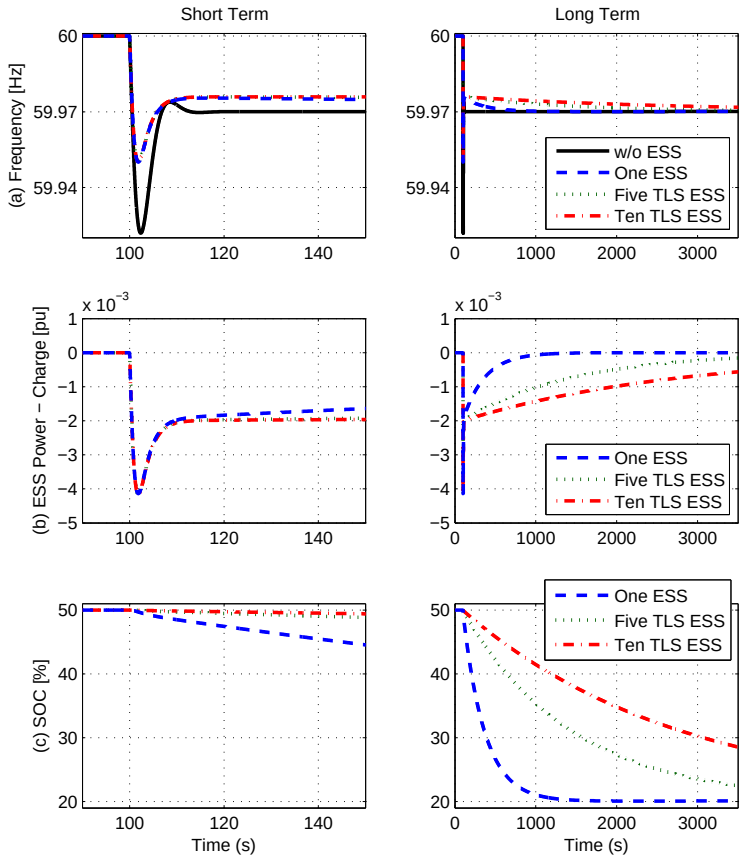

Figure 6.15: The influence of increased ESS size with Constant droop rate: w/o ESS, Single ESS, Five times larger size (TLS) ESS, and Ten times larger size (TLS) ESS.

The Influence of ESS Size

When ESS size (K_E) increases without droop rate (R) change, the initial power support regarding droop rate is not influenced, as initial power depends only on ($1/R$). The rise of ESS size (K_E) results in the the change of response characteristics; the decreases of cut-off frequency as in (6.26), and the increases of settling time as in (6.27).

Observe in Fig. 6.15(a) that initial responses of frequency are identical in short term and the decaying characteristics in long term exhibit different tendency, which implies that the supporting powers are equally initiated due to droop rate. However, supporting duration and its cut-off frequency become different due to ESS size, as can be shown in Fig. 6.15(b). Additionally, the SOC change has also different characteristics in Fig. 6.15(c).

6.6.3 Coordination with Load Frequency Control

ESS and Generator can cooperate with each other to complementarily cover drawbacks of the others and to offer mutual compensations, because the inborn characteristics of ESS can be defined as limited energy and faster action, while that of generator can be defined as unceasing energy and slower action.

More precisely, the operation of Load Frequency Control (LFC) drives system frequency to become nominal value, and it provides enormous energy within few minutes to match the balance between consumption and generation. On the other hand, when system frequency returns to nominal value (f_n), ESS recovers the central SOC (SOC_{cen}) after providing ancillary service within few second, as noted in Fig. 6.2(b) and Fig. 6.3.

Namely, for the second frame, ESS takes the responsibility of the ancillary service to support governor action, and for minute frame, the generator takes the responsibility of the ancillary service through LFC, where ESS should launch energy management, thus DaSOF method can be explained as negative LFC. Fig. 6.16 presents harmonious operation between ESSs and generators installed with parallel ESS with LFC control based on Fig. 6.10. The fleet of ESSs supports the power for short term in Fig. 6.16(b) and lessens frequency deviation in Fig. 6.16(a), and for the longer term, the operation of LFC is carried out to recover frequency to nominal value and the DaSOF ESS method manages its energy by adjusting SOC to central value in Fig. 6.16(c) as explained in Fig. 6.2.

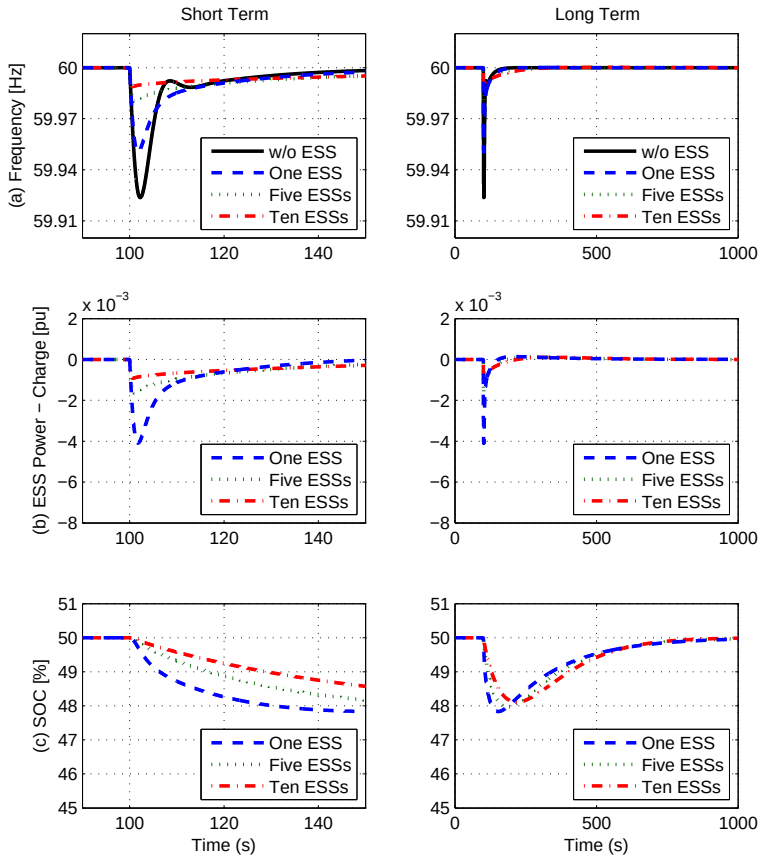

Figure 6.16: Coordinated frequency regulation with increased number of ESS: w/o ESS, Single ESS, Five times larger size (TLS) ESS, and Ten times larger size (TLS) ESS.

6.7 Efficacy in Renewable Integrated System

The fluctuation of renewables in small sized network critically affects the frequency stability, especially in reduced inertia constant generation system. This chapter aims to observe how much DaSOF method reduces frequency fluctuation and manages its energy compared to No-ESS case and droop only case.

6.7.1 System Configuration and Parameters

The case studies are organized as in Table 6.3; Case A: No-ESS, Case B: ESS with droop only (w/o DaSOF method), Case C: five DaSOF ESSs, and Case D: ten DaSOF ESSs. All of the parameters regarding the inertia constant of the system and the size of ESS are equal. Owing to the uncertainty of renewables, the variation of total generation is the inevitable facts; consequently, rapid fluctuation of generation shakes the network frequency as can be seen in Fig. 6.11(a).

6.7.2 The Results of DaSOF Application on Renewable Source Integration Case

Against the backdrop above, ESS can resolve the insecure behaviour as in Fig. 6.11, presenting that the operation of Case C and D manages SOC to confine energy in operation range around 50% in Fig. 6.11(b), and supports power to reduce frequency deviation in Fig. 6.11(a), while Case B compensates the higher power than the cases of DaSOF ESS in Fig. 6.11(b) but shows unstable operation trajectory of SOC by integrating the error of SOC and goes to 0% of SOC in Fig. 6.11(c).

It can be noticed that even though the frequency trajectory between Case B and C in Fig. 6.11(a) is nearly identical, the SOC behaviour in 6.11(c) is totally different, which indicates DaSOF ESS effective way to manage SOC.

6.8 Effect on A Highly Penetrated Bulk System

6.8.1 Simulation Environments

On the basis of the Australian Future Grid Scenario [23, 24], the highly complex system is designed, as can be seen in Fig. 6.17. In this system, most of Concentrating Solar

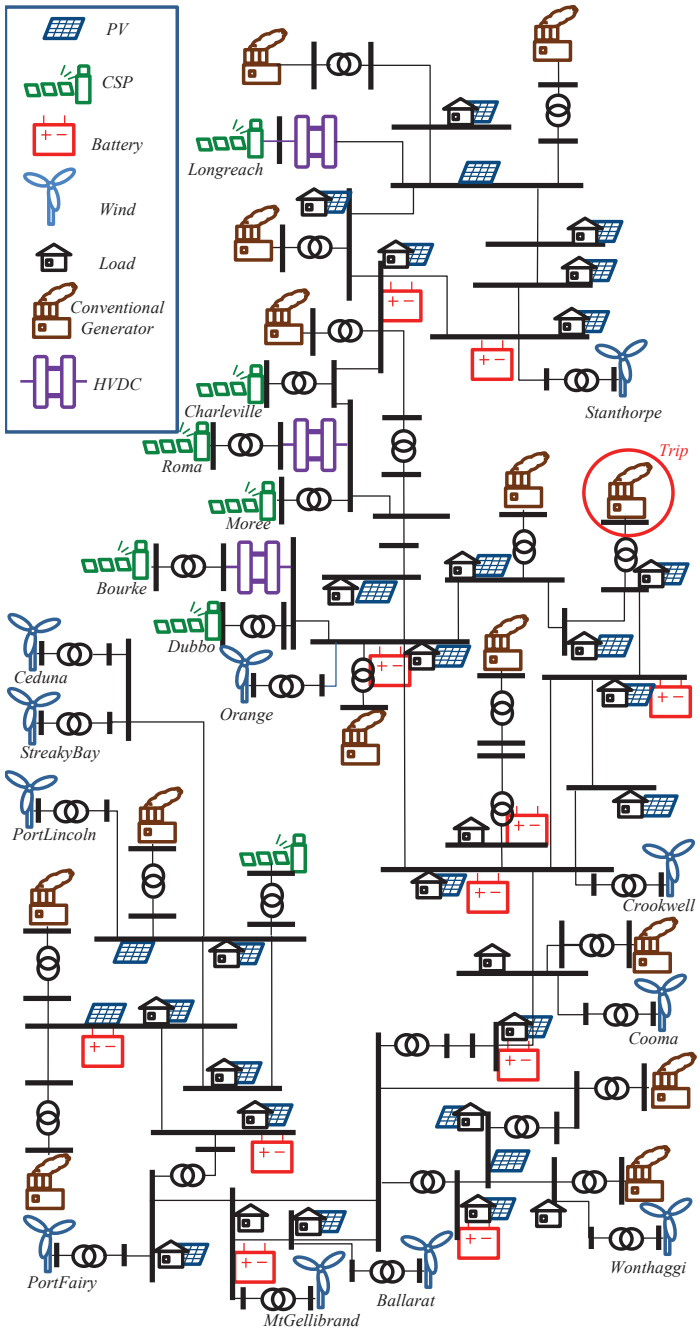

Figure 6.17: The 14 Generator Model (Simplified Australian System) based on the Australian Future Grid Scenario

thermal power Plant (CSP) is located in central area of Australia, and WPPs are spread along the sea especially in the south of Australia.

Under the circumstance with fewer conventional generators, the inertia constant of the network can be reduced, and the increase of penetration level may increase the vulnerability of frequency stability. Aggregated inertia constants within coherent generation areas can be calculated through (6.31). As frequency is a global problem, widely spread ESS can enhance conventional system performance.

$$H_{tot} = \sum_{i=1}^{n_{gen}} H_i n_i \frac{S_i}{S_{base}} \tag{6.31}$$

where n_{gen}: the number of generators, n_i: the number of the i_{th} generator, S_i: the rating of the i_{th} generator; H_i: the inertia constant of the i_{th} generator; and S_{base}: the base of the system.

6.8.2 Generator Trip

When frequency deviation occurs due to an unexpected generator trip as marked in Fig. 6.17. Case 1 in Fig. 6.18 shows the frequency deviates almost 0.1 Hz; however, the reduced system inertia constant indicated in Table 6.4 makes the system highly vulnerable: frequency deviation in the same contingency case is highly affected, almost 0.7 Hz in Fig. 6.18.

Table 6.4: System Condition for Bulk System

	Case 1	Case 2	Case 3
Generation of Conventional Units	22,212.9 MW	13,984.7 MW	13,984.7 MW
Generation of RES Units	0MW	8,230MW	8,230MW
Inertia Constant(s) (S_{base}:1GW)	93.01 s	56.01 s	56.01 s
Penetration level (%)	0	32.18	32.18
Static Reserve (ESS)	-	-	220 MW

As a counterpart of this phenomenon, widely spread ESSs for frequency regulation are adopted to assist frequency regulation; as a result, the frequency profile is considerably improved but shows a delayed tendency because of ESS support during the short term and ESS SOC recovery during the long term.

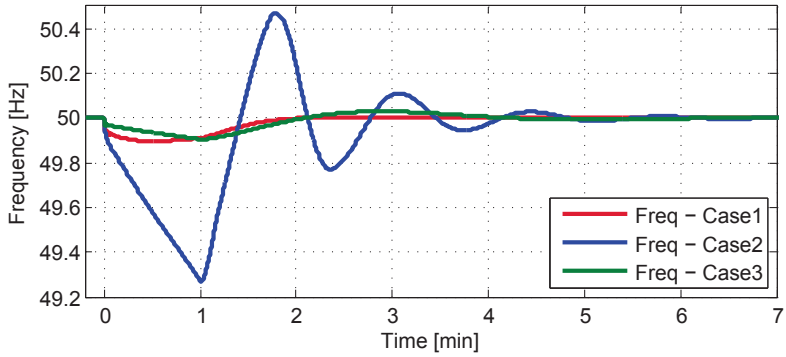

Figure 6.18: Single generator trip case in 14 Generator Model

6.8.3 Renewable Integration

In the renewable fluctuation case, the Photovoltaic (PV) and WPP data are applied to the system as in Fig. 6.19(a) and (b), and the extremely uncertain characteristics of RES raise an imbalance between production and demand. As a consequence, it causes a frequency fluctuation problem; moreover, the reduced inertia constant can deteriorate the existing problem.

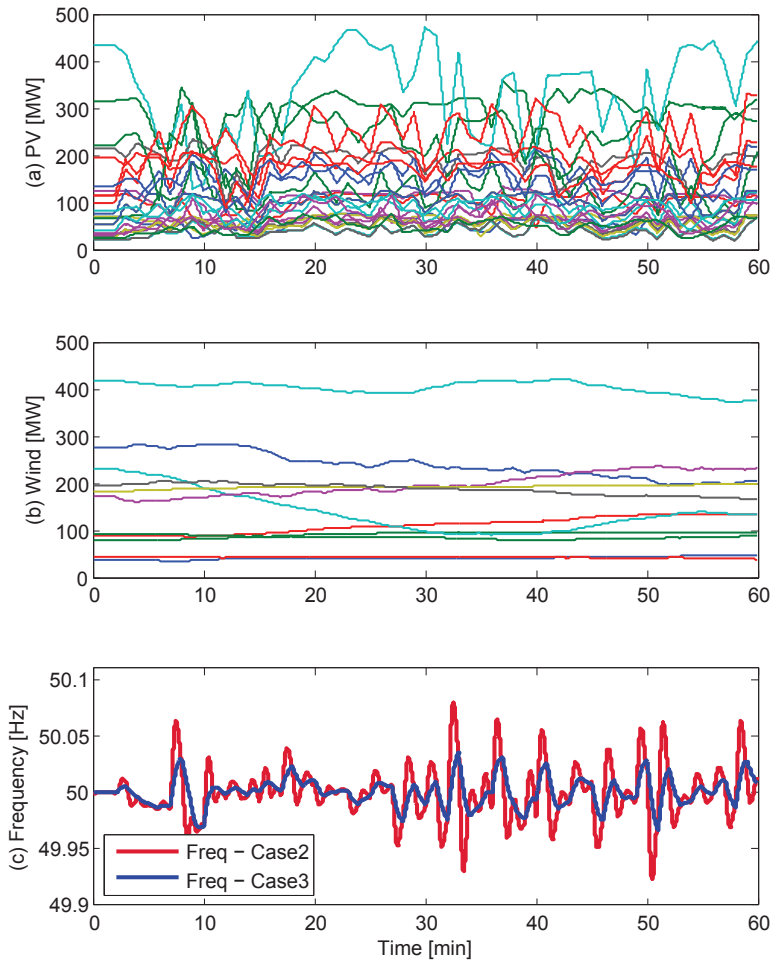

Figure 6.19: Renewable fluctuation case on 14 Generator Model: (a) PV power (b) Wind power, and (c) System frequency

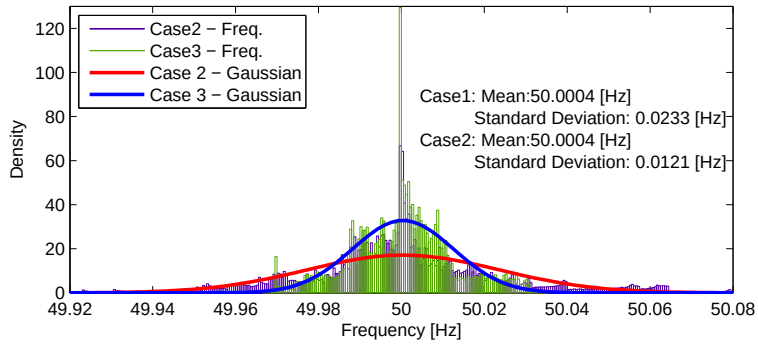

Figure 6.20: Frequency data profile and its Gaussian distribution graph for Case 2 and Case 3.

The governor and AGC action have relatively longer time delay and longer time constant than ESS operation; furthermore, the most influential factor is located in the faster time frame as explained earlier with Fig. 6.13. The system frequency with and without ESS is presented in Fig. 6.19(c). The contribution of ESS in Fig. 6.19(c) provides evidence of the explanation, which shows the ESS eliminates and takes charge of the high frequency band.

The frequency distribution of the collected data from Fig. 6.19(c) is illustrated in Fig. 6.20 for Case 2 and 3. In both cases, the data of the frequency concentrate on the nominal frequency, as mean values are nearly 50 Hz; nonetheless, the Case 2 shows an obviously wider distribution of frequency than that of Case 3.

The curve fitting of the Gaussian distribution based on (6.32) indicates that the density around the nominal frequency of Case 3 is higher than that of Case 2 thereby demonstrating the effectiveness of the proposed method. Most importantly, frequency deviation is nearly two times smaller according to the standard deviation in (6.33).

$$f(x,\mu,\sigma) = \frac{1}{\sigma\sqrt{2\pi}} exp[\frac{-(x-\mu)^2}{2\sigma^2}] \tag{6.32}$$

$$\sigma = \sqrt{\frac{n\sum x_i^2 - (\sum x_i)^2}{n(n-1)}} \tag{6.33}$$

where σ: standard deviation, μ: mean value, n: the number of data points, and x: data.

6.9 Summary

This chapter has attempted to sketch out novel methodology of frequency regulation purposed ESS enabling parallel operation with droop control method and the SOC management. This chapter provides a stepping-stone for developing mathematical theories and its analysis of method. Furthermore, the suggested analysis has strengthened theoretical basis using response indications and has examined the effects of size and parallel numbers of ESS. In the aspect of power system operation, the implications of ESS on governor system with droop and LFC operation cases have been investigated and it is tried to take a look into influences of ESS on the frequency fluctuating system due to renewable sources. The efficacy of the method in a practical bulk system underpins various analytical and theoretical foundations. As may be ascertained from the evidence above, this method facilitates ESS to manage SOC, to compensate frequency, to harmoniously operate with coordination of existing frequency regulation in several circumstances.

The results of the study may lead to various promising applications for future research and application.

Chapter 7

Bifunctional Methodology Maximizing EV Capability to Arrange for Ancillary Service on Frequency Coordination

Abstract– **This chapter unveils a V2G methodology of EV which is able to perform charging and frequency regulation together. This methodology combines Smart Charging method with Droop control and SOC Feedback (DaSOF) method to exhibit bifunctionality in regard to charging EV and providing ancillary service. This method can extract the benefits of DaSOF to execute decentralized parallel operation, filtering frequency, and harmonious operation with frequency control coordination. the phenomenon of the proposed charging method with transfer functions and state-space models on the basis of automatic control theory is also scrutinized. The feasibility of this method is verified on practical mid-sized island system to investigate efficacy of charging/non-charging status and harmoniousness with other generating units. The outcomes indicates the V2G service by EV compensation filters out the high frequency component without huge influence of charging status.**

7.1 Introduction

In regards to renewable sources embracing inherent variability and intermittency, some of the scholarly work has found that the possibility exists for renewable sources to endanger power system resiliency, and the growing concerns towards the high penetration level and reduced inertia constant inspire the scholars to conduct research concerning the way of alleviation of the facing problems.

Against this backdrop, ESS and Electric Vehicle (EV) are anticipating the emergence of the equipment to resolve these technical issues for grid modernization, as EV is promising methods of future transportation, expected to take large portion of vehicle market share and to geographically and widely spread around the power network [28], [29]. Subsequently, the academic efforts regarding EV have been widely rising through extensive studies and publications, and the countless research suggests and develops the methods of EV operation aiming at compensation of frequency as a supplementary frequency regulation. For instance, autonomous control of Vehicle to Grid (V2G) for frequency support with SOC balance [91] and decentralized V2G control considering charging demands from EVs [90] are studied. A tuning method of ESS controller is suggested for robust Load Frequency Control (LFC) under highly penetrated system [103]. The frequency regulation method with data acquisition via limited communication for Plug-in Electric Vehicle (PEV) is investigated [104]. A method that aggregator coordinates EV communication with AGC system is suggested [99]. EV stabilization for frequency support of Microgrid using Multiple Model Predictive Control is researched [105]. Regarding V2G issues, the review of V2G on distribution system is extensively executed [106]. Energy Storage System (ESS) is also emerging equipment for the future to stabilize power system in case of the increase of penetration level.

This chapter suggests the new method, a combination of two previous methods, to exploit both capabilities of previously introduced Droop control and SOC Feedback (DaSOF) method onto Smart Charging method. The suggested method intends to take both advantages, enabling EV to harmoniously mitigate the frequency deviations with previously established frequency coordination while charging.

The rest of the chapter organized as follows: Section 7.2 introduces previous study, and Section 7.3 sheds light on proposed method. In Section 7.5, proposed method is verified on Jeju Island and its effectiveness is indicated in Section 7.6. The chapter is

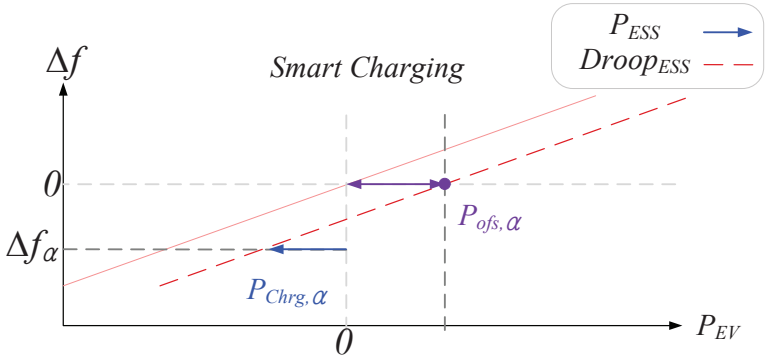

Figure 7.1: Smart Charging Method.

concluded in last of the chapter in Section 7.7.

7.2 Existing V2G and ESS Control Method

7.2.1 Smart Charging Method

The Smart Charging method attracts scholars attention after the first introduction in [91], which illuminates V2G methodology to protect frequency instability against intermittency of renewable resources in use of EVs and PHEVs.

Conceptually, in case contingency happens and frequency deviation takes place, EV can provide ancillary service proportional to the droop rate during the time when EV is charging the power as can be observed in Fig. 7.1. Namely, the quantity of charging power decreases or increases during the charging status, for the time frequency deviates.

This previous research also presents the SOC management scheme named Battery SOC balance control by inclining droop slope; however, the proposed method in this chapter places dissimilar scheme using an offset concept to manage SOC, which can be formed into transfer function.

7.2.2 Droop control and SOC Feedback Method

The DaSOF method was invented for the management of SOC by means of droop control for purpose of the ESS frequency regulation in Fig. 7.2.

The transfer function of DaSOF in (7.1) can be derived from (6.6)-(6.8), denoting the power of ESS theoretically responds as the type of high pass filter. This transfer function can be reformulated to the state space model as can be observed in (7.2), which would be the stepping-stone for the state-space model of the bifunctional EV operation methodology in following sections.

$$\frac{\Delta P_{ESS}(s)}{\Delta f(s)} = \frac{K_E s}{R_{ESS} K_E s + K_f} \tag{7.1}$$

$$\begin{aligned} \dot{X}(s) &= -\frac{K_f}{K_E R} \cdot X(s) + U(s) \\ Y(s) &= -\frac{K_f}{K_E R^2} \cdot X(s) + \frac{1}{R} \cdot U(s) \end{aligned} \tag{7.2}$$

where $X(s)$ is the state, $U(s)$ is the input and $Y(s)$ is the output of state space matrix.

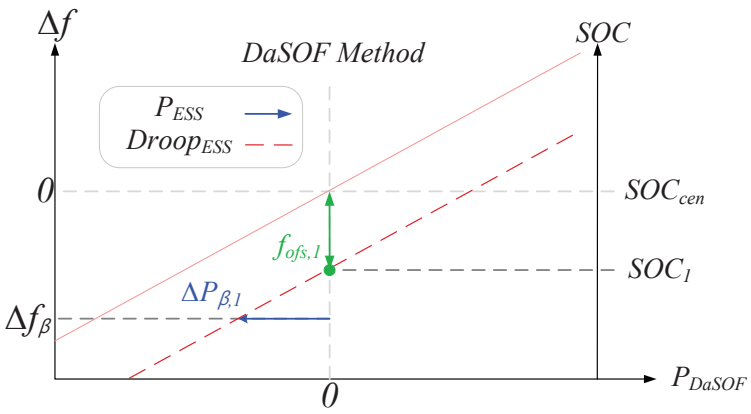

Figure 7.2: Droop control and SOC feedback method.

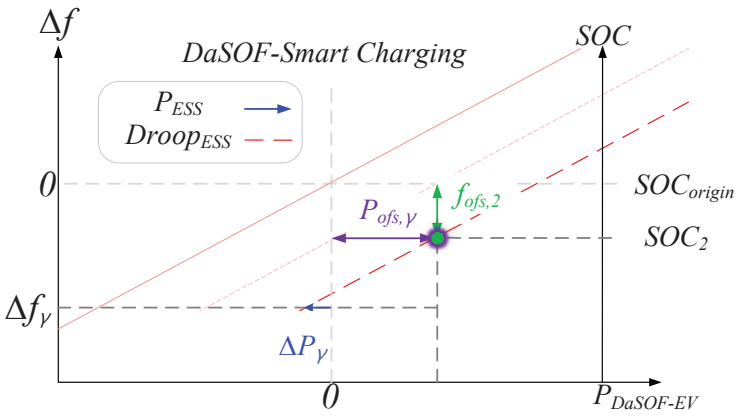

Figure 7.3: Proposed DaSOF-Smart Charging method.

7.3 Proposed DaSOF-Smart Charging for EV

Apart from the previous research that introduces managing SOC by inclining droop rate in [91], this method manages SOC with f_{ofs} and charges EV by linear change of SOC. The distinct advantage of this method is to enhance the analysability of ESS system and its output through the transfer function and state space matrix.

7.3.1 Operation Methodology

Operation at Contingency Condition

The basic principles of DaSOF-Smart Charging method posses the capability of both charging the power to EV and supporting the grid for the frequency deviation in accordance with droop rate during the charging state.

Fig. 7.3 sheds light on the suggested DaSOF-Smart Charging method with the combination of Fig. 7.1 and Fig. 7.2, and in this figure, x-axis presents the charging power of ESS and y-axis represents two factors; SOC and the frequency.

This method can be characterized as both P_{ofs} and f_{ofs} in combined fashion, which enables the energy on the battery to be filled in conjunction with the management of SOC considering frequency depth simultaneously. The green mark in Fig.3 manifests the central point (CP) of the droop rate and can serve as a meaningful indication of this

method.

When this method initiates, the CP shifts to right side of x-axis for EV charging, and y-axis is determined by SOC level of the EV battery based on the y-axis on the left as much as the distance between SOC reference and current SOC. Furthermore, the reference of the SOC corresponds to frequency deviation in y-axis on the left, and f_{ofs} calculated by current SOC is designed to follow frequency deviation.

Observe Fig. 7.3 that SOC_2 determines the f_{ofs2} (y-axis of CP) and the charging power for the EV exists as $P_{ofs\gamma}$. If frequency deviation happens as Δf_{γ}, ESS decreases the power as P_{γ}, and after the contingency situation, ESS supports the system as the moment of contingency would be relatively short compared to charging. Explicitly, the SOC level of the battery determines y-axis of CP and measured frequency determines the power of the battery in Fig.3.

EV Charging Principles

The case in Fig. 7.4 exhibits EV charging principle for the steady state without the contingency, and it is assumed as initial SOC settles down to SOC_3. If initial CP is located in point A (SOC_3) and EV charges as much as P_{ofs}, point A moves up to point B.

In this moment of charging, the command of EV charging power is maintained constantly as much as $P_{ev,ref}$ as can be presented in (7.3); consequently, the movement of point A to B, the change of $SOC_{ev,ref}$, rises linearly in Fig. 7.4.

In this sense, the position of nominal frequency in y-axis is sliding as in Fig. 7.4 and this can be explained in (7.4) denoting that $\Delta f = 0$ becomes $SOC_{FR,ref} = 0$, while SOC_{ref} constantly escalates due to linearly rising $SOC_{ev,ref}$ and constant $P_{ev,ref}$, although frequency deviation Δf equals zero. Thus, the value of y-axis on the right for SOC is fixed and $SOC_{ev,ref}$ value itself rises, when the value of y-axis on the left $\Delta f = 0$ is sliding up.

The charging power signal $P_{ev,ref}$ is changed to SOC reference signal $SOC_{ev,ref}$ in (7.4) and EV charging offset signal for f_{chrg}. The f_{chrg} plays a charging reference role as indicated in Fig. 7.5 and (7.5), as $f_{chrg}+\Delta f$ becomes f_{ref}.

Subsequently, f_{ref} is followed by f_{ofs}, and the deviation between f_{ref} and f_{ofs} proportional to the inverse droop rate turns into the EV power P_{ev} , which becomes a constant value, when frequency deviation is zero as aforementioned.

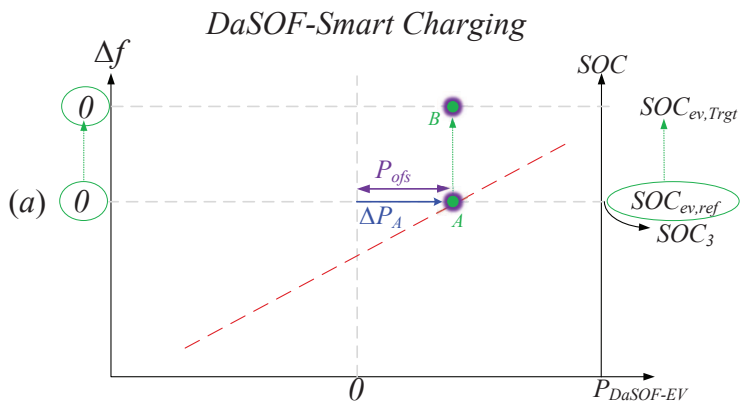

Figure 7.4: The movement of Central Point (CP) during the charging.

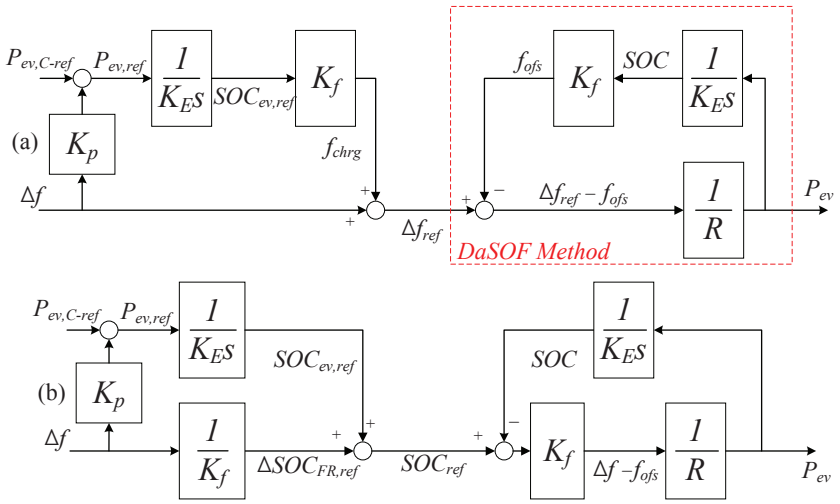

Figure 7.5: Transfer function of DaSOF-Charging method: (a) frequency based representation (b) SOC based representation.

$$SOC_{ev,ref} = \frac{1}{K_E s} P_{ev,ref} = \frac{1}{K_E s}(P_{ev,C\text{-}ref} + K_p \Delta f) \tag{7.3}$$

$$SOC_{ref} = SOC_{ev,ref} + SOC_{FR,ref} = \frac{1}{K_E s} P_{ev,ref} + \frac{1}{K_f} \Delta f \tag{7.4}$$

$$\Delta P_{ESS} = \frac{1}{R}(\Delta f_{ref} - f_{ofs}), \quad (\Delta f_{ref} = \Delta f + f_{chrg}) \tag{7.5}$$

$$\Delta f_{chrg} = K_f \cdot SOC_{ev,ref} = \frac{K_f}{K_E s} \cdot P_{ev,ref}(s) \tag{7.6}$$

where $SOC_{ev,ref}$ is EV SOC reference, $P_{ev,ref}$ is EV power reference considering frequency deviation, $P_{ev,C\text{-}ref}$ is constant EV power reference, K_p is the factor to change the power reference during the frequency deviation, $SOC_{FR,ref}$ is SOC for frequency regulation without considering EV charging signal, and f_{chrg} is frequency offset reference for EV charging.

7.3.2 Block Diagram of DaSOF-Smart Charging Method

Fig. 7.5 indicates the block diagram of the method, and the two equivalent block diagrams is illustrated in Fig. 7.5(a), (b) to be readily understandable. Fig. 7.5(a) focused and based on the left y-axis (frequency) in Fig. 7.3. This method assists to easily understand DaSOF method side and the function of droop rate, which can be explained as the output power is calculated by multiplying inverse droop rate with subtracted value from f_{ref} to f_{ofs}. Fig. 7.5(b) is depicted to assist understanding of the charging principles to express how ramp input $SOC_{ev,ref}$ functions in this methodology.

This block diagram consists of two inputs and one output noticeably; hence, it can be defined as Multiple Input Single Output (MISO) type, and each input has its own meaning as below. The first input from $P_{ev,ref}$ represented as constant value, and integration of $P_{ev,ref}$ value is changed to an energy concept. That is to say, constant injection of power

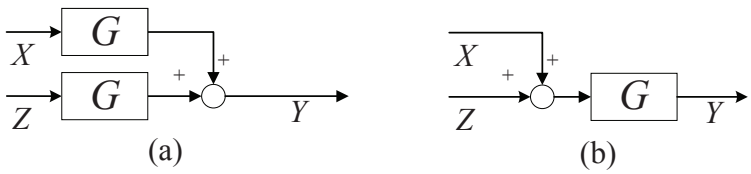

Figure 7.6: Basic rule of equivalent transfer function

to fill up the battery of EV is reflected into linearly rising SOC, which is an indication of energy. The second input, frequency deviation, aims to compensate frequency deviation and fluctuation by response only for high frequency band.

During the contingency, $SOC_{ev,ref}$ constantly and linearly increases due to constant $P_{ev,C\text{-}ref}$ whether frequency deviates or not; thus, after the contingency, the quantity of the EV power is little bit higher than set up value to follow up the $SOC_{ev,ref}$. For this reason, K_p is to reduce or increase the power reference $P_{ev,ref}$ when frequency deviation happens. The advantage of K_p=0 is to match the charging-time, and SOC is tracking the linear increasing $SOC_{ev,ref}$ with higher charge of P_{ev}; however, when K_p has a high value, the EV participates in ancillary service more actively, because $P_{ev,ref}$ itself decreases or increases to prevent the linear increase of $SOC_{ev,ref}$, depending on the frequency deviation.

7.3.3 Numerical Expressions of the Method

As this method is the type of MISO, it can be transformed to transfer function. In order to conduct the transformation, DaSOF part can be divided to the side of Δf and Δf_{chrg} as indicated as (7.7).

$$P_{ESS}(s) = \frac{K_E s}{R_{ESS} K_E s + K_f} \cdot \Delta f(s) + \frac{K_E s}{R_{ESS} K_E s + K_f} \cdot \Delta f_{chrg} \tag{7.7}$$

This transfer function can be developed to state space model in (7.8) on the basis of (7.2), which is added by both terms of transfer functions, frequency deviation side Δf and EV charging power $P_{ev,ref}$ in (7.7). This method allows for increasing the capability of analysis when EV applied on the power system.

$$\begin{bmatrix} \dot{x}_1(s) \\ \dot{x}_2(s) \end{bmatrix} = \begin{bmatrix} -\frac{K_f}{K_E R} & 0 \\ 0 & -\frac{K_f}{K_E R} \end{bmatrix} \begin{bmatrix} x_1(s) \\ x_2(s) \end{bmatrix} + \begin{bmatrix} 1 & 0 \\ K_p & 1 \end{bmatrix} \begin{bmatrix} P_{ref}(s) \\ \Delta f(s) \end{bmatrix}$$

$$P_{ESS}(s) = \begin{bmatrix} \frac{K_f}{K_E R} & -\frac{K_f}{K_E R^2} \end{bmatrix} \begin{bmatrix} x_1(s) \\ x_2(s) \end{bmatrix} + \begin{bmatrix} 0 & \frac{1}{R} \end{bmatrix} \begin{bmatrix} P_{ref}(s) \\ \Delta f(s) \end{bmatrix} \tag{7.8}$$

The response from EV charging reference $P_{ev,ref}$ to EV charging P_{ESS} becomes such as first order filtered output as can be expressed in (7.9). In case the EV charging reference changes into ramp input based on (7.3), the response from the input $SOC_{ev,ref}$ to P_{ev} can be expressed as (7.10), and steady state error in this transfer function may exist. According to the control theory, if the input is defined as in (7.11), steady state error can be defined as (7.12), and It can be noticed as the relation of SOC (7.10) has steady state error.

$$\frac{\Delta P_{ESS}(s)}{\Delta P_{ev,ref}(s)} = \frac{K_f}{RK_E s + K_f} \tag{7.9}$$

$$\frac{\Delta P_{ESS}(s)}{\Delta SOC_{ev,chrg}(s)} = \frac{K_f K_E s}{RK_E s + K_f} \tag{7.10}$$

$$r(t) = A \cdot t \cdot u(t), \;\; R(s) = \frac{A}{s^2} \tag{7.11}$$

$$e_{ss}(s) = A/(\lim_{s \to 0} s \cdot [G(s)] \cdot R(s)) \tag{7.12}$$

7.3.4 Verification of EV Charging Theorem

This chapter intends to verify our theory with regards to linear change of SOC reference, first order characteristic for power charging, HPF characteristic against frequency deviation, and steady-state error of SOC with the three cases.

Fundamentally, when inertial energy and governor control of generator support the

Table 7.1: The Cases for Performance Verification

	The Cases
Case A	DaSOF only
Case B	DaSOF-Smart Charging
Case C	No EV

power against the frequency deviation, both DaSOF EV (fully charged) and DaSOF-Smart Charging EV with 20kWh size assist the ancillary service. Afterwards, while AGC recovers the frequency, EV also recovers SOC and starts charging.

In this system, the underlying assumption is established as the power system operates with Load Frequency Control (LFC), which can maximize the functionality of DaSOF.

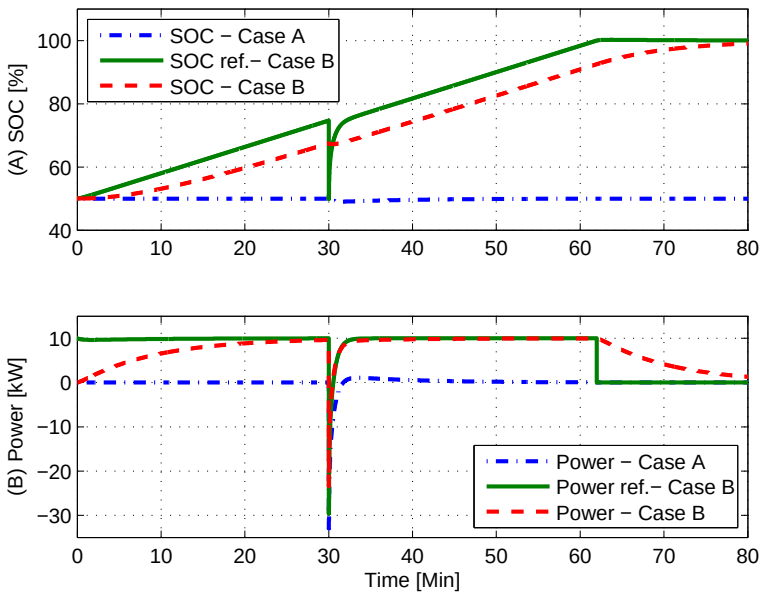

Figure 7.7: Charging graph of DaSOF-Smart Charging method and reaction of contingency; (a) SOC (b) Power

Case A in Table 7.1 intends to observe the functionality of non-charging EV, only supporting the grid and maintaining predetermined SOC value in this method. Case B aims to verify the theory of steady state error and to observe EV support of charging EV. Case C is to compare the system change without EV.

When EV initiates the charging at 0 [s] as can be shown in Fig. 7.7(a), the SOC reference of the charging increases gradually and lead to steady state error compared to the real SOC as aforementioned in (7.10)-(7.12).

According to (7.9), the trajectory of EV power in Fig. 7.7(b) exhibits filtered value to follow the power reference. The temporary mismatch between the power reference and the power injection leads to steady state error of SOC. As can be shown in Fig. 7.7(a) Case B, SOC reference increases linearly, and the SOC value follows it with the steady state error due to the slow response of the power as in Fig. 7.7(b) Case B.

If frequency deviation occurs, the SOC_{ref} is temporarily decreased, and EV releases the supporting power. Fig. 7.7(a),(b) indicates that a contingency takes place at 30 [min], and the reference of SOC sharply drops to release the power. The discharging time corresponds only to relatively short few minutes; thus, SOC does not experience severe drop as low as SOC reference.

Fig. 7.8 illustrates the frequency trajectory of three case studies, which presents the compensated frequency (Case A,B) and uncompensated frequency (Case C) shows stark differences. In this figure, the compensation between Case A and B bears remarkable similarity and overlaps each other, which implies the operation of AGC corrects frequency to be nominal value before the occurrence of contingency, and the supplying power of EV from the initial value analogizes with each other.

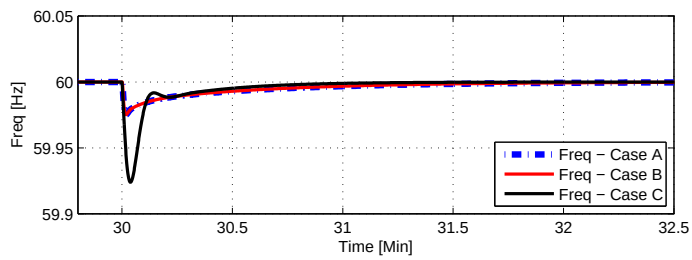

Figure 7.8: Frequency deviation; Case A: DaSOF Method only, Case B: DaSOF-Smart Charging Method, Case C: No EV

7.3.5 Results of Charging Principles

The constant charging trajectory on the SOC-Power domain such as Fig. 7.3 and Fig. 7.4 can be presented as Fig. 7.9 without contingency, which indicates trajectory of the charging reference EV as green indication rises constantly up from 50% to 100%. The measured trajectory of the charging EV, as red indication from the 0kW to 10kW like a form of first order filter such as a shape of a bowl. When SOC reaches 100 [%], it goes back to idle state; meanwhile, Power and SOC trajectory linearly changes as both tracks such as first order filter.

Under the contingency case in Fig. 7.10 , the process from start to finish has significant similarity to the case in Fig. 7.9, but when the frequency drop happens, SOC reference plummets and EV discharges. After this moment, generators recover the frequency through the LFC in accordance with frequency control sequence; hence, the recovery action of SOC is achieved, and supporting power turns into charging power. After the contingency recovery, if K_p=0, this method allows charging slightly higher power to meet the charging time.

7.4 The Charging Time

As a result of previous chapter, the time delay of power and the steady state error of SOC result in the unpunctuality of the charging time. Thus, this chapter intends to provide a guideline to charge the energy right on time with this method.

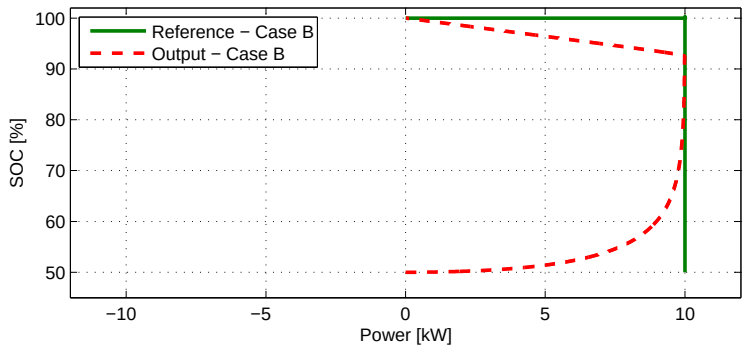

Figure 7.9: Trajectory of DaSOF Smart Charging without contingency

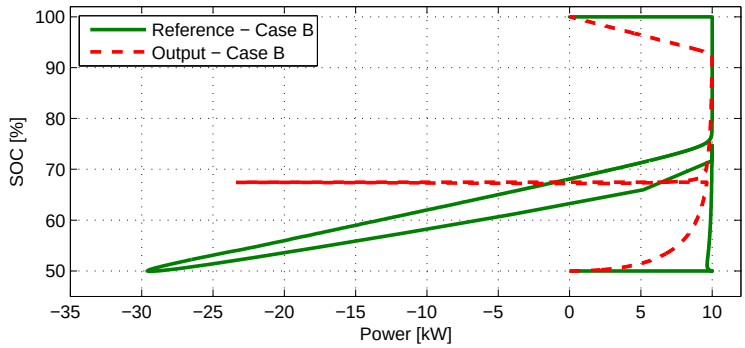

Figure 7.10: Trajectory of DaSOF Smart Charging with contingency

The EV charging rate will be discussed with C-rate, which defined as the current-rate with a unit [C], which is able to charge a battery for an hour, for instance 0.5 [C] can fully charge in 2 hours, and 2 [C] charging spends 30 mins for the full charging. In terms of this, C-rate is expressed as α which is approximated as power in pu.

7.4.1 The Response of a Square Wave Pulse

Fig. 7.11 indicates square wave as an input (P_{ref}) and its output of 1st order LPF (P_{ESS}). In this regard, equation (7.13) indicates mathematical expressions of power trajectory for the square wave change of reference power in each time slot. If we assume the pulse reference charges as much as α during the time T as in Fig. 7.11, the actual power (P_{ESS}) follows it such as 1st order filtered output such as second line of (7.13). After the time T, in case power reference drops to 0 in Fig. 7.11, P_{ESS} gradually diminished to 0 as third

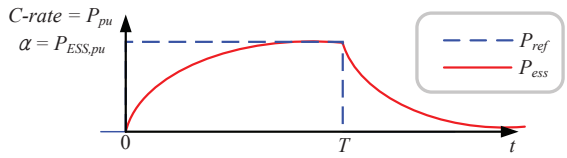

Figure 7.11: The response of a square wave type reference

line of (7.13).

$$P_{ESS,pu}(t) = \begin{cases} 0 & t < 0 \\ \alpha(1 - e^{-t/\tau}) & 0 < t < T \\ \alpha(1 - e^{-t/\tau})e^{-(t-T)/\tau} & T < t \end{cases} \tag{7.13}$$

where α is the value of C-rate, τ is the time constant, T is time duration of reference, and t is the time.

7.4.2 The Charging Time of the Normal Charger

Equation (7.14) is the relation of C-rate (α), charging time (T_{chr}), and chargeable SOC ($\%SOC$). $\%SOC$ indicates remaining capacity, calculated as dividing fully charged SOC (100%) from the value of remaining SOC as indicated as (7.15).

The calculation of time in regards to C-rate is with the hour unit, and T_{chr} presents the charging time in second unit, which is changed to hour unit by dividing h as in (7.14).

With (7.14), if C-rate and $\%SOC$ are given, the charging time T_{chr} can be calculated; otherwise, if $\%SOC$ and T_{chr} are given, C-rate can be calculated. For instance, $\%SOC$ and T_{chr} equal 0.5 and 3600 respectively, α can be 0.5 [C] for the 1 hour charging.

$$\%SOC \cdot \frac{1}{\alpha} = \frac{T_{chr}}{h} \tag{7.14}$$

$$\%SOC = \frac{SOC_{full} - SOC_{ini}}{SOC_{full}} \tag{7.15}$$

where $SOC_{full} = 100\%$, $\%SOC$ is the rate of chargeable capacity, α is the value of C-rate, SOC_{ini} is the value of SOC before charging, and T_{chr} is charging time.

7.4.3 The Charging Time of This Method

In proposed DaSOF-Smart Charging Method, since the response of power charges as low pass filtered, settling time of delayed power should be included in charging time.

As indicated in Fig. 7.7, when SOC reference reaches to 100%, SOC cannot be fully charged due to the steady state error; meanwhile, power reference becomes 0, and the power gradually decreases until SOC becomes 100%. In this regard, the charging time

Table 7.2: The Cases for Performance Verification

	The Cases
Case α	Normal Charging
Case β	Charging considering Time Delay

Table 7.3: Parameters of DaSOF Smart Charging EV

Variable	K_E	R	K_f	SOC_{ini}	SOC_{full}	h	T_{chr}
Value	18	0.05	0.1/60	50	100	3600	3600

is delayed as much as gradually decreasing power, which is after 60 [min] in Fig. 7.7. So, this time should be included in the charging time.

Regarding this, to charge ESS right on time, the C-rate should be higher value than normal charging to include the delayed time into charging time, as actual SOC is to become 100%.

$$t_s = \frac{4.5\zeta}{\omega_n} = \frac{4.5RK_E}{K_f} \qquad (\zeta > 0.69) \tag{7.16}$$

$$\%SOC \cdot \frac{1}{\alpha} = (T_{chr} - \frac{4.5RK_E}{K_f})/h \tag{7.17}$$

$$\alpha = P_{ref,pu} = \frac{\%SOC}{(T_{chr} - \frac{4.5RK_E}{K_f})/h} \tag{7.18}$$

where ζ is damping ratio, ω_n is angular velocity of natural characteristics, $SOC_{ss} = SOC_{ref} - SOC$, h is the coefficient to change the unit from seconds to hours (i.e. h = 3600).

First, settling time can be calculated as in (7.16) as the 1st order filter has damping ratio equal to 1, and settling time can be approximated as (7.16) based on [102].

Therefore, charging time without settling time can be decreased with the increase

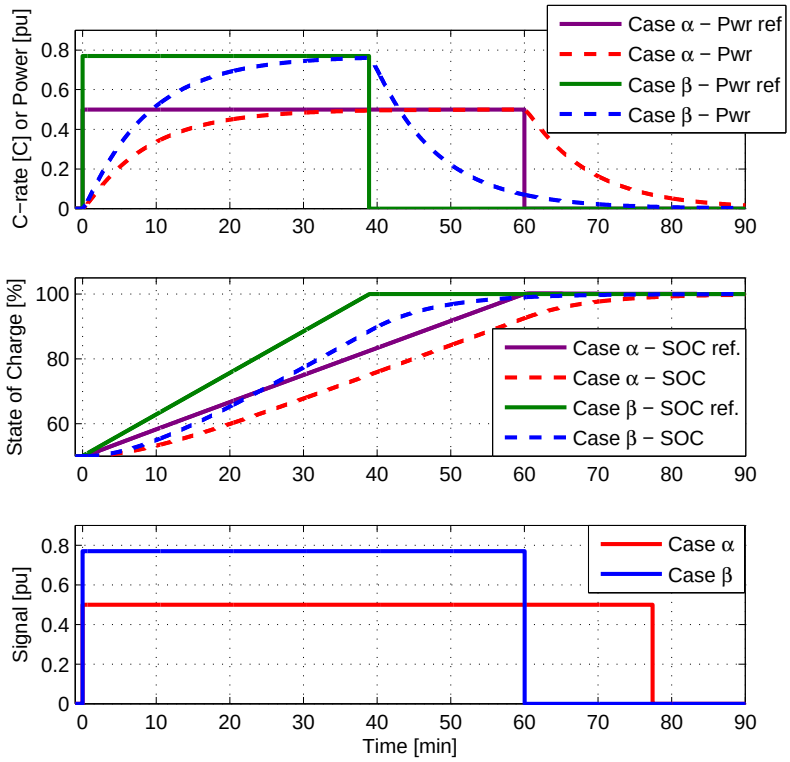

Figure 7.12: The increased charging rate to charge right on time ; (a) Power in pu or C-rate; (b) SOC (c) Charging signal

of C-rate . T_{chr} in (7.14) is reduced as much as the result in (7.16); thus, the time part can be changed to $T_{chr} - t_s$ as in (7.17). This equation (7.17) is derived for the value of C-rate in increased manner as in (7.18). For the verification of our theory in (7.18), we establish the case studies as in Table 7.2. Fig. 7.12 shows the result of Case studies; Case α is with normal charging demand and without the increase of C-rate; Case β is with proposed charging reference including the increased C-rate.

Case α intends to charge 0.5 [c] to increase 50% of SOC in 60 [min] without considering the time delay based on (7.14), and Case β is to charge 60 [min] right on time including the time delay based on (7.18) with the parameters in Table 7.3.

In Fig. 7.12(a) Case α, the power reference inject the signal to charge ESS by in-

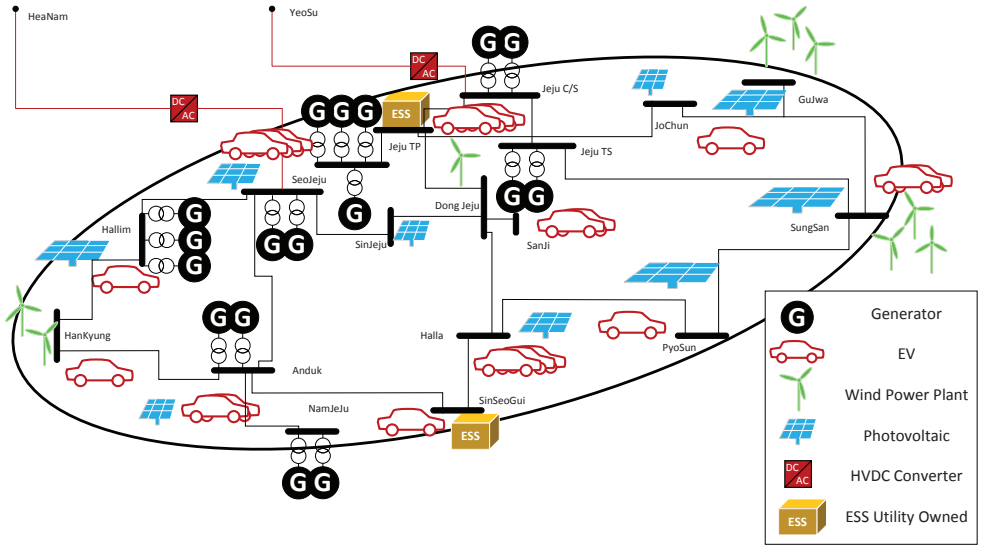

Figure 7.13: System configuration of Jeju island future grid.

creasing SOC linearly to 100% for an hour. However, because actual power does not change instantly and changes such as low pass filtered, actual SOC increases with steady state error, and the timing of full charge is indicated as 18 [min] later.

In Case β, ESS is charged with higher power based on (7.18); therefore, SOC reference in Case β reaches to 100% faster than SOC reference in Case α. The actual power in Case β is also charged higher value than that in Case α; subsequently, SOC in Case β is faster than Case α.

Fig. 7.12(c) indicates the charging signal of both cases, which is triggered during the charging states and becomes zero during the non-charging states. The magnitude of Fig. 7.12(c) is the same value of C-rate of each case to graphically distinguish each case.

As can be seen in (c), full charging timing in Case β is finished in 60 [min] right on time, although full charging timing in Case β is finished in 78 [min] as delayed as 18 [min]. This chapter provides a guideline for the change of charging magnitude, when proposed method is used, and we have verified the underlying suggestion operates well.

Table 7.4: The Location and Rating of WTG and PV

Wind	Rating [MW]	Wind	Rating [MW]	Wind	Rating [MW]
Hankyung	3.	Hengwon	10.	Jeju Univ.	5.5
Kimnyung	1.5	Samdal	3.	Sinchaing	0.85
Susan	2.	Susan2	2.	Walljung	1.5
PV	**Rating [MW]**	**PV**	**Rating [MW]**	**PV**	**Rating [MW]**
Anduk	0.611	Gujwa	0.711	Halla	1.719
Hallim	1.846	Jochun	0.615	Pyosun	4.317
Seojeju	0.873	Sinjeju	0.176	Sungsan	4.702

7.5 Future Grid of Jeju Island

7.5.1 System Configuration of Jeju Island

The test bed to investigate effectiveness of the EV is configured as in Fig. 7.13 on Jeju island based on existing information and the future plan of system expansion. Jeju island has been subject to Smart Grid demonstration test bed and to installation of fleet of clean energy sources as well as the large number of EV charger to promote EV. Due to the short of the generation, first HVDC in Fig. 7.13 is currently under the operation to flexibly meet the requirement of load demand, while the installation of second HVDC is planning stage by the government. Nevertheless, in this scenario, we assume the installation of second HVDC is completed and is presumably under the operation to investigate phenomenon of the future system. The capability of generators in the island to satisfy the demand of the load are restricted, and it relies on HVDCs characterized as faster acting equipment; hence, HVDCs are in charge of frequency control and operate LFC with several generators to balance the supply and generation, although most of the generators conducts governor control for the frequency control. The detailed information in regard with Jeju island is configured from the data in [107]. EVs are highly distributed on the load centers and most of the tourist attraction sites, and two large scaled ESSs are installed by utility, placed on nearby two dominantly large cities (Jeju and Seogwipo) to

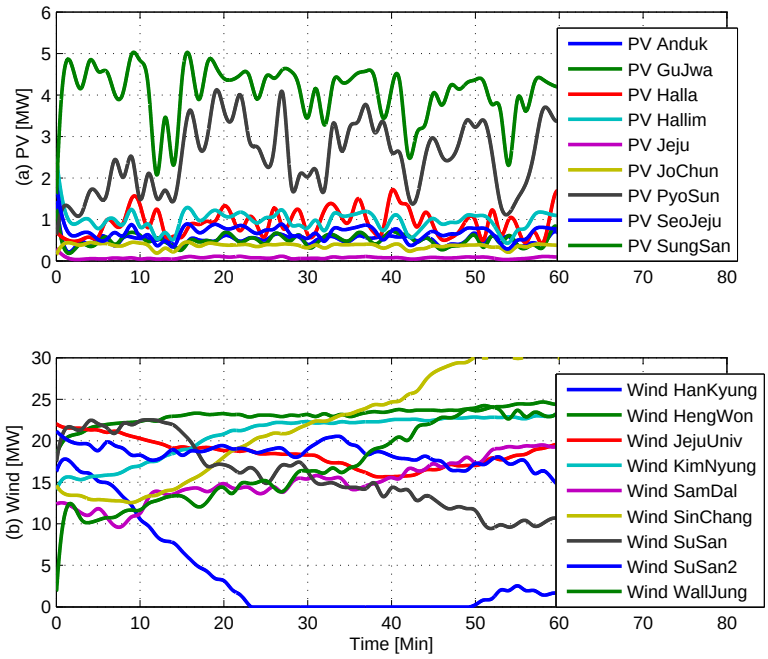

Figure 7.14: The power of renewable sources injected in Jeju Island.

ensure the reinforcement of the system resiliency.

7.5.2 Renewable Fluctuation

In order to investigate the strengthening of the system stability in regards to frequency against circumstance of renewable variation, the fluctuating components of the renewable energy are injected into the system, which potentially deteriorates Jeju island stability.

Regarding renewable generators, utility owned PV and WTG are geographically scattered around the Jeju island and are implemented as Table 7.4, which location is determined based on the installation site and rating information [108], [109]. From these renewable sources, the quantity of the renewable generation is provided into the power network as can be shown in Fig. 7.14.

Table 7.5: The Location and Size of EV

Location	Size [MWh]	Location	Size [MWh]	Location	Size [MWh]
1. Pyosun	0.28	5. Hallim C/C	0.25	9. Sanji	1.23
2. Sinseogui	0.7	6. Hallim	0.6	10. Sin-Jeju	1.9
3. SungSan	0.75	7. Halla	0.9	11. Dong-Jeju	1.25
4. Jochun	0.75	8. Jeju TP	0.06	12. Anduk	0.95

7.6 Effectiveness of ESS and EV Integration

The battery capacities of single EV sedan and single EV bus are assumed as 20-30 [kWh] and 80-110 [kWh] [16], respectively. We assumed in here the group of EVs' SOC and power in each location in Table 7.5 are identical, although the practical system consists of mixed EV charging situations.

7.6.1 Study Cases

Case 1 in Table 7.6 intends to observe fully charged case of the EV providing ancillary service, and full charging may have the possibility to absolve further energy from the grid; thus, fully charged reference is assumed as 95%, and all SOC values of the ESS initiate with slightly different level of SOC.

Case 2 aims to investigate the compensation capability of EV during the charging stage. EV is scheduled to charge the EV battery for 2 hours with 0.5 [C] and exhibits analogous performance with non-charging status, because the compensation from the initial point is equal to each case. Case 3 will indicate the frequency stabilizing case by the two times larger number of EVs to investigate the influence of the increased EV participation on the frequency stability.

7.6.2 The Case 1

Observe in Fig. 7.15 all of the EV are already charged approximately 95% of SOC and are commanded not to charge. We can observe two important points in this figure;

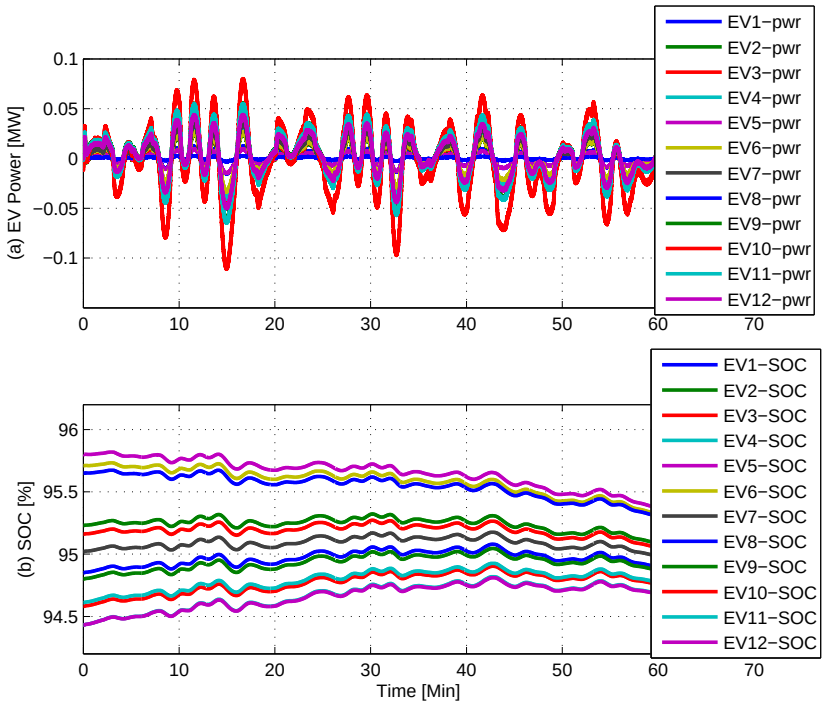

Figure 7.15: Frequency regulation of fully charged EV; (a) Power, (b) SOC.

Table 7.6: The Case Study for Jeju Island

	Frequency Supporting Equipments	C-rate [C]
Case 1	Fully Charged EV (Non-Charging)	0
Case 2	Charging EV	0.5
Case 3	Non-Charging EV, Charging EV, (Twice EVs in total)	0.5 & 0
Case 4	No EVs	-

first, DaSOF method corrects SOC level to 95% of the EV SOC in Fig. 7.15(b) such as what DaSOF does correct SOC level to 50%, the center of the SOC. Second, all of the power provides ancillary service around 0 [MW] for the fluctuating renewable sources Fig. 7.15(a).

7.6.3 The Case 2

In the regard of Case 2, corresponding EVs are subject to charging with 0.5 [C] that increase 50% of SOC level within 60 [min], which implies SOC ramp rate from the diverse size of EV are all identical due to the same C-rate, although the power of aggregated EV does not equal as indicated in Fig. 7.16(a) and Table 7.5. In Fig. 7.16(a), EVs conduct well its responsibility of V2G service, which charges power and compensates fluctuating component; in the meantime, accumulated EV energy is constantly rising in smooth and linear manner, where it has minor fluctuation of SOC.

The differences between charging and non-charging cases in Case 1 and 2 can be clearly distinguished by the power and SOC changes; however, the influence on the frequency is almost negligible, when frequency is controlled by LFC.

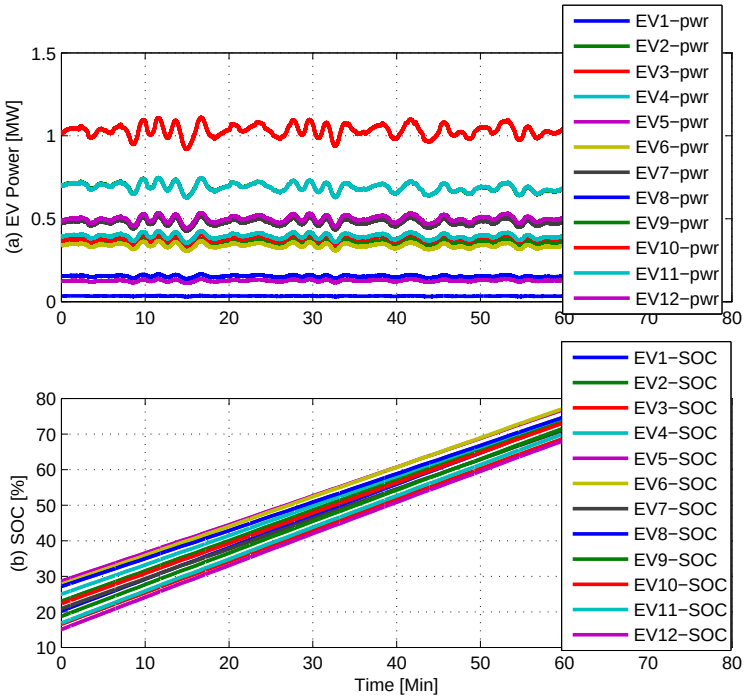

Figure 7.16: Frequency regulation of charging EV; (a) Power, (b) SOC.

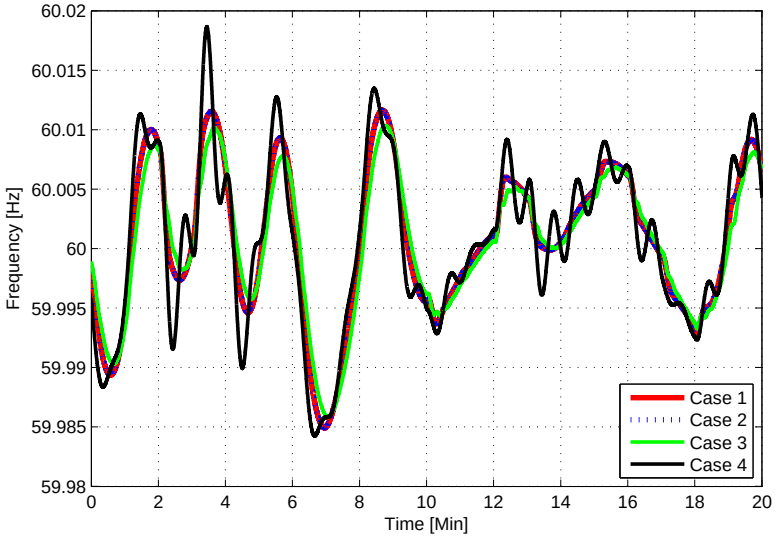

Figure 7.17: The result of frequency; Case1: EV with fully charged status, Case2 EV with charging status, Case3: The larger number of EV with the mix of charging and non-charging status.

7.6.4 The Case 3

Case 3 presents the compensation ability of the larger fleet of EV to strengthen frequency stability under the situation with the larger number of EVs and the mix of EV charging and non-charging. The larger number of EVs have better compensation capability, which is reflected into the less frequency deviation in following section. The number of EVs is double of the previous cases in Table 7.6, which implies more EVs can participate the frequency regulation.

7.7 Summary

This chapter has attempted to introduce a novel methodology of V2G service enabling the fleet of EV to regulate frequency together with EV charging. Basically, the advantage of the DaSOF method can be defined as harmoniously operable functionality with existing frequency control sequence especially AGC operation and easily definable to transfer function. In this regard, DaSOF-Smart Charging method embedded with DaSOF characteristics enables EV to show bifunctional fashion; charging and grid supporting. The phenomena during the charging in this method is described in terms of reference and output change of SOC and power, and the effects of the proposed method on Jeju island during the charging and non-charging are introduced. The results of the study may conclude V2G service facilitating EV to support power system with the advantages of the DaSOF method to operate harmoniously with existing frequency control sequence of conventional generation system.

Chapter 8

Conclusions and Future Plans

This dissertation has attempted to investigate stability issues of power systems regarding small-signal stability and frequency stability for the renewable integration cases.

From small signal perspectives, the dissertation has tried to take a look at how much the power system stability is influenced by the dynamic and the probabilistic output of the renewable resource characteristics using system identification (N4SID) and Monte Carlo simulations. Furthermore, this research also has been elaborated to scrutinize the change of the inertia constant, Eigen-characteristics, and the penetration level. The overall outcome provides the information of influences of the renewable integration on small signal stability in Ch. 3 and 4.

Frequency stability issues centre on the countermeasure by means of ESS. This dissertation has attempted to introduce the invented novel methodology of ESS for frequency regulation, enabling parallel operation with droop control method and the SOC management. This dissertation provides several theoretical basis strengthening the applicable methodology on power system in Ch. 5. The advantage of this method includes independent, decentralized control for the global frequency stability with the conventional frequency regulation sequences. The frequency band coverage of this method is located on the high frequency band of the bode plot. In this regard, as conventional frequency regulation method covers the low frequency band, this method can bring the advantage of the complementary allocation and coordination of response time between ESS and conventional generators. In the aspect of power system operation in Ch. 6,

I have investigated the practical implications of ESS for the renewable integration on governor system with droop and LFC operation cases on the Australian system and Jeju island. The successful compensation of ESS has been proved to stabilize the frequency fluctuation due to renewable sources by offering the power with regards to the high frequency band of frequency fluctuation. As to the EV in Ch. 7, the one of advantage of this method is to be applied on the highly distributed system, so this method is grafted on the Smart Charging method for the EV application. The EV application also has the same functionality as suggested method with its unique characteristics while charging and non-charging.

To sum up, this research tried to deliver the various stability issues should be considered, when the renewable generators are integrated on the power system. In this regard, I tried to suggest and develop the method of the analysis and solution for these issues.

Future plans can be ESS application for the small signal stability stabilization and Microgrid in highly distributed fashion. Moreover, the issues with the control of HVDC/ FACTS to minimize the small signal stability with PMUs in the diverse location also have possibility for the further research.

Chapter 9

Appendix

A document of Student Cotutelle Agreement for Joint Ph.D Degree between Yonsei University and the University of Sydney is attached at following pages.

Student Cotutelle Agreement

This Agreement **is made on date of last signature**

Between

The College of Engineering, Yonsei University Korea

and

The Faculty of Engineering and Information Technologies,

The University of Sydney, Australia (ABN 15 211 513 464,CRICOS Provider 00026A)

and

Jae Woong SHIM, Korea (‘**the Student**’)

(‘**the Parties**’)

Background

A. The University of Sydney and Yonsei University have entered into a Principal Cotutelle Agreement, dated December 2011.

B. The Faculty of Engineering and Information Technologies at the University of Sydney and the College of Engineering at Yonsei University share an ongoing commitment to cooperative research collaboration.

C. **Mr Jae Woong Shim** desires to undertake a doctoral degree jointly offered and awarded by the University of Sydney and Yonsei University.

D. The Parties have agreed to enter into a Cotutelle arrangement for Mr Jae Woong Shim on the terms set out in this Agreement.

Agreed Terms

1. Definitions and Interpretation

1.1 Definitions

In this Agreement:

Academic Year:

(a) at the University of Sydney, means from March to November in the same year;

(b) at Yonsei University, means from March to February in the next year;

Intellectual Property means all registered and unregistered rights, titles and interests in relation to present and future copyright, trademarks, designs, know-how, patents, confidential information and all other intellectual property as defined in article 2 of the Convention establishing the World Intellectual Property Organisation 1967;

Jointly Awarded Degree means PhD Cotutelle.

Supervisor means an appropriately qualified employee of the University of Sydney or Yonsei University who is jointly responsible for supervising the conduct and progress of the Student's candidature, including by means of instruction, advice and mentoring.

1.2 Interpretation

In this Agreement:

(a) headings are for convenience only and do not affect the interpretation of this Agreement;

(b) all references to clauses and schedules are references to clauses and schedules to this Agreement, unless otherwise specified;

(c) words importing the singular include the plural and vice versa;

(d) an expression importing a natural person includes any University, partnership, joint venture, association, corporation or other body corporate and vice versa;

(e) a reference to legislation includes any subordinate legislation, and includes that legislation and any subordinate legislation as amended or replaced;

(f) a reference to a document or agreement includes all amendments or supplements to, or replacements or novations of, that document or agreement.

2. Term of Agreement

2.1 This Agreement is effective from the date of last signature and ends on the date of the Student's graduation, unless it is terminated at an earlier time in accordance with **clause 2.2**.

2.2 This Agreement may be terminated at any time by any of the Parties giving written notice to the other Parties of the suspension or termination of the Student's candidature.

3. Administration

3.1 The Student will offer himself for the Jointly Awarded Degree on the basis of research undertaken in the field of ***"Operation and Analysis of Hybrid AC/HVDC Super Grids".***

3.1 For Students from Yonsei University, the Student's candidature will be divided between the University of Sydney and Yonsei University with a minimum of one (1) year of the candidature to be undertaken at each institution.

3.2 Upon completion of 2 years of coursework, Yonsei students would be enrolled in a four (4) year PhD Research Program at the University of Sydney.

3.3 The Student will be based and spend the majority of their time in attendance at the University of Sydney and Yonsei University as follows:

(a) Academic Year July 2013 – July 2014: The University of Sydney
(b) Academic Year July 2014– December 2014: Yonsei University
(c) Academic Year 2015: Yonsei University

3.4 Unless otherwise agreed by the Parties in writing (noting the potential impact on the Student's insurance coverage), the Student will simultaneously enrol at the University of Sydney and Yonsei University for each year of the candidature.

3.5 The Student will be entitled to the same rights and privileges (including library services and student support services) at the University of Sydney and Yonsei University as other enrolled students.

3.6 Yonsei University will be responsible for administering the Student's candidature.

3.7 Yonsei Candidates are required to undertake one unit of study worth 6 credit points (according to the University of Sydney credit system) in the Faculty of Engineering and Information Technologies at the University of Sydney during their attendance at the University of Sydney.

3.8 To the extent of any inconsistency between the rules and regulations of the University of Sydney and Yonsei University, the rules and regulations Yonsei University will apply to the Student's candidature.

4. Supervision

4.1 The University of Sydney and Yonsei University will each appoint a Supervisor.

4.2 The University of Sydney and Yonsei University may change or substitute a Supervisor at any time.

4.3 At the date of this Agreement, the Supervisors are:

(a) The University of Sydney: Dr Gregor Verbic; and

(b) Yonsei University Dr Kyeon Hur.

5. Thesis and Examination

5.1 The student's Home Institution will be responsible for organising and administering the examination process. The examination will take place at the student's home institution in accordance with its rules and regulations.

5.2 The earliest date for submission of a thesis by the Student for examination is August 2015.

5.3 The latest date for submission of a thesis by the Student for examination is August 2016.

5.4 The examiner(s) will be appointed by written agreement between the University of Sydney and Yonsei University.

5.5 The Student will submit a thesis for examination and thereafter present himself for examination at Yonsei University and the University of Sydney in accordance with the rules and regulations of the Yonsei University and the University of Sydney subject to the following conditions:

(a) the Student will write and (where applicable) defend the thesis in English, and will include in the thesis a substantial abstract written in Korean.

(b) the Student will submit two copies of the thesis to the University of Sydney, of which one will be for the University of Sydney's use and retention;

(c) the Student will submit six copies of the thesis to Yonsei University, all of which will be for Yonsei University's use and retention.

5.6 Both institutions will respect the examination outcome, provided the process above is followed. In the event of a dispute between the University of Sydney and Yonsei University regarding the examination outcome (due to incorrect procedures), the University of Sydney and Yonsei University will jointly appoint a suitably qualified external person to re-examine the thesis and, if necessary, conduct an additional oral examination ('**External Re-Examiner**'). The decision of the External Re-Examiner will be final.

6. Graduation

6.1 If the conditions for graduation are met, the Jointly Awarded Degree will be conferred by Yonsei University.

6.2 The Student is entitled to receive a testamur that:

(a) states that the Jointly Awarded Degree was undertaken by the Student through a Cotutelle arrangement; and

(b) lists the names of both the University of Sydney and Yonsei University.

6.3 The University of Sydney may also confer a testamur in accordance with **clause 6.2**, at its sole discretion.

7. Financial Arrangements

7.1 Unless otherwise agreed in writing by the University of Sydney and Yonsei University the Student will pay tuition fees at the home institution and be exempt from payment of tuition fees at the other institution for the duration of the candidature.

7.2 Unless otherwise agreed in writing by the Parties, the Student will be responsible for all other personal costs in connection with the candidature, including all living, travel, insurance (including additional medical coverage, liability and accident insurance) and ancillary costs.

7.3 The student stipend details as follows:

- *Travel support provided by the National Research Foundation Korea*

7.4 Unless otherwise agreed in writing by the University of Sydney and Yonsei University the supervisors will be responsible for the cost of any flights and accommodation required for a Supervisor or examiner to attend any oral or other examination.

8. Intellectual Property

8.1 Unless otherwise agreed by the Parties in writing, all Intellectual Property rights developed by the Student during his candidature will vest in Mr Jae Woong Shim.

8.2 The University of Sydney and Yonsei University will not assert copyright ownership over the Student's doctoral thesis, as the copyright vests in the Student.

9. Student Accommodation

9.1 The Student will be responsible for organising his own accommodation.

9.2 The University of Sydney and Yonsei University will provide information to the Student regarding temporary and longer-term accommodation on and off campus.

9.3 Neither the University of Sydney nor Yonsei University guarantees that accommodation on campus will be available.

10. Student obligations

10.1 The Student will:

(a) at all times comply with and be bound by any relevant laws, rules, regulations and codes of practice applicable to the candidature, including in respect of:

a. any entry and visa requirements;

b. the research conducted by the Student; and

c. the Student's presence in or on land or buildings owned, occupied or under the control of the University of Sydney or Yonsei University ;

(b) obtain medical insurance for the duration of the Student's time at Yonsei University

(c) if enrolled at the University of Sydney as an overseas student, be solely responsible for the purchase and maintenance of Overseas Student Health Cover (OSHC) while staying in Australia, as a condition of the Student's visa.

11. Indemnification

11.1 Subject to applicable laws, the University of Sydney and Yonsei University indemnify and agree to keep indemnified ('**Indemnifying Institution**') the other institution ('**Indemnified Institution**') against all liability, loss, costs, damages or expenses (including legal costs and expenses) incurred or suffered by the Indemnified Institution as a result of any wilful misconduct or negligent act or omission by the Indemnifying Institution, or a material breach of this Agreement by the Indemnifying Institution.

11.2 Subject to applicable laws, the University of Sydney and Yonsei University will not be liable to one another for incidental damages, such as loss of profits, revenue, goodwill or opportunities, and each institution's liability under this Agreement is reduced to the extent that any liability, loss, costs, damages or expenses arise from or are attributable to any wilful or negligent act or omission by the Indemnified Institution.

11.3 References to the Indemnifying Institution and the Indemnified Institution in this clause include the institution's directors, officers, employees, agents and students,

11.4 The University of Sydney and Yonsei University will maintain adequate insurance protections for public liability and professional indemnity (which may be self-insurance) to cover their obligations under this Agreement, and will provide to the other institution a certificate of currency and renewals of such insurance, if requested to do so.

12. Force Majeure

12.1 Neither institution will be held responsible or liable, or be deemed to be in default or breach of this Agreement, for any delay, failure or inability to meet its obligations under this Agreement (other than any obligation to pay money) caused by or arising from any cause that is unavoidable or beyond the reasonable control of the institution, including war, warlike operations, riot, insurrection, orders of government, strikes, lockouts, public health emergencies, quarantines, disturbances or any act of God or other cause which frustrates the performance of this Agreement.

13. Nature of Agreement and Amendment

13.1 This Agreement is binding and constitutes the entire agreement between the Parties, in addition only to a Principal Agreement between the parties which has been agreed to by both parties and which sets out their general obligations regarding Cotutelle arrangements.

13.2 Nothing contained or implied in this Agreement is intended to create a partnership between any of the Parties or, except as otherwise provided in this agreement, establish any of the Parties as an agent or representative of any other party.

13.3 This Agreement and any Schedule to it may be amended, modified, extended or renewed only with the written, mutual consent of the Parties.

13.4 The Parties agree that this Agreement and all documents related to may be written in both English and the language chosen by Yonsei University with the English version prevailing.

Signed:

[redacted]

Mr Jae Woong Shim
Candidate

Date: 29/07/2013

On behalf of:

The College of Engineering, Yonsei University

[redacted]

Dr Kyeon Hur
Supervisor

Date: 29/07/2013

Yonsei University

[redacted]

Professor Jinho Lee
Dean, Graduate School

Date: 12/08/2013

The University of Sydney

[redacted]

Dr Gregor Verbic
Supervisor

Date: 23/08/2013

The University of Sydney

[redacted]

Professor Marie Carroll
Pro-Vice-Chancellor (Academic Affairs)

Date: 2/9/13

References

[1] IEC, "Grid integration of large-capacity Renewable Energy sources and use of large-capacity Electrical Energy Storage," IEC, Tech. Rep., 2012.

[2] N. Mathur, S. Ravinder, P. Batra, and P. Jindal, "Large scale grid integration of renewable energy sources - Way Forward," Central Electricity Authority, Tech. Rep., Nov. 2013.

[3] J. Nikoletatos and S. Tselepis, "Renewable energy integration in power grids: Technology brief," IEA-ETSAP and IRENA, Tech. Rep., Apr 2015.

[4] J. Balke, "Integration of Renewable Energy in Europe," KEMA Consulting GmbH - Imperial College London and NERA Economic Consulting, Tech. Rep. 9011-700, Jun. 2014.

[5] C. DeMarco, G. T. Heydt, and S. Oren, "A Grand Challenge for the Future Grid," PSERC, Tech. Rep. PSERC Document 14-4, Oct. 2014.

[6] J. Heydt, S. Oren, M. Ilic, P. Sen, T. Mount, S. Meliopoulos, J. Momoh, P. Sauer, J. McCalley, M. Kezunovic, A. Bose, C. DeMarco, V. Vittal, W. Jewell, and D. Ray, "Challenges in Integrating Renewable Technologies into an Electric Power System," PSERC, Tech. Rep. PSERC Document 10-07, April 2010.

[7] J. Weiss and B. Tsuchida, "Integrating Renewable Energy into the Electricity Grid: Case studies showing how system operators are maintaining reliability," Advanced Energy Economy Institute (AEEI) and The Brattle Group, Inc., Tech. Rep., June 2015.

[8] K. Forsten and P. Myrda, "Grid Transformation Workshop Results," EPRI, Tech. Rep., April 2012.

[9] D. Lew, N. Miller, K. Clark, G. Jordan, and Z. Gao, "Impact of High Solar Penetration in the Western Interconnection," NREL, Tech. Rep. NREL/TP-5500-49667, Dec. 2010.

[10] B.-M. Hodge, D. Lew, and M. Milligan, "The Impact of High Wind Power Penetrations on Hydroelectric Unit Operations in the WWSIS," NREL, Tech. Rep. NREL/TP-5500-52251, 2011 Jul.

[11] V. Vittal, G. T. Heydt, S. Hariharan, S. Gupta, G. Hug, R. Yang, A. Pandey, and H. Franchetti, "Tools and Techniques for Considering Transmission Corridor Options to Accommodate Large Scale Renewable Energy Resources," PSERC, Tech. Rep. PSERC Publication 12-23, Aug. 2012.

[12] D. Corbus, M. Schuerger, L. Roose, J. Strickler, T. Surles, D. Manz, D. Burlingame, and D. Woodford, "OAHU Wind Integration and Transmission Study Summary Report," NREL, Tech. Rep. NREL/ TP-5500-48632, Nov 2010.

[13] P. Pourbeik, "Generic Models and Model Validation for Wind and Solar PV Generation: Technical Update," EPRI, 942 Corridor Park Blvd. Knoxville, TN, Tech. Rep. 1021763, Dec. 2011.

[14] J. Manobianco, C. Alonge, J. Frank, and M. Brower, "Development of Regional Wind Resource and Wind Plant Output Datasets for the Hawaiian Islands," NREL, AWS Truepower, LLC Albany, New York, Tech. Rep. NREL/SR-550-48680, July 2010.

[15] E. Muljadi, V. Gevorgian, M. Singh, and S. Santoso, "Understanding Inertial and Frequency Response of Wind Power Plants," NREL, Tech. Rep. NREL/CP-5500-55335, Jul. 2012.

[16] W. Jewell, Z. Hu, N. Li, K. W. Hedman, J. R. Ruggiero, and G. T. Heydt, "The Economic Case for Bulk Energy Storage in Transmission Systems with High Percentages of Renewable Resources," PSERC, Tech. Rep. PSERC Publication 14-9, Sep. 2014.

[17] S. Inwood and A. Tuohy, "Impacts of wind generation integration," EPRI Energy Technology Assessment Center, Tech. Rep., April 2012.

[18] B. Kaun, "Cost-effectiveness of energy storage in california," EPRI, Tech. Rep. 3002001162, Jun. 2013.

[19] D. Rastler, "Electricity Energy Storage Technology Options: A White Paper Primer on Applications, Costs, and Benefits," EPRI, 3420 Hillview Avenue Palo Alto, California 94304, Tech. Rep. 1020676, Dec. 2010.

[20] ABB ltd, "Battery Energy Storage for Renewable Integration: Managing generation to improve grid stability," ABB, Tech. Rep.

[21] F. M. Kezunovic, R. Baldick, I. Damnjanovic, C. Pang, S. Kim, D. Tuttle, and M. Peydaayesh, "PHEVs as Dynamically Configurable Dispersed Energy Storage," PSERC, Tech. Rep. PSERC Publication 11-03, Aug. 2011.

[22] G. Gross, A. Dominguez-Garcia, C. Singh, and A. Sprintson, "Integration of Storage Devices into Power Systems with Renewable Energy Sources," PSERC, Tech. Rep. PSERC Publication 12-24, Sep. 2012.

[23] The University of Melbourne Energy Research Institute, "Zero Carbon Australia Stationary Energy Plan," The University of Melbourne Energy Research Institute, Tech. Rep., 2010.

[24] Australian Energy Market Operator (AEMO), "100 Per Cent Renewables Study–Modelling Outcomes," AEMO, Tech. Rep. July, 2013.

[25] M. Gibbard and D. Vowles, "IEEE PES Task Force on Benchmark Systems for Stability Controls: Simplified 14-generator model of the south east australian power system," The University of Adelaide, South Australia, Tech. Rep., 2010.

[26] Korea Electric Power Corporation (KEPCO). [Online]. Available: http://home.kepco.co.kr/kepco/EN/

[27] Ministry of Trade, Industry, and Energy: Korea Government, "4th Fundamental Planning of Renewable Energy," Ministry of Trade, Industry and Energy, Korea Government, Tech. Rep., Sep. 2014.

[28] J. Shim, G. Verbic, K. Hur, and D. Hill, "Impact analysis of variable generation on small signal stability," in *2014 Australasian Universities Power Engineering Conference (AUPEC)*, Perth, Australia, Sep. 2014, p. 16.

[29] ——, "Impact of Large Scale Penetration of Concentrated Solar Thermal Power on Oscillatory Stability of the Australian Future Grid," in *Solar Integration Workshop 2014*, Berlin, Germany, Nov. 2014, pp. 85–92.

[30] P. Kundur, J. Paserba, V. Ajjarapu, G. Andersson, A. Bose, C. Canizares, N. Hatziargyriou, D. Hill, A. Stankovic, C. Taylor, T. V. Cutsem, and V. Vittal, "Definition and classification of power system stability IEEE/CIGRE joint task force on stability terms and definitions," *IEEE Trans. Power Syst.*, vol. 19, no. 3, p. 13871401, Aug. 2004.

[31] P. Kundur, *Power System Stability and Control*, ser. The EPRI Power System Engineering Series. New York: McGraw-Hill, 1994.

[32] NERC, "Industry Advisory: Generator Governor Frequency Response," NERC, Atlanta, GA, Tech. Rep., Nov. 2012.

[33] N. Jaleeli, L. S. VanSlyck, D. N. Ewart, L. H. Fink, and A. G. Hoffmann, "Understanding automatic generation control," *IEEE Trans. Power Syst.*, vol. 7, no. 3, pp. 1106–1122, Aug 1992.

[34] Ibraheem, P. Kumar, and D. P. Kothari, "Recent philosophies of automatic generation control strategies in power systems," *IEEE Trans. Power Syst.*, vol. 20, no. 1, pp. 346–357, Feb 2005.

[35] M. Yao, R. Shoults, and R. Kelm, "AGC logic based on NERC's new control performance standard and disturbance control standard," *IEEE Trans. Power Syst.*, vol. 15, no. 2, pp. 852–857, May 2000.

[36] J. Slootweg and W. Kling, "The impact of large scale wind power generation on power system oscillations," *Electric Power Systems Research*, vol. 67, no. 1, pp. 9–20, Oct. 2003.

[37] G. Tsourakis, B. Nomikos, and C. Vournas, "Contribution of Doubly Fed Wind Generators to Oscillation Damping," *IEEE Trans. Energy Convers.*, vol. 24, no. 3, pp. 783–791, Sep. 2009.

[38] J. Sanchez-Gasca, N. Miller, and W. Price, "A modal analysis of a two-area system with significant wind power penetration," in *IEEE PES Power Systems Conference and Exposition, 2004.* IEEE, 2004, pp. 1537–1541.

[39] S. Eftekharnejad, V. Vittal, G. T. Heydt, B. Keel, and J. Loehr, "Small Signal Stability Assessment of Power Systems With Increased Penetration of Photovoltaic Generation: A Case Study," *IEEE Trans. Sustain. Energy*, vol. 4, no. 4, pp. 960–967, Oct. 2013.

[40] D. Gautam, V. Vittal, and T. Harbour, "Impact of Increased Penetration of DFIG-Based Wind Turbine Generators on Transient and Small Signal Stability of Power Systems," *IEEE Trans. Power Syst.*, vol. 24, no. 3, pp. 1426–1434, Aug. 2009.

[41] B. Tamimi, C. Canizares, and K. Bhattacharya, "System Stability Impact of Large-Scale and Distributed Solar Photovoltaic Generation: The Case of Ontario, Canada," *IEEE Trans. Sustain. Energy*, vol. 4, no. 3, pp. 680–688, Jul. 2013.

[42] CIGRE, "Grid Integration of Wind Generation," Working Group 08 of Study Committee C6, Tech. Rep., 2009.

[43] Australian Energy Market Operator (AEMO), "Integrating Renewable Energy–Wind Integration Studies Report," Australian Energy Market Operator (AEMO), Tech. Rep., 2013.

[44] D. K. Mugwanya and J. E. Van Ness, "Mode Coupling in Power Systems," *IEEE Trans. Power Syst.*, vol. 2, no. 2, pp. 264–269, 1987.

[45] M. Klein, G. Rogers, S. Moorty, and P. Kundur, "Analytical investigation of factors influencing power system stabilizers performance," *IEEE Trans. Energy Convers.*, vol. 7, no. 3, pp. 382–390, 1992.

[46] J. F. Manwell, J. G. McGowan, and A. L. Rogers, *Wind Energy Explained: Theory, Design and Application*. Wiley, 2010.

[47] T. Burton, N. Jenkins, D. Sharpe, and E. Bossanyi, *Wind Energy Handbook*. John Wiley & Sons, 2011.

[48] P. Van Overschee and B. De Moor, *Subspace identification for linear systems: theory, implementation, applications, Volume 1*. Kluwer Academic Publishers, 1996.

[49] Y. Pipelzadeh, N. Chaudhuri, B. Chaudhuri, and T. Green, "System stability improvement through optimal control allocation in voltage source converter-based high-voltage direct current links," *Generation, Transmission Distribution, IET*, vol. 6, no. 9, pp. 811–821, September 2012.

[50] J. Hauer, W. Mittelstadt, K. Martin, J. Burns, H. Lee, J. Pierre, and D. Trudnowski, "Use of the WECC WAMS in Wide-Area Probing Tests for Validation of System Performance and Modeling," *IEEE Trans. Power Syst.*, vol. 24, no. 1, pp. 250–257, Feb 2009.

[51] Australian Government, Department of Resources and Tourism, "Energy facts, statistics and publications," Australian Government, Tech. Rep., 2012.

[52] DESERTEC Foundation, "Clean Power from Deserts: The DESERTEC Concept for Energy, Water and Climate Security," DESERTEC Foundation, Tech. Rep., 2009.

[53] S. Taggart, G. James, Z. Dong, and C. Russell, "The future of renewables linked by a transnational asian grid," *Proceedings of the IEEE*, vol. 100, no. 2, pp. 348–359, Feb 2012.

[54] B. Elliston, I. MacGill, and M. Diesendorf, "Comparing least cost scenarios for 100% renewable electricity with low emission fossil fuel scenarios in the Australian National Electricity Market," *Renewable Energy*, vol. 66, no. 0, pp. 196 – 204, 2014.

[55] C. Budischak, D. Sewell, H. Thomson, L. Mach, D. E. Veron, and W. Kempton, "Cost-minimized combinations of wind power, solar power and electrochemical storage, powering the grid up to 99.9% of the time," *Journal of Power Sources*, vol. 225, no. 0, pp. 60 – 74, 2013.

[56] K. Knorr, "Abschätzung der Netzstabilität einer rein regenerativen Stromversorgung," in *17. Kasseler Symposium Energie-Systemtechnik*, 2012.

[57] N. Mithulananthan, R. Shah, and K. Lee, "Small-disturbance angle stability control with high penetration of renewable generations," *Power Systems, IEEE Transactions on*, vol. 29, no. 3, pp. 1463–1472, May 2014.

[58] M. Geyer, "Potential of solar trough installations in europe," in *Concentrating Solar Power towards the 7th FW RTD Program*, June 2008.

[59] International Renewable Agency (IRENA), "Renewable Energy Cost Analysis–Concentrating Solar Power," IRENA, Tech. Rep., June 2012.

[60] I. L. Garca, J. L. lvarez, and D. Blanco, "Performance model for parabolic trough solar thermal power plants with thermal storage: Comparison to operating plant data," *Solar Energy*, vol. 85, no. 10, pp. 2443 – 2460, 2011.

[61] J. Chow, R. Galarza, P. Accari, and W. Price, "Inertial and slow coherency aggregation algorithms for power system dynamic model reduction," *IEEE Trans. Power Syst.*, vol. 10, no. 2, p. 680685, May 1995.

[62] J. Quintero, V. Vittal, G. Heydt, and H. Zhang, "The Impact of Increased Penetration of Converter Control-Based Generators on Power System Modes of Oscillation," *IEEE Trans. Power Syst.*, vol. 29, no. 5, pp. 2248–2256, Sep. 2014.

[63] S. Savulescu, *Realtime Stability Assessment In Modern Power System Control Centers*, ser. IEEE Press Series in Power Engineering. New York: Wiley, 2009.

[64] S. Bu, W. Du, H. Wang, Z. Chen, L. Xiao, and H. Li, "Probabilistic Analysis of Small-Signal Stability of Large-Scale Power Systems as Affected by Penetration of Wind Generation," *IEEE Trans. Power Syst.*, vol. 27, no. 2, p. 762770, May 2012.

[65] Australian PV Institute. [Online]. Available: http://pv-map.apvi.org.au/

[66] Australian Government, Bureau of Meteorology, Climate Data Online. [Online]. Available: http://www.bom.gov.au/climate/data/

[67] Y. Agalgaonkar, B. Pal, and R. Jabr, "Stochastic Distribution System Operation Considering Voltage Regulation Risks in the Presence of PV Generation," *IEEE Trans. Sustainable Energy*, vol. 6, no. 4, p. 13151324, Oct. 2015.

[68] M. Tabone and D. Callaway, "Modeling Variability and Uncertainty of Photovoltaic Generation: A Hidden State Spatial Statistical Approach," *IEEE Trans. Power Syst.*, vol. 30, no. 6, p. 29652973, Nov. 2015.

[69] P. J. Jones and P. Smith, *Stochastic Processes, An Introduction*, 2nd ed. Boca Raton, FL, USA: CRC Press, 2010.

[70] R. Yates and D. Goodman, *Probability and Stochastic Processes*. New York: Wiley, 2005.

[71] N. Soleimanpour and M. Mohammadi, "Probabilistic Load Flow by Using Nonparametric Density Estimators," *IEEE Trans. Power Syst.*, vol. 28, no. 4, pp. 3747–3755, Nov. 2013.

[72] J. Chow, *Power System Coherency and Model Reduction*, ser. Power Electronics and Power Systems. New York: Springer, 2013, vol. 94.

[73] R. Preece and J. V. Milanovi, "Efficient Estimation of the Probability of Small-Disturbance Instability of Large Uncertain Power Systems," *IEEE Trans. Power Syst.*, vol. 31, no. 2, pp. 1063–1072, March 2016.

[74] Z. Xu, Z. Y. Dong, and P. Zhang, "Probabilistic small signal analysis using Monte Carlo simulation," in *IEEE Power Engineering Society General Meeting, 2005.*, June 2005, pp. 1658–1664 Vol. 2.

[75] W. M. Grady and D. Costello, "Implementation and application of an independent Texas synchrophasor network," in *2010 63rd Annual Conference for Protective Relay Engineers*, March 2010, pp. 1–12.

[76] J. Eyer and G. Corey, "Energy Storage for the Electricity Grid: Benefits and Market Potential Assessment Guide," Sandia National Laboratories, Albuquerque, NM and Livermore, CA, Tech. Rep. SAND2010-0815, Feb. 2010.

[77] KERMIT Study Report, "To determine the effectiveness of the AGC in controlling fast and conventional resources in the PJM frequency regulation market," KEMA Inc., Chalfont, PA, Tech. Rep. Statement of Work 11-3099, Dec. 2011.

[78] D. Allen, C. Brown, J. Hickey, V. Le, and R. Safuto, "Energy storage in the New York electricity market," New York Independent System Operator (NYISO), Rensselaer, NY, Tech. Rep., Mar. 2010.

[79] ERCOT, "Future Ancillary Services in ERCOT," Electric Reliability Council of Texas (ERCOT), Austin, TX, Tech. Rep., Sep. 2013.

[80] W. Hur, Y. Moon, K. Shin, W. Kim, S. Nam, and K. Park, "Economic Value of Li-ion Energy Storage System in Frequency Regulation Application from Utility Firm's Perspective in Korea," *Energies*, vol. 8, no. 6, pp. 5000–5017, May 2015.

[81] M. van der Hoeven, "Technology Roadmap: Energy Storage," International Energy Agency (IEA), Paris, France, Tech. Rep., Mar. 2014.

[82] The DOE Global Energy Storage Database, Sandia National Laboratories. [Online]. Available: http://www.energystorageexchange.org/

[83] M. Atanacio, R. Fioravanti, W. Katzenstein, and K. Vu, "Emission II Study of Advanced Storage used for Frequency Regulation," Sandia National Laboratories, Albuquerque, NM, Tech. Rep. Sandia Negotiation 96362, Dec. 2011.

[84] FERC, "Third-Party Provision of Ancillary Services; Accounting and Financial Reporting for New Electric Storage Technologies: 18 CFR Parts 35, 101 and 141,," Federal Energy Regulatory Commission (FERC), Washington, D.C., Tech. Rep., Jul. 2013.

[85] G. Zhang, "EPRI power systems dynamics tutorial," EPRI, Palo Alto, CA, Tech. Rep. 1016042, Jul. 2009.

[86] NERC, "Frequency Response Standard Background Document," NERC, Atlanta, GA, Tech. Rep., Nov. 2012.

[87] C. Hill, M. Such, D. Chen, J. Gonzalez, and W. Grady, "Battery Energy Storage for Enabling Integration of Distributed Solar Power Generation," *IEEE Trans. Smart Grid*, vol. 3, no. 2, pp. 850–857, Jun. 2012.

[88] I. Y. Chung, W. Liu, D. A. Cartes, E. G. Collins, and S. I. Moon, "Control Methods of Inverter-Interfaced Distributed Generators in a Microgrid System," *IEEE Trans. Ind. Appl.*, vol. 46, no. 3, pp. 1078–1088, May 2010.

[89] J. Dang, J. Seuss, L. Suneja, and R. G. Harley, "SOC feedback control for wind and ESS hybrid power system frequency regulation," in *IEEE Power Electronics and Machines in Wind Applications (PEMWA) 2012*, Jul. 2012, pp. 1–7.

[90] H. Liu, Z. Hu, Y. Song, and J. Lin, "Decentralized Vehicle-to-Grid Control for Primary Frequency Regulation Considering Charging Demands," *IEEE Trans. Power Syst.*, vol. 28, no. 3, pp. 3480–3489, Aug. 2013.

[91] Y. Ota, H. Taniguchi, T. Nakajima, K. M. Liyanage, J. Baba, and A. Yokoyama, "Autonomous Distributed V2G (Vehicle-to-Grid) Satisfying Scheduled Charging," *IEEE Trans. Smart Grid*, vol. 3, no. 1, pp. 559–564, Mar. 2012.

[92] H. Mahmood, D. Michaelson, and J. Jiang, "Decentralized Power Management of a PV/Battery Hybrid Unit in a Droop-Controlled Islanded Microgrid," *IEEE Trans. Power Electron.*, vol. 30, no. 12, pp. 7215–7229, Dec. 2015.

[93] X. Lu, K. Sun, J. M. Guerrero, J. C. Vasquez, and L. Huang, "State-of-Charge Balance Using Adaptive Droop Control for Distributed Energy Storage Systems in DC Microgrid Applications," *IEEE Trans. Ind. Electron.*, vol. 61, no. 6, pp. 2804–2815, Jun. 2014.

[94] X. Lu, K. Sun, J. M. Guerrero, J. C. Vasquez, and L. Huang, "Double-Quadrant State-of-Charge-Based Droop Control Method for Distributed Energy Storage Systems in Autonomous DC Microgrids," *IEEE Trans. Smart Grid*, vol. 6, no. 1, pp. 147–157, Jan. 2015.

[95] C. Gavriluta, J. I. Candela, J. Rocabert, A. Luna, and P. Rodriguez, "Adaptive Droop for Control of Multiterminal DC Bus Integrating Energy Storage," *IEEE Trans. Power Del.*, vol. 30, no. 1, pp. 16–24, Feb. 2015.

[96] J. W. Shim, Y. Cho, S. J. Kim, S. W. Min, and K. Hur, "Synergistic Control of SMES and Battery Energy Storage for Enabling Dispatchability of Renewable Energy Sources," *IEEE Trans. Appl. Supercond.*, vol. 23, no. 3, pp. 5 701 205–5 701 205, Jun. 2013.

[97] J. Xiao, P. Wang, and L. Setyawan, "Hierarchical Control of Hybrid Energy Storage System in DC Microgrids," *IEEE Trans. Ind. Electron.*, vol. 62, no. 8, pp. 4915–4924, Aug. 2015.

[98] J. Pahasa and I. Ngamroo, "PHEVs Bidirectional Charging/Discharging and SoC Control for Microgrid Frequency Stabilization Using Multiple MPC," *IEEE Trans. Smart Grid*, vol. 6, no. 2, pp. 526–533, Mar. 2015.

[99] H. Liu, Z. Hu, Y. Song, J. Wang, and X. Xie, "Vehicle-to-Grid Control for Supplementary Frequency Regulation Considering Charging Demands," *IEEE Trans. Power Syst.*, vol. 30, no. 6, pp. 3110–3119, Nov. 2015.

[100] O. Tremblay and L. Dessaint, "Experimental validation of a battery dynamic model for EV applications," *World Electric Vehicle Journal*, vol. 3, p. 1316, 2009.

[101] C. M. Shepherd, "Design of Primary and Secondary Cells - Part 2. An equation describing battery discharge," *Journal of Electrochemical Society*, vol. 112, pp. 657–664, Jul. 1965.

[102] B. Kuo and F. Golnaraghi, *Automatic Control Systems*, 9th ed. New York: Wiley, 2009.

[103] S. Vachirasricirikul and I. Ngamroo, "Robust LFC in a Smart Grid With Wind Power Penetration by Coordinated V2G Control and Frequency Controller," *IEEE Trans. Smart Grid*, vol. 5, no. 1, pp. 371–380, Jan 2014.

[104] H. Yang, C. Y. Chung, and J. Zhao, "Application of plug-in electric vehicles to frequency regulation based on distributed signal acquisition via limited communication," *IEEE Trans. Power Syst.*, vol. 28, no. 2, pp. 1017–1026, May 2013.

[105] J. Pahasa and I. Ngamroo, "PHEVs Bidirectional Charging/Discharging and SoC Control for Microgrid Frequency Stabilization Using Multiple MPC," *IEEE Trans. Smart Grid*, vol. 6, no. 2, pp. 526–533, March 2015.

[106] M. Yilmaz and P. T. Krein, "Review of the Impact of Vehicle-to-Grid Technologies on Distribution Systems and Utility Interfaces," *IEEE Trans. Power Electron.*, vol. 28, no. 12, pp. 5673–5689, Dec 2013.

[107] Korea Wind Energy industry Association (KWEIA). [Online]. Available: http://www.kweia.or.kr/

[108] Electric Power Statistics Information System Available (EPSIS) . [Online]. Available: http://epsis.kpx.or.kr/epsis/

[109] Electric Vehicle Charging Information System. [Online]. Available: http://www.ev.or.kr/